
# Pattern Formation Through Synchronization in Systems of Nonidentical Autonomous Oscillators

Dissertation
zur Erlangung des akademischen Grades
Doctor Rerum Naturalium (Dr. rer. nat.)
im Fach Physik / Nichtlineare Dynamik

eingereicht an der
Mathematisch-Naturwissenschaftlichen Fakultät
der Universität Potsdam

von

Ralf Tönjes

Potsdam, October 31, 2007

Elektronisch veröffentlicht auf dem
Publikationsserver der Universität Potsdam:
http://opus.kobv.de/ubp/volltexte/2008/1597/
urn:nbn:de:kobv:517-opus-15973
[http://nbn-resolving.de/urn:nbn:de:kobv:517-opus-15973]

# Kurzzusammenfassung

Die vorliegende Arbeit beschäftigt sich in Theorie und Simulation mit den raum-zeitlichen Strukturen, die entstehen, wenn nicht-identische, diffusiv gekoppelte Oszillatoren synchronisieren. Wir greifen dabei auf die von Kuramoto [1] hergeleiteten Phasengleichungen zurück. Eine entscheidene Rolle für die Musterbildung spielt die Symmetrie der Kopplung. Wir untersuchen den ordnenden Einfluss von Asymmetrie (Nichtisochronizität) in der Phasenkopplungsfunktion auf das Phasenprofil in Synchronisation und das Zusammenspiel zwischen dieser Asymmetrie und der Frequenzheterogenität im System. Die Arbeit gliedert sich in drei Hauptteile. Kapitel 2 und 3 beschäftigen sich mit den grundlegenden Gleichungen und den Bedingungen für stabile Synchronisation. Im Kapitel 4 charakterisieren wir die Phasenprofile in Synchronisation für verschiedene Spezialfälle sowie in der von uns eingeführten exponentiellen Approximation der Phasenkopplungsfunktion. Schliesslich untersuchen wir im dritten Teil (Kap. 5) den Einfluss von Nichtisochronizität auf die Synchronisationsfrequenz in kontinuierlichen, oszillatorischen Reaktions-Diffusionssystemen und diskreten Netzwerken von Oszillatoren.

# Abstract

This work is concerned with the spatio-temporal structures that emerge when non-identical, diffusively coupled oscillators synchronize. It contains analytical results and their confirmation through extensive computer simulations. We use the Kuramoto model [1] which reduces general oscillatory systems to phase dynamics. The symmetry of the coupling plays an important role for the formation of patterns. We have studied the ordering influence of an asymmetry (non-isochronicity) in the phase coupling function on the phase profile in synchronization and the intricate interplay between this asymmetry and the frequency heterogeneity in the system. The thesis is divided into three main parts. Chapter 2 and 3 introduce the basic model of Kuramoto and conditions for stable synchronization. In Chapter 4 we characterize the phase profiles in synchronization for various special cases and in an exponential approximation of the phase coupling function, which allows for an analytical treatment. Finally, in the third part (Chap. 5) we study the influence of non-isochronicity on the synchronization frequency in continuous, reaction diffusion systems and discrete networks of oscillators.

# Acknowledgments

Now that my time here at the Nonlinear Dynamics group (AGNLD) at Potsdam University draws to its conclusion I look back to three years and six months of fruitful and enjoyable work. Much of the comfort is due to my fellow colleagues of the Theoretical Ecology research group and my advisor Prof. Bernd Blasius. I am fond of the inspiring discussions with him, often on the train to Potsdam, which have led to one or another tangent project just because I got hooked by a challenging problem. I was amazed by Bernd's capacity to work on several ecological and mathematical problems simultaneously and draw connections between them, at the same time applying for grants, organizing workshops, always looking for cooperations and still taking all the time needed to discuss my work or the work of my colleagues. I had the privilege to work in a department which is internationally renowned in the non-linear dynamics community and, in particular, for its work in the field of synchronization. I have to thank Changsong Zhou for many discussions and suggestions. Through the special topic of Theoretical Ecology, on the other hand, I was also exposed to scientists from biological fields, Lars Rudolph and Andrea Kölzsch, who taught me to look closer at the plants and birds around us, Carlos Dommar D'Lima, working in the far-out field of adaptive evolutionary dynamics, Nina Kuckländer, who proofread parts of this Thesis and is often found to count sheep, and last but not least Thilo Groß , who I admire for his knowledge and experience. I am very grateful that I was given the opportunity to work, and at times, live here with my co-workers and friends.

Particular acknowledgment is due to the head of our department Prof. Jürgen Kurths, who extended my contract for six months which is even longer than I had asked for. I am thankful for the stimulating working environment and hope to have the opportunity of cooperations in the future. I also need to acknowledge the funding of this Ph.D. Project, including salary and conference participations, by The German Volkswagen Stiftung as well as the Joint Research Project SfB555 of the DFG.

# Contents

# Chapter 1

# Introduction

The process of self-organization to global nonstationary phenomena from local interaction rules is so striking and universal that recent publications [2, 3] celebrate synchronization to be among the fundamental ordering principles of nature, along with evolution, self-organized criticality [4] or neutral theories [5]. It is in fact an aspect of Synergetics, the science of self-organization in non-equilibrium macroscopic systems consisting of many nonlinearly interacting subsystems [6, 7]. Synchronization as collective behavior also plays an important part in the field of cybernetics and in particular control theory (e.g. [8, 9]). With basic conceptual mathematical models effects of synchronization can be studied in detail and predicted qualitatively as well as quantitatively [10, 11, 12, 13, 14, 15]. Phase models in general allow for a unified treatment of a great variety of chemical [1, 16], biological [9, 17, 18, 19, 20, 21, 22] and physical [23, 24, 25, 26] spatially extended, rhythmically recurrent systems. The main interest in these works is the transition between incoherent and coherent collective behavior due to local neighborhood or global mean field interaction. Both regimes can be desirable in some applications, for instance in arrays of coupled lasers [25] or Josephson junctions [27] or undesirable, as is the case for large amplitude oscillations in ensembles of neurons in the brain [9, 20] or resonance effects in technical constructions [28].

Yoshiki Kuramoto in his monograph *Chemical Oscillations, Waves, and Turbulence* from 1985 [1] was the first to systematically derive phase equations for autonomous oscillators with a perturbation approach and averaging techniques. The Kuramoto phase equations are obtained from a reduction of limit cycle systems to the dynamics of a single parameter, the phase of the system (Chap. 2, [1]). An excellent review about the Kuramoto model, its various generalizations and phase transitions in the thermodynamical limit has recently been published by Acebrón et al. [29]. They focus on analytical results for oscillatory subsystems with all to all coupling and remark that

the solution of the Kuramoto model with short range interaction is a hopeless task except for special cases like one-dimensional models or Cayley-tree structures. The field of statistical mechanics of complex networks [30, 31, 32], dynamical systems on complex networks (e.g. [11, 33]) and ultimately the interaction and co-evolution between dynamics on the nodes of a network with the system topology [34, 35, 36, 37, 38] has spun, however, a lot of interest in exactly the problem of local short range interaction. It has been shown numerically and analytically (e.g. [39, 40, 41, 42]) that the structure of the coupling network is of importance for the ability of a system to synchronize.

A rather peculiar effect is that of pattern formation through synchronization. Synchrony in the sense of a mutual adjustment of internal frequencies or even general synchronization [2] does not necessarily mean a total reduction of the system dimension to that of a single component, i.e. completely uniform dynamics. Instead, parameters like phase can vary across the system while the phase differences remain bounded or locked in synchronization. In that case one can define waves that travel along the phase gradient. If the wavelength is smaller than the diameter of the system these waves are perceived as time periodic spatial patterns. Such waves are a prominent feature in regular low-dimensional reactor topologies of chemical oscillating reaction diffusion systems [43, 44]. Wave propagation, although experimentally more expensive to assess, is also observed in ecological and epidemiological context [45, 46, 47]. It is important to understand the mechanisms leading to pattern formation and to know the time and length scales involved in order to utilize or control these patterns [48]. The Kuramoto model is especially suited to study target patterns [1].

This thesis is a collection of details and results obtained by us during the years 2004 through 2007 on the particular subject of Kuramoto phase oscillators in complete phase locked synchronization. Pattern formation through synchronization is explored from the spatial as well as the temporal perspective. We argue the importance of symmetry and show that breaks in symmetry are actually responsible for spatio-temporal patterns and their regularity. Both, heterogeneity and the nonlinear effect of nonisochronicity break symmetries. Nonisochronicity measures the dependence of the angular velocity on the amplitude of the oscillations. Nonidentical oscillators will adapt their amplitudes and accelerate as an ensemble. On one hand, this leads to a shift of the synchronization frequency from the mean frequency of all oscillators. On the other hand it breaks the symmetry of the coupling in phase variables. An asymmetric coupling has an ordering effect on the phase profile in synchronization and can lead to the appearance of quasi-regular concentric waves in one or two dimensional systems [10].

Chapter 2 serves as a reference where we review the derivation of the Ku-

ramoto phase equations for weakly coupled, weakly anharmonic oscillators. The continuum limit of the equations is discussed in Section 2.3. It will be used as an approximation for phase oscillators in large regular cubic lattices or on the surface of a sphere in Sections 5.3 and 5.4.

Chapter 3 defines what we want to understand as the synchronized solution of the Kuramoto phase equations. We make general statements about the existence and the stability of such a solution and show that the problem of finding a solution, if the natural frequencies of the oscillators are given, amounts to the inversion of a high-dimensional nonlinear map.

Chapter 4 is mainly concerned with the spatial aspect of pattern formation. We start by studying different mechanisms for multistability in Section 4.1. Different initial conditions can lead to different phase profiles in synchronization. In particular, different topological charges, i.e. non-zero winding numbers over closed paths, are found as stable inhomogeneous synchronized states for *identical* oscillators. Heterogeneity in the natural frequencies can perturb these synchronization states but topological charges are structurally stable and can persist. In the remaining Sections 4.2-4.4 we discuss the ordering effect of an asymmetric phase coupling function on the phase profile in synchronization.

In the last Chapter (Chap. 5) we derive expressions for the shift of the synchronization frequency in response to small heterogeneity in the oscillator frequencies. We find the perturbation expansions up to the second order in the standard deviation of the natural frequencies around synchronized states of identical oscillators. For random natural frequencies the synchronization frequency is a random variable for which we calculate the expected value in regular cubic lattices with periodic boundary conditions and topological charge, for an almost homogeneous lattice on the surface of a sphere and for connected random graphs with binomial degree distribution and without topological charges (Sec. 5.3-5.5).

The appendices present details and additional information which are self-contained and can be read independently from the main text. Appendix A documents our bifurcation analysis for a chain of three nonidentical, non-isochronous oscillators in a short hand way. Appendix D presents a method which samples uniformly from all connected random networks (with labeled vertices) of a certain size. The other appendices do not present new results.

# Chapter 2

# Phase Equations

## 2.1 Derivation of the Kuramoto Phase Equations

In his monograph *Chemical Oscillations, Waves, and Turbulence* from 1985 [1] Yoshiki Kuramoto studied the properties of oscillatory dynamical systems from a very general perspective. The first half of the book is dedicated to the derivation of phase equations for extended systems, like oscillatory reaction-diffusion systems or coupled limit cycle oscillators, by means of a perturbative analysis. Since these phase equations are also the main subject of this thesis we will briefly review Kuramoto's method of phase reduction in this section.

Central to the approach of Kuramoto is the notion of a phase $\phi(\mathbf{X})$ defined for the states $\mathbf{X}$ of a dynamical system $\dot{\mathbf{X}} = \mathbf{F}(\mathbf{X})$. A limit cycle $\{\mathbf{X}^0(t), t \in \mathbb{R}\}$ is a periodic trajectory and an asymptotically stable invariant set of the dynamics with $\mathbf{X}^0(t+T) = \mathbf{X}^0(t)$. On the limit cycle the phase $\phi = \phi(\mathbf{X}^0)$ can be defined as a scalar which increases uniformly in time as $\dot{\phi} = 2\pi/T = \omega$. The difference between two phases $\phi_1$ and $\phi_2$ is the minimal arclength on the unit cycle between these phases. The equality of phases is defined as

$$\phi_1 = \phi_2 \quad \Longleftrightarrow \quad \phi_1 - \phi_2 \;=\; 0 \mod [-\pi, \pi) \tag{2.1}$$

so that $\phi + 2\pi = \phi + T\omega = \phi$ in consistence with $\phi(\mathbf{X}^0(t+T)) = \phi(\mathbf{X}^0(t))$. The definition of a phase can be extended to the basin of attraction of the periodic orbit by introducing isochrons. Isochrons are submanifolds $I_\phi$ of constant phase $\phi$ that contain $\mathbf{X}^0$ with $\phi = \phi(\mathbf{X}^0)$ and all $\mathbf{X}$ with $\lim_{t\to\infty}(\mathbf{X}(t) - \mathbf{X}^0(t)) = 0$. If $\mathbf{X}^0(t)$ and $\mathbf{X}(t)$ are on the same isochron then so are $\mathbf{X}^0(t+\tau)$ and $\mathbf{X}(t+\tau)$ for all time shifts $\tau$. In consequence $\dot{\phi}(\mathbf{X}) = \dot{\phi}(\mathbf{X}^0) = \omega$ for all $\mathbf{X}$ in the basin of attraction of the limit cycle.

We must keep in mind that this definition of phase is different from the angular argument in two dimensional oscillations which we would obtain by methods of projections and Hilbert transforms [2, 49]. It has, however, by construction the property

$$\omega = \dot{\phi}(\mathbf{X}) = \nabla^{\dagger}\phi \cdot \dot{\mathbf{X}} = \nabla^{\dagger}\phi \cdot \mathbf{F}(\mathbf{X}) \tag{2.2}$$

where $\nabla\phi$ is the phase gradient at point $\mathbf{X}$ and the multiplication is a vector product.

We are interested in systems of $N$ coupled, nonidentical oscillators. In order to find equations for the dynamics of the phases we will now closely follow the argument made by Kuramoto for a pair of oscillators [1] but in our case for a general network of coupled, nonidentical limit cycle oscillators. Let the dynamics of $N$ coupled oscillators be given as

$$\dot{\mathbf{X}}_n = \mathbf{F}_n(\mathbf{X}_n) + \sum_{m=1}^{N} A_{nm}\mathbf{V}(\mathbf{X}_m, \mathbf{X}_n) \qquad n = 1 \ldots N \tag{2.3}$$

where $\mathbf{A}$ is a matrix that describes the strength of interaction between each two oscillators in the network and $\mathbf{V}(\mathbf{X}_m, \mathbf{X}_n)$ is the functional form of interaction for two systems in the states $\mathbf{X}_n$ and $\mathbf{X}_m$. For attractive coupling, which we will consider throughout this thesis, we require $\mathbf{V}(\mathbf{X}, \mathbf{X}) = 0$. The dynamics $\mathbf{F}_n(\mathbf{X})$ may be slightly different for each oscillator $n$. The first step, in order to compare the non-identical systems, is to look at an average dynamics of period $T$ (natural frequency $\omega$) and treat heterogeneity and coupling as a perturbation. We define

$$\begin{aligned} \mathbf{F}(\mathbf{X}) &= \frac{1}{N}\sum_{n=1}^{N}\mathbf{F}_n(\mathbf{X}) \\ \mathbf{H}_n(\mathbf{X}) &= \mathbf{F}_n(\mathbf{X}) - \mathbf{F}(\mathbf{X}) \qquad \text{and} \\ \mathbf{p}_n &= \mathbf{H}_n + \sum_{m=1}^{N} A_{nm}\mathbf{V}(\mathbf{X}_m, \mathbf{X}_n) \end{aligned} \tag{2.4}$$

so that $\dot{\mathbf{X}}_n = \mathbf{F}(\mathbf{X}_n) + \mathbf{p}_n$. The phases $\phi_n$ of the oscillators with respect to the averaged dynamics yield

$$\dot{\phi}_n = \omega + \nabla^{\dagger}\phi_n \cdot \mathbf{p}_n \qquad . \tag{2.5}$$

If the perturbation is small enough and the oscillators are close to the limit cycle of the averaged dynamics then in zero$^{\text{th}}$ order of perturbation the $\mathbf{X}_n$ can be replaced by $\mathbf{X}_n^0$ where $\phi(\mathbf{X}_n) = \phi(\mathbf{X}_n^0)$. This enables us to close the equations (Eq. 2.5) with respect to the phases as

$$\dot{\phi}_n = \omega + f_n(\phi_n) + \left(\sum_{m=1}^{N} A_{nm}\ G(\phi_m, \phi_n)\right) \tag{2.6}$$

with

$$\begin{aligned} \mathbf{Z}(\phi) &= \nabla\phi(\mathbf{X}^0(\phi)) \\ f_n(\phi) &= \mathbf{Z}^\dagger(\phi)\cdot\mathbf{H}_n(\mathbf{X}^0(\phi)) \qquad \text{and} \\ G(\phi_m,\phi_n) &= \mathbf{Z}^\dagger(\phi_n)\cdot\mathbf{V}(\mathbf{X}^0(\phi_m),\mathbf{X}^0(\phi_n)) \quad . \end{aligned} \tag{2.7}$$

The vector $\mathbf{Z}(\phi)$ is called *phase response function* and is orthogonal to the tangent space of the isochron $I_\phi$ at $\mathbf{X}^0(\phi)$. This space can be analyzed from a linearization of $\mathbf{F}(\mathbf{X}^0)$ around the limit cycle using Floquet theory [1]. In general $\mathbf{Z}(\phi)$ is only experimentally accessable [16]. Moreover, for anharmonic limit cycle oscillations $f_n(\phi)$ is not constant and $G(\phi_m,\phi_n)$ is not a function of just the phase difference $\phi_m-\phi_n$. In order to obtain simpler expressions Kuramoto introduced a moving averaging approach, assuming that during a time period $T$ phase differences do not change significantly. This amounts to the assumption of weakly coupled, weakly anharmonic oscillators. We can then define

$$\dot\vartheta_n = \frac{1}{T}\int_{t-T}^{t}\dot\phi_n \tag{2.8}$$

$$\omega_n = \omega + \frac{1}{2\pi}\int_0^{2\pi} f_n(\varphi)\,d\varphi \tag{2.9}$$

$$g(\vartheta_m-\vartheta_n) = \frac{1}{2\pi}\int_0^{2\pi} G(\vartheta_m-\vartheta_n+\varphi,\varphi)\,d\varphi \tag{2.10}$$

and obtain the Kuramoto phase equations

$$\dot\vartheta_n = \omega_n + \sum_{m=1}^{N} A_{nm}\; g(\vartheta_m-\vartheta_n) \quad . \tag{2.11}$$

The quantity $\omega_n$ is the natural frequency of the unperturbed oscillator on its limit cycle. The function $g(\Delta\vartheta)$ is the (averaged) phase coupling function. Note that $g(0)$ is zero, if $\mathbf{V}(\mathbf{X},\mathbf{X})=0$. We will show in (Sec. 3.1) that the coupling is attractive if $g'(0)>0$ and repulsive if $g'(0)<0$. The phase coupling function is $2\pi$-periodic and often very well approximated by its first harmonic component as

$$g(\Delta\vartheta) \;\sim\; \sin(\Delta\vartheta+\alpha)-\sin\alpha \;\sim\; \sin\Delta\vartheta+\gamma\,(1-\cos\Delta\vartheta) \quad . \tag{2.12}$$

In fact, we will show in the next section (Sec. 2.2) that for Stuart-Landau oscillators, a normal form of the supercritical Hopf-bifurcation and thus a paradigm for weakly anharmonic limit cycle oscillators, the phase coupling function has exactly the form (Eq. 2.12). Because of the rotational symmetry of the equations the function $G(\phi_m,\phi_n)$ only depends on the phase difference $\phi_m-\phi_n$ and $f_n(\phi_n)=\omega_n$ is independent of $\phi_n$. An averaging (Eqs. 2.8-2.10) is not necessary. The parameter $\gamma$, which breaks the symmetry of the phase

coupling function has a direct physical interpretation. We will see in the next sections that it measures the change of the angular velocity in the vicinity of the limit cycle. It is called the nonisochronicity of the oscillator.

The Kuramoto phase equations we are studying throughout this thesis are thus

$$\dot{\vartheta}_n = \omega_n + \sum_{m=1}^{N} A_{nm} \left( sin(\vartheta_m - \vartheta_n) + \gamma \left(1 - \cos(\vartheta_m - \vartheta_n)\right)\right) \tag{2.13}$$

for all $n = 1 \ldots N$.

## 2.2 Phase Coupling Function for Stuart Landau Oscillators

For the Kuramoto phase reduction method described in Chapter 2 an expression for the phase gradient $\mathbf{Z}(\phi)$ orthogonal to the isochrons of a limit cycle is required. This is in general not analytically feasible. However, for two dimensional systems with rotational symmetry a general expression can be found [50].

Suppose in cylindrical coordinates with local base $\mathbf{e}_r$ and $\mathbf{e}_\theta$ we have $\mathbf{X} = r\mathbf{e}_r(\theta)$, $\dot{\theta} = f(r)$ and $\dot{r} = g(r)$. A point on the isochron $I_\phi$ with distance $r$ from the origin may be found at an angle

$$\theta = \phi + h(r) \tag{2.14}$$

Differentiating this equation with respect to time we find

$$f(r) = \dot{\phi} + g(r)h'(r) \tag{2.15}$$

The phase velocity $\dot{\phi}$ is constant within the basin of attraction since all points on an isochron remain on that isochron. The phase gradient $\nabla\phi$ is found from (Eqs. 2.14, 2.15) as

$$\nabla\phi \;=\; \frac{1}{r}\,\mathbf{e}_\theta - h'(r)\mathbf{e}_r \;=\; \frac{1}{r}\,\mathbf{e}_\theta - \frac{f(r) - \dot{\phi}}{g(r)}\mathbf{e}_r \tag{2.16}$$

A Stuart-Landau oscillator is a system in the complex plane with the dynamics

$$\dot{z} = (1 - i\alpha)z + (1 - i\gamma)|z|^2 z \qquad . \tag{2.17}$$

The scale has been chosen so that the limit cycle is on the unit circle. In polar coordinates we have

$$\dot{\theta} = f(r) = \alpha - r^2\gamma \qquad \dot{r} = g(r) = (1 - r^2)r \qquad \dot{\phi} = \omega = \alpha - \gamma \qquad . \tag{2.18}$$

Here the role of the parameter $\gamma$ in the nonlinear term of (Eq. 2.17) becomes apparent. For positive values $\gamma > 0$ the angular velocity $\dot{\theta}$ decreases as the radius $r$ increases. The phase gradient with respect to the isochrons on the unit circle follows with (Eq 2.16) in the limit $r \to 1$ as

$$\mathbf{Z}(\phi) = \mathbf{e}_\phi - \gamma \mathbf{e}_r \qquad . \tag{2.19}$$

In the case of linearly coupled, nonidentical Stuart-Landau oscillators

$$\dot{z}_n = (1 + i\alpha_n) z_n - (1 + i\gamma_n)|z_n|^2 z_n + \sum_{m=1}^{N} A_{nm}(z_m - z_n) \qquad , \tag{2.20}$$

we find for the perturbation terms (Eqs. 2.4,2.7)

$$\begin{aligned} \mathbf{H}_n &= ((\alpha_n - \alpha) - (\gamma_n - \gamma))\, \mathbf{e}_{\phi_n} \\ \mathbf{V}(\phi_m, \phi_n) &= \mathbf{e}_{\phi_m} - \mathbf{e}_{\phi_n} \\ \omega_n &= \alpha - \gamma + f_n(\phi) \;=\; \alpha_n - \gamma_n \\ G(\phi_m, \phi_n) &= \sin(\phi_m - \phi_n) + \gamma\,(1 - \cos(\phi_m - \phi_n)) \end{aligned} \tag{2.21}$$

where $\alpha$ and $\gamma$ are the ensemble averages of $\alpha_n$ and $\gamma_n$.

## 2.3 Continuum limit

Kuramoto points out that equation (Eq. 2.5) remains valid if a continuum of oscillators with phases $\phi(\mathbf{r})$ at positions $\mathbf{r} \in \mathbb{R}^d$ is considered and the perturbation $\mathbf{p}(\mathbf{r}) = \mathbf{H}(\mathbf{X}, \mathbf{r}) + \nabla^2 \mathbf{D}\mathbf{X}(\mathbf{r})$ is due to heterogeneity and diffusion. For normal diffusion $\mathbf{D}$ is diagonal and $\nabla^2$ is to be applied component wise. In this thesis we will only discuss homogeneous, continuous media with integer dimension $d$ for which the Laplacian is known. After the averaging (Eq. 2.8), the Kuramoto phase equations take the form of a nonlinear phase diffusion equation

$$\dot{\vartheta} = \omega(\mathbf{r}) + \alpha \nabla^2 \vartheta + \beta (\nabla \vartheta)^2 \tag{2.22}$$

with

$$\begin{aligned} \omega(\mathbf{r}) &= \omega + \frac{1}{2\pi} \int_0^{2\pi} \mathbf{Z}^\dagger(\varphi) \cdot \mathbf{H}(\mathbf{X}^0(\varphi), \mathbf{r})\; d\varphi \\ \alpha &= \frac{1}{2\pi} \int_0^{2\pi} \mathbf{Z}^\dagger(\varphi) \cdot \mathbf{D} \frac{d\mathbf{X}^0(\varphi)}{d\varphi}\; d\varphi \\ \beta &= \frac{1}{2\pi} \int_0^{2\pi} \mathbf{Z}^\dagger(\varphi) \cdot \mathbf{D} \frac{d^2\mathbf{X}^0(\varphi)}{d\varphi^2}\; d\varphi \qquad . \end{aligned} \tag{2.23}$$

Our aim here is to derive continuous equations which approximate a regular lattice of phase oscillators with nearest neighbor interaction and vice versa.

Let $\{\mathbf{r}_n\}$ be a grid of $N$ discrete points on a differential manifold. We will specifically consider a rectangular patch in $\mathbb{R}^d$ with open or periodic boundary conditions and the sphere $S^3$. The phases of these oscillators are $\vartheta_n = \vartheta(\mathbf{r}_n)$ and their frequencies $\omega_n = \omega(\mathbf{r}_n)$. The fields $\vartheta(\mathbf{r})$ and $\omega(\mathbf{r})$ shall be continuations of the respective values at the grid points $\mathbf{r}_n$ so that $\vartheta(\mathbf{r})$ is smooth. The discrete Kuramoto phase equations for this grid-network of phase oscillators are

$$\dot{\vartheta}(\mathbf{r}_n) = \omega(\mathbf{r}_n) + \sum_m A_{nm} g(\vartheta(\mathbf{r}_m) - \vartheta(\mathbf{r}_n)) \qquad . \tag{2.24}$$

We want to assume a local nearest neighbor coupling, i.e. for $A_{mn} \neq 0$ the difference vectors $\mathbf{h}_{mn} = \mathbf{r}_m - \mathbf{r}_n$ are small. We can then approximate the manifold locally with its tangent space and $\mathbf{h}_{mn}$ becomes the directional derivative $\mathbf{h}_{mn} = \sum_i h^i_{mn} \partial_i$ where $\partial_i$ is a local orthonormal base of the tangent space [51]. Next we expand the equations (Eq. 2.24) to the order $O(h^2)$ at each grid point. For that we first expand the phase as

$$\vartheta(\mathbf{r}_n + \mathbf{h}_{mn}) \approx \vartheta(\mathbf{r}_n) + \mathbf{h}_{mn}\vartheta(\mathbf{r}_n) + \frac{1}{2}\mathbf{h}_{mn}\mathbf{h}_{mn}\vartheta(\mathbf{r}_n) \tag{2.25}$$

Now the phase coupling function $g(\vartheta_m - \vartheta_n)$ in (Eq. 2.24) can be expanded keeping only terms of order $O(h^2)$ as

$$\dot{\vartheta}(\mathbf{r}_n) \approx \omega(\mathbf{r}_n) + \sum_m A_{nm} \left[ g'(0) \left( \mathbf{h}_{mn}\vartheta(\mathbf{r}_n) + \frac{1}{2}\mathbf{h}_{mn}\mathbf{h}_{mn}\vartheta(\mathbf{r}_n) \right) + \frac{1}{2} g''(0) \left( \mathbf{h}_{mn}\vartheta(\mathbf{r}_n) \right)^2 \right] \tag{2.26}$$

In order to obtain an equation of the form (Eq. 2.22) we have to impose the conditions

$$\begin{aligned} \sum_m A_{nm}\mathbf{h}_{mn} &= 0 \\ \sum_m A_{nm} h^i_{mn} h^j_{mn} &= \mu^2 \delta^{ij} \qquad . \end{aligned} \tag{2.27}$$

The first condition in (Eq. 2.27) means that each grid point should be in the center of weight of its neighbor points. The second condition can be relaxed to requiring that the matrix $\mu^{-2} \sum_m A_{nm}\mathbf{h}_{mn}\mathbf{h}^\dagger_{mn}$ is special orthogonal for some value $\mu^2$ and can be brought to yield (Eq. 2.27) after an appropriate rotation. We then obtain the continuous equations

$$\dot{\vartheta} \;=\; \omega \;+\; \frac{1}{2}\mu^2 \left[ g'(0) \nabla^2 \vartheta \;+\; g''(0) \left( \nabla \vartheta \right)^2 \right] \tag{2.28}$$

or after a scaling $\tau = \frac{1}{2}\mu^2 t$ of time

$$\frac{d\vartheta}{d\tau} = \frac{2}{\mu^2}\omega + g'(0)\nabla^2\vartheta \;+\; g''(0)\left(\nabla\vartheta\right)^2 \qquad . \tag{2.29}$$

The error introduced by a continuous approximation (Eq. 2.28) is due to the change into tangent space proportional to the curvature of the medium times the distance of the oscillators squared. If the medium is flat the error scales with the oscillator distance to the power of three $O(h^3)$.

We can take the continuous limit of (Eq. 2.24) by refining the grid and choosing the coupling strengths $A_{mn}$ so that $\mu^2/2$ is kept constant. The value $\mu^2/2$ can also be kept constant by changing the length scale and keeping the ratio between number of oscillators and the volume of the differential manifold constant. We use this in Section 5.3 and 5.4 to find the expected synchronization frequency in large grids of phase oscillators.

# Chapter 3

# Existence and Stability of Synchronization

## 3.1 Complete phase synchronization of Kuramoto phase oscillators

The Kuramoto phase equations for coupled oscillators with phases $\vartheta_n$ on a network of size $N$ are

$$\dot{\vartheta}_n = \omega_n + \sum_{m=1}^{N} A_{nm}\ g(\vartheta_m - \vartheta_n) \qquad n = 1 \ldots N \tag{3.1}$$

where $\omega_n$ is the natural frequency of the $n^{\text{th}}$ oscillator. The coupling strength between two oscillators $n$ and $m$ is given by the value $A_{nm}$ of an interaction matrix. By an appropriate scaling of time the strongest interaction in the network can be set to unity. If all couplings are either identical and positive or zero, then $A_{nm}$ becomes the adjacency matrix of the network with entries $A_{nm} = 1$ if two oscillators are coupled and zero otherwise. For attractively coupled oscillators the coupling function $g(\Delta\vartheta)$ has to be zero for identical phases $g(0) = 0$ and must have a positive first derivative $g'(0) = 0$. The heterogeneity in the system can be quantified by the sample variance $\sigma^2 = \mathrm{var}(\omega)$ of the natural frequencies.

We will recite the general Kuramoto phase equations (Eq. 3.1) at various points throughout the text. As an example we will also repeatedly look at a

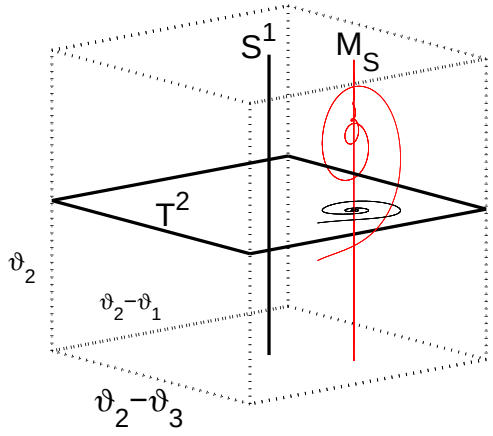


Figure 3.1: The phase space for a chain of three coupled phase oscillators is a 3-torus $T^3 = S^1 \times T^2$, here illustrated as a cube with periodic boundary conditions. Shown is a trajectory (red) of system (Eq. 3.2) with $\gamma = 4$, $\omega_1 - \omega_3 = 0$ and $\omega_1 - \omega_2 = 3$. After a transient the oscillators reach phase synchronization on a synchronization manifold $M_S$ corresponding to a stable focus in the space of relative phases $T^2$ (black projection of red trajectory on $T^2$).

chain of three phase oscillators

$$\begin{aligned} \dot{\vartheta}_1 &= \omega_1 + g(\vartheta_2 - \vartheta_1) \\ \dot{\vartheta}_2 &= \omega_2 + g(\vartheta_1 - \vartheta_2) + g(\vartheta_3 - \vartheta_2) \\ \dot{\vartheta}_3 &= \omega_3 + g(\vartheta_2 - \vartheta_3) \\ g(\Delta\vartheta) &= \sin\Delta\vartheta + \gamma\,(1 - \cos\Delta\vartheta) \qquad . \end{aligned} \tag{3.2}$$

Here the first and the third oscillator are only indirectly coupled through the second oscillator.

The state space of the system is an $N$-torus $T^N$ so that the shift of any phase by $2\pi$ maps that phase identically onto itself. The coupling function $g(\Delta\vartheta)$ must therefore be $2\pi$-periodic and since only the phase differences enter the equations they are invariant to arbitrary global shifts of phase $\vartheta_n \to \vartheta_n + C$ for all $n$. This important symmetry separates the state space $T^N = S^1 \times T^{N-1}$ at each point into a circle $S^1$ corresponding to a global shift of phases and an $(N-1)$ torus $T^{N-1}$ of phase differences orthogonal to it (Fig. 3.1).

This work is concerned with the problem of synchronization which can be

formulated in different ways, either statistically in a weak sense or absolutely on the level of the dynamics. The heterogeneity $\sigma^2$ plays the role of a bifurcation parameter. Partial synchronization is a phase transition of the absolute value of the order parameter $R = \frac{1}{N}\sum_{n=1}^{N} e^{i\vartheta_n}$, a macroscopic observable in a many-oscillator system, from near zero ($O(N^{-\frac{1}{2}})$) above a critical frequency disorder to increasing values below. This phase transition is commonly meant when the transition to synchronization is discussed [1, 11]. A nonzero order parameter $R$ is associated with the formation of synchronized clusters and in particular a dominant cluster of oscillators which rotate unisonous for long periods of time. The phases between the oscillators do not need to be locked [12]. We are interested, however, in the problem of full phase synchronization. In complete phase synchronization all phase velocities are equal

$$\dot{\vartheta}_n = \Omega \tag{3.3}$$

and the relative phases $\vartheta_n - \vartheta_m$ are stationary. Synchronization therefore corresponds to a fixed point of the phase dynamics in $T^{N-1}$ and a synchronization manifold $M_S$ orthogonal to it (Fig. 3.1). According to their stability these fixed points can be classified as stable or unstable nodes or focuses and saddles. By varying the natural frequencies $\omega_n$ of the oscillators these fixed points can undergo bifurcations of various co-dimensions, in particular, a saddle node bifurcation at a critical heterogeneity where a stable synchronization manifold is created or destroyed.

Combining equations (Eqs. 3.1 and 3.3) we obtain

$$\Omega = \omega_n + \sum_{m=1}^{N} A_{nm}\ g_{mn} \qquad n = 1 \ldots N \tag{3.4}$$

with $g_{mn} = g(\vartheta_m - \vartheta_n)$. The stability of the synchronization manifold follows from the eigenvalues of a linearization of the phase dynamics around $M_S$. If $\varphi_n = \vartheta_n - \vartheta_n^0$ is a small displacement of the phases $\vartheta_n$ from a point $\vartheta^0$ on $M_S$, then with (Eqs. 3.1 and 3.4) follows

$$\dot{\varphi}_n \ \approx\ \sum_{m=1}^{N} A_{nm} g'_{mn} \cdot (\varphi_m - \varphi_n) \ =\ \sum_{m=1}^{N} L_{nm}\ \varphi_m \tag{3.5}$$

with the first derivatives $g'_{mn} = g'(\vartheta_m^0 - \vartheta_n^0)$. The Jacobian $\mathbf{L}$ on the right hand side is, in fact, the Laplacian of a weighted graph with weights $A_{nm}g'_{mn}$ across the edges $l = (n, m)$.

$$\mathbf{L} : T^{N-1} \to \mathbb{R}^{N\times N} \quad \text{with} \quad L_{nm} = A_{nm}g'_{mn} - \delta_{nm}\sum_{l=1}^{N} A_{nl}g'_{nl} \qquad . \tag{3.6}$$

The definitions for the Laplacian of a graph found in the literature [52] can differ in sign and scaling factor. Since we will look at the continuous limit we use in (Eq. 3.6) the definition for which $\mathbf{L}$ becomes the Laplacian differential operator on a regular square lattice in that limit.

The sums $\sum_m L_{nm}$ over the rows of the Laplacian $\mathbf{L}$ defined in (Eq. 3.6) are identically equal to zero. Therefore, $\mathbf{L}$ has at least one eigenvalue equal to zero corresponding to neutral stability in the direction of the synchronization manifold $M_S$ (global phase shift). If the weights $A_{nm}g'_{mn}$ are non-negative, the Laplacian has eigenvalues $E_k$ with non-positive real parts. This follows from Gershgorin's Circle Theorem [53], which states that each eigenvalue $E_k$ of a square matrix $\mathbf{L}$ lies in at least one of the circles in the complex plane of radii $R_n = \sum_{m\neq n} |L_{nm}| = \sum_{m\neq n} |A_{nm}g'_{mn}|$ around the diagonal elements $L_{nn} = -\sum_{m\neq n} A_{nm}g'_{mn}$. If all weights are non-negative then the discs in the complex plane touch the imaginary axis at zero because $L_{nn} = -R_n$. If the eigenvalue $E_0 = 0$ is not degenerate, then all other eigenvalues $E_n$ must have negative real parts and the synchronization manifold where $\varphi \parallel \mathbf{1}$ is asymptotically stable.

The linear stability analysis (Eq. 3.5) shows, that the Jacobian of the phase dynamics and thus the stability of a synchronization manifold does not directly depend on the frequencies $\omega_n$. Therefore the areas $S \subset T^{N-1}$ in phase space where asymptotically stable synchronization manifolds are possible are directly determined by the coupling network $\mathbf{A}$ and the coupling function $g(\Delta\vartheta)$.

The eigenvalues $E_k$ and the left, as well as the right eigenvectors $\mathbf{P}_k$ and $\mathbf{p}_k$ of $\mathbf{L}$ are defined by

$$\mathbf{L}\mathbf{p}_k = E_k\mathbf{p}_k \tag{3.7}$$

$$\mathbf{L}^\dagger\mathbf{P}_k = E_k^*\mathbf{P}_k \tag{3.8}$$

$$\mathbf{P}_k^\dagger \cdot \mathbf{p}_m = \delta_{km} \qquad \sum_k \mathbf{p}_k\mathbf{P}_k^\dagger = \mathbb{I} \tag{3.9}$$

$$\mathbf{p}_0 \sim \mathbf{1} \qquad \mathbf{L}\mathbf{p}_0 = 0 \quad . \tag{3.10}$$

The eigenvectors and eigenvalues are functions of $T^{N-1}$. The eigenvectors can be made orthonormal and to fulfill the completness relation (Eq. 3.9) with the identity matrix $\mathbb{I}$. The uniform right eigenvector $\mathbf{p}_0$ has the eigenvalue $E_0 = 0$ (Eq. 3.10). We can define the region of stability $S$ as

$$S \subset T^{N-1}: \quad \max_n \ \mathrm{Re}E_n(S) = 0 \quad . \tag{3.11}$$

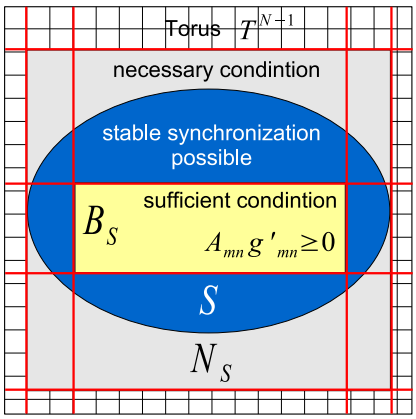


Figure 3.2: Venn diagram for necessary and sufficient conditions of stability. If a set of relative phases $\Delta\vartheta \in T^{N-1}$ is a solution to the Kuramoto phase equations in synchronization (Eq. 3.4) then its stability is completely determined. The Jacobian of the phase dynamics around the synchronization manifold has eigenvalues with non-positive real parts in the area $S$ (blue ellipse). In the yellow box $B_S$ all off-diagonal elements of the Jacobian are larger or equal to zero from which follows with Gershgorin's circle theorem that all eigenvalues have non-positive real parts. Outside the gray box $N_S$, on the other hand, all eigenvalues must have positive real parts. The red lines indicate submanifolds where $g_{mn}$ is zero across some edge $(n, m)$. These submanifolds form the borders of $B_S$ and $N_S$ as defined in (Eqs. 3.12, 3.13) and may be easier to check conditions than $\Delta\vartheta \in S$.

The set $S$ (Fig. 3.2) is that subset of $T^{N-1}$ where all eigenvalues of the Laplacian have non-positive real parts. All synchronization manifolds $M_S$ that intersect with $T^{N-1}$ within int$(S)$ are asymptotically stable. Using Gershgorin's theorem we can also formulate necessary and sufficient regions for stability $B_S$ and $N_S$

$$B_S \subset T^{N-1}: \quad \min_{n,m} A_{nm} g'_{mn}(B_S) = 0 \tag{3.12}$$

$$N_S \subset T^{N-1}: \quad \max_{n,m} A_{nm} g'_{mn}(N_S) > 0 \quad . \tag{3.13}$$

We have seen that $A_{nm}g'_{mn} \geq 0$ for all $n, m$ is a sufficient condition for synchronization. Similarly one can show that from $A_{nm}g'_{mn} \leq 0$ for all $n, m$ follows that the synchronization manifold is not asymptotically stable. The condition $A_{nm}g'_{mn} > 0$ *for at least some* $n, m$ is hence necessary for synchronization. The sets $B_S$ and $N_S$ (Eq. 3.12, 3.13) give easy to check conditions $B_S \subseteq S \subseteq N_S$ for synchronization (Fig. 3.2). They consist, in fact, of boxes defined by the roots of $g'(\Delta\vartheta)$. We have illustrated the different regions in $T^{N-1}$ schematically in figure (Fig. 3.2).

Figures (Figs. 3.3a,c and 3.4a,c) show the space $T^2$ of relative phases for

the system of three oscillators and different coupling schemes. The area $S$ has been determined numerically while $B_S$ and $N_S$ are confined between the straight lines obtained as solutions of $A_{nm}g'_{mn} = 0$.

## 3.2 The image of the phase space in the parameter space

We ask now for which frequencies $\omega_n$ complete phase synchronization exists, what the corresponding phase profiles look like and whether they are stable. This question is addressed by various approximations for the coupling function [10, 54], trough perturbation theory for small frequency disorder (Chap. 5) or directly for special coupling networks as will be discussed in Sections 4.2 and 4.3. Due to the nonlinearity and noninvertability of the coupling function $g(\Delta\vartheta)$ it is not trivial to find phases $\vartheta_n$ that yield (Eq. 3.4). The frequencies, on the other hand, enter equation (Eq. 3.4) linearly. So for a given set of phases $\vartheta_n$ the relative frequencies $\omega_n - \omega_m$ that make these phases a point on a synchronization manifold $M_S$ are uniquely determined as

$$\omega_n - \omega_m = \sum_k (A_{mk}\ g_{km} - A_{nk}\ g_{kn}) \tag{3.14}$$

The equations (Eq. 3.14) define a map $\Delta\omega(\Delta\vartheta)$ from relative phases $\Delta\vartheta \in T^{N-1}$ to relative frequencies $\Delta\omega \in \mathbb{R}^{N-1}$ (Figs. 3.3-3.5). If the coupling function $g(\Delta\vartheta)$ is continuous then $\Delta\omega(\Delta\vartheta)$ is continuous. In consequence, the parameter range $\Delta\omega(T^{N-1})$ where synchronization manifolds exist at all is compact. It is bounded by a box $B_\omega$, given by the minimum $g_{\min}$ and the maximum $g_{\max}$ of $g(\Delta\vartheta)$ as

$$\begin{aligned} \min(\omega_n - \omega_m) &= \sum_k (A_{mk}\ g_{\min} - A_{nk}\ g_{\max}) \\ \max(\omega_n - \omega_m) &= \sum_k (A_{mk}\ g_{\max} - A_{nk}\ g_{\min}) \quad . \end{aligned} \tag{3.15}$$

While equation (Eq. 3.15) can be used to quickly check the necessary condition $\Delta\omega \in B_\omega$ for synchronization to be possible it does not guarantee synchronization. Especially for large systems $N \gg 1$ the area $B_\omega$ in parameter space is much larger than $\Delta\omega(T^{N-1})$. The following set relations define sufficient and necessary conditions for the relative frequencies $\Delta\omega(S)$ for which stable synchronization is possible

$$\Delta\omega(B_S) \subseteq \Delta\omega(S) \subseteq \Delta\omega(N_S) \subseteq \Delta\omega(T^{N-1}) \subseteq B_\omega \tag{3.16}$$

The mapping from phase space to parameter space is illustrated in Fig. 3.3 and Fig. 3.4 at the example of three oscillators and different coupling schemes.

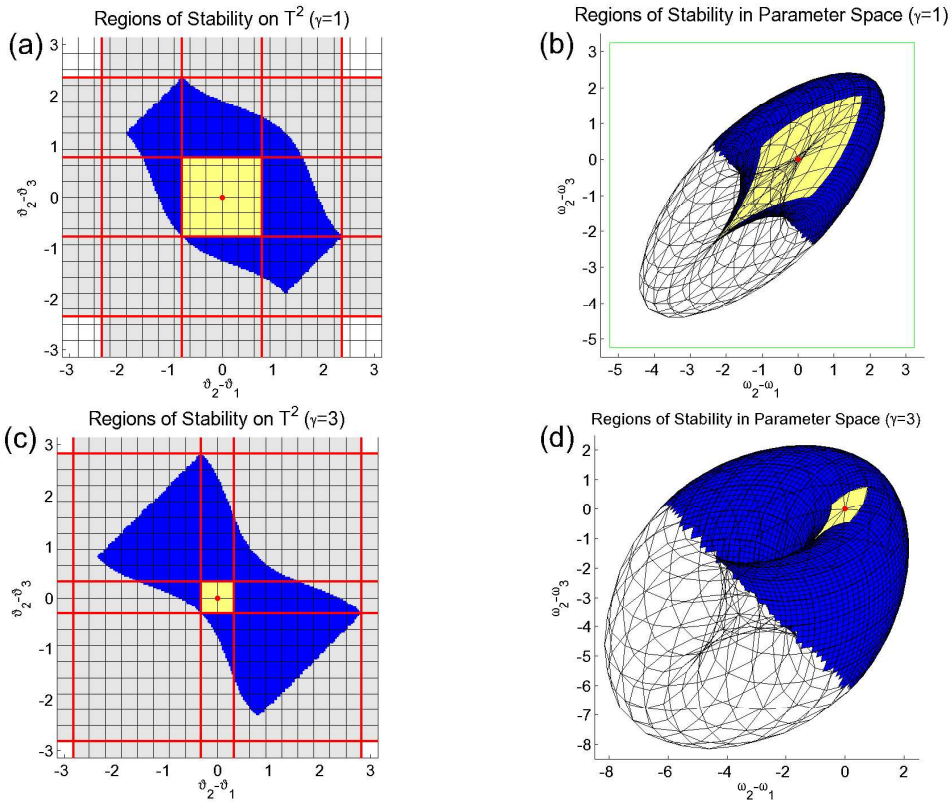


Figure 3.3: Phase space $T^2$ (Fig.(a,c)) and parameter space (Fig.(b,d)) for a chain (Eq. 4.12, $g(\Delta\vartheta) = \sin\Delta\vartheta + \gamma(1 - \cos\Delta\vartheta)$) of three phase oscillators. The region $B_S$ where the Laplacian (Eq. 3.6) has non-negative off-diagonal elements (yellow area) is bounded by the lines where the first derivative of the coupling function across a link is zero (red lines Fig.(a,c)). The same lines also separate the region $N_S$ (gray area Fig.(a,c)), where at least one off diagonal element is zero, from the regions where the Laplacian is guaranteed to have no negative eigenvalue real parts (white area Fig.(a,c)). The region $S$ of stable synchronization manifolds (blue area) contains $B_S$. The non-isochronicity for subfigures (a,b) is $\gamma = 1$ and for subfigures (c,d) we have used $\gamma = 3$. Subfigures (b,d) show the image $\Delta\omega$ of $T^2$ in the parameter space. Following the mesh lines one can see the region where the Torus is folded in a cusp bifurcation. The green box in subfigure (b) is the area $B_\omega$ defined by the maximum and the minimum of the coupling function (Eq. 3.15). The corresponding box for subfigure (d) is omitted because it is too large. The red circle at the origin marks the homogeneous system of identical oscillators.

For a homogeneous system with $\omega_n = \omega_m$ for all $n$ and $m$ the trivial synchronization manifold where $\vartheta_n^0 - \vartheta_m^0 = 0$ always exists and is stable because a Laplacian matrix with non-negative off-diagonal elements $A_{nm}g'(0)$ is negative-semidefinite.

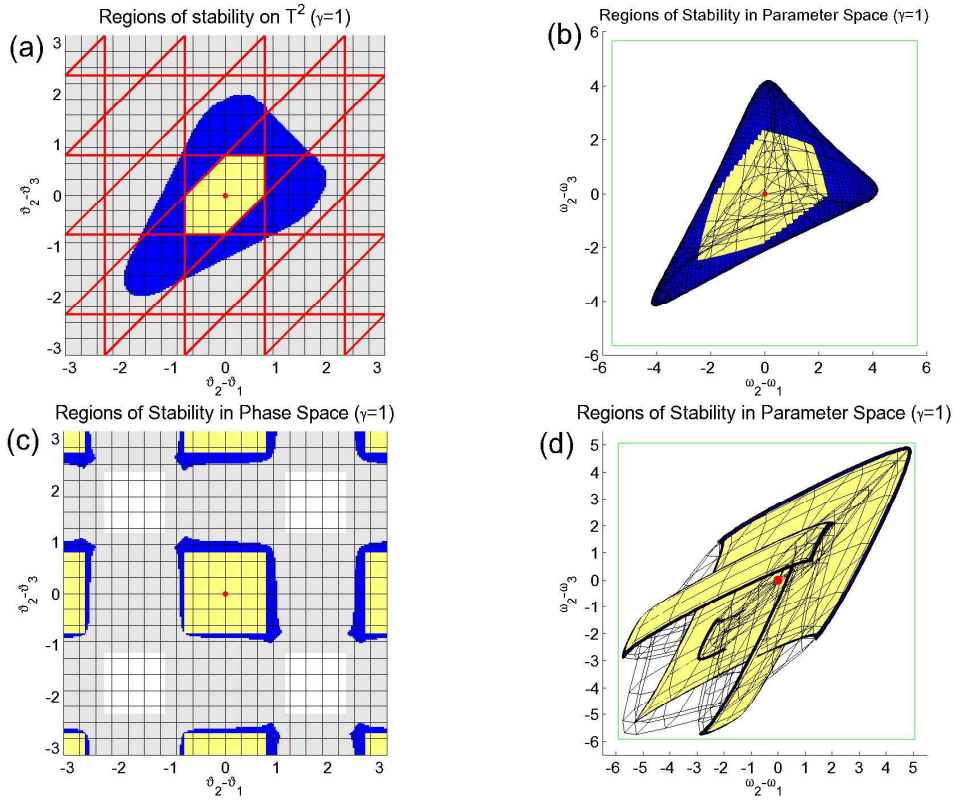


Figure 3.4: Phase space $T^2$ (a,c) and parameter space (b,d) for three coupled phase oscillators. The coupling scheme for Fig.(a,b) is all to all and $g(\Delta\vartheta) = \sin\Delta\vartheta + (1 - \cos\Delta\vartheta)$ while Fig.(c,d) shows the results for a chain of three oscillators (Eq. 3.2) and a coupling function $g(\Delta\vartheta) = \sin\Delta\vartheta + (1 - \cos\Delta\vartheta) + \sin 2\Delta\vartheta$ with a pronounced second harmonic. The region $B_S$ where the Laplacian (Eq. 3.6) has non-negative off-diagonal elements (yellow area) is bounded by the lines where the first derivative of the coupling function across a link is zero (red lines Fig.(a)). These lines also separate the region $N_S$ (gray area Fig.(a,c)), where at least one off diagonal element is positive, from the regions where the Laplacian is guaranteed to have no negative eigenvalue real parts (white area (c)). The red lines were omitted in Fig.(c). The region $S$ of stable synchronization manifolds (blue area) contains $B_S$. Subfigures (b,d) show the image $\Delta\omega$ of $T^2$ in the parameter space. The green box in Fig.(b,d) is the area $B_\omega$ defined by the maximum and the minimum of the coupling function (Eq. 3.15). The red circle at the origin marks the homogeneous system of identical oscillators. In comparison with (Fig. 3.3) we see how a change in the coupling function or the coupling network can fundamentally effect the topology of the phase space.

The effect of nonisochronicity or loops in a network of coupled oscillators makes a closed analytical solution for the stationary phase profile of the Kuramoto phase equations in synchronization (Eq. 3.4) a highly nonlinear problem and in general impossible. The inverse problem, however, given a set of phases

(a) 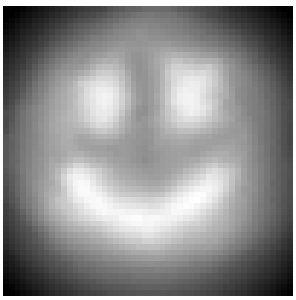 (b) 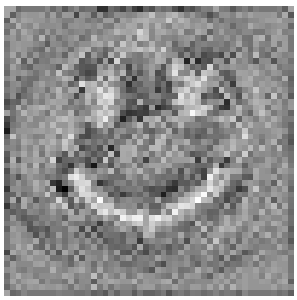 (c) 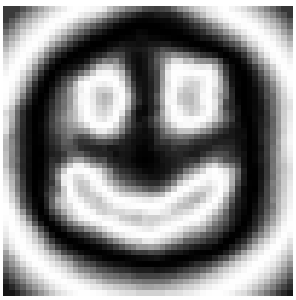

Figure 3.5: Estimation of local natural frequencies from observed phase profile or design of a wave pattern by control of frequencies. We created a template for the phases in the synchronized state (a) for a regular lattice of $50 \times 50$ oscillators with nearest neighbor coupling and open boundary conditions, with phases ascending from black ($\vartheta = 0$) to white ($\vartheta = 10$). With a nonisochronicity $\gamma = 1$ the frequencies that according to (Eq. 3.14) lead to this stationary phase profile were calculated. Here shown in subfigure (b) are the frequencies in gray levels, from low frequencies in dark to high frequencies (white). Finally we integrated the Kuramoto phase equations for this system with homogeneous initial conditions $\vartheta_n = 0$. Synchronization was achieved and the sine of the phases (subfig. c, gray level) follows the prescribed phase gradient closely.

to check whether these phases are on an asymptotically stable synchronization manifold and to estimate the frequencies of the oscillators that make these phases a stationary phase profile, is surprisingly simple (Eqs. 3.5, 3.14, 3.15), with possible applications for the control of synchronization patterns and parameter estimation (Fig. 3.5).

# Chapter 4

# Synchronized Solutions and Approximations

Given a set of natural frequencies $\omega_n$ and the coupling structure $A_{nm}$ of a network of Kuramoto phase oscillators we are interested in the spatial pattern that emerges if and when the oscillators synchronize and eventually yield

$$\Omega = \omega_n + \sum_{m=1}^{N} A_{nm}\ g(\vartheta_m - \vartheta_n) \quad . \tag{4.1}$$

In order to obtain the relative phases $\vartheta_m - \vartheta_n$ we need to invert the function $\Delta\omega(\Delta\vartheta)$. We have seen in the previous chapter that this problem has no unique solution and that the folding of the space of relative phases $\Delta\vartheta \in T^{N-1}$ into the space of relative frequencies $\Delta\omega \in \mathbb{R}^{N-1}$ is not trivial and depends intricately on the coupling structure. In [54] we discuss a perturbation approach to this problem. The results of this work can be found in Chapter 5. In this following chapter, we look for special solvable cases and approximate solutions.

A first step to find the phase differences in synchronization would be to find the values $g_{mn} = g(\vartheta_m - \vartheta_n)$ of the coupling function in equation (Eq. 4.1). The equations seem to be linear in the values of the coupling function across the edges. While this is true, there are usually much more edges in a graph than nodes and in general for each edge two values $g_{nm} \neq g_{mn}$ of the coupling function are needed. The values $g_{mn}$ are under-determined by the equations (Eq. 4.1) and have to be complemented by nonlinear equations. With a coupling function of the form $g(\Delta\vartheta) = \sin\Delta\vartheta + \gamma(1 - \cos\Delta\vartheta)$, for instance, for the harmonics

$s_{mn} = \sin(\vartheta_m - \vartheta_n)$ and $c_{mn} = \cos(\vartheta_m - \vartheta_n)$ one has to solve the equations

$$\Omega = \omega_n + \sum_m A_{nm} \left( s_{mn} + \gamma(1 - c_{mn}) \right) \quad \text{for all} \quad n = 1 \ldots N \tag{4.2}$$

$$s_{mn} = -s_{nm} \qquad c_{mn} = c_{nm} \qquad s_{mn}^2 + \quad c_{mn}^2 = 1 \quad (\text{for} \quad A_{mn} \neq 0) \tag{4.3}$$

$$\sin \left( \sum_{l=(n,m)} (\vartheta_m - \vartheta_n) \right) = \operatorname{Im} \prod_{l=(n,m)} (c_{mn} + i s_{mn}) \quad = \quad 0 \tag{4.4}$$

where the sum inside the sine function in equation (Eq. 4.4) is telescopic along the edges $l = (n, m)$ of some directed circle $(n_1, n_2, \ldots, n_L, n_1)$. Equation (Eq. 4.4) reflects the periodic boundary conditions for closed paths in the network. The phase differences are defined as the shortest arclength $\vartheta_m - \vartheta_n \in [-\pi, \pi)$ on the unit circle between two phases. In a network with $N$ vertices and $E$ undirected edges ($A_{mn} = A_{nm}$) there are $4E + 1$ unknowns $\Omega, s_{mn}$ and $c_{mn}$. If the network is connected, there are also $E - N + 1$ independent circles which form a base of the circle space of the network [55]. The number of equations $N$ (4.2) + $3E$ (4.3) + $(E - N + 1)$ (4.4) $= 4E + 1$ is sufficient to determine the unknown values, even though the equations (Eqs. 4.3, 4.4) are nonlinear of second and higher order and in general no closed analytical solution exists.

This is not the case, however, if the coupling function is odd or even $g_{mn} = \pm g_{nm}$ and the network is a tree network, that is, a connected graph without circles. In Section 4.2 we will solve the equations (Eq. 4.1) for the value $g(\vartheta_m - \vartheta_n)$ of an odd coupling function across an edge that separates the network into two subnetworks. A similar approach for coupling functions with even symmetry is more involved. In that case the Kuramoto phase equations are conservative, i.e. **div** $\dot{\vartheta} = 0$ (see e.g. [56]) and no stable synchronization manifold can exist.

## 4.1 Multistability

Coexistence of two or more attractors of a dynamical system is called multistability. Multistabile systems are of interest for applications of information storrage and processing [57]. Any bistable system is capable of storing one bit of information. Flip-flops, for instance, are bistable electronic circuits which have been common in microprocessors since the beginning. Arrays of Flip-flops are used as memory elements. The basins of attraction for different attractors in the state space of a system may have different sizes and shapes. They may be fractal so that the attractor a system ends up on depends very sensitively on the initial conditions in some areas of the state space. An important question

is the control of multistable systems, e.g. how they can be perturbed to switch from one attractor to another. The role of noise for this switching has spurred the whole field of stochastic resonance [58, 59].

Coexisting stable synchronization manifolds can be found in the Kuramoto model (Eq. 3.1,4.1) in the presence of higher harmonics in the coupling function $g(\Delta\vartheta)$. Besides the homogeneous solution, with zero phase differences between identical oscillators, different cluster states can be stabilized [16]. By changing the coupling strength between the oscillators one can change the basins of attraction. Phase oscillators with a coupling function with higher harmonics can, for instance, be used for the construction of adaptive neural networks [60].

A different source of multistability are periodic boundary conditions for phase variables. We will briefly discuss the twisted wave states that arise in the presence of closed circles in a network of phase oscillators in the next Section (Sec. 4.1.1). In our perturbation approach (Chap. 5) we also expand explicitely around such inhomogeneous synchronization states which makes the analysis somewhat more complicated. There are still open questions concerning the geometry of the basins of attraction [61] which we hope to address in future work.

Finally, not only higher harmonics but strong asymmetry in the coupling function $g(\Delta\vartheta)$ can lead to multiple stable synchronization states, as well. In contrast to the other two mechanisms for multistability this effect is only observed in networks of nonidentical oscillators. In Section 4.1.2 we present the results of the bifurcation analysis for a chain of three nonidentical, nonisochronous oscillators and find multistability for $\gamma^2 \geq 3$.

We want to emphasize that multistability is a common feature in networks of coupled phase oscillators [14, 54, 61] and should not be neglected in favor of the analysis of complete synchronization of identical oscillators, for which the trivial synchronization manifold is known analytically.

### 4.1.1 Topological charges and multistability

The enormous success of the master stability function approach [33] may have focused the attention of the scientific community disproportionately on the stability of the homogeneous synchronization manifold $\mathbf{X}_1 = \mathbf{X}_2 = \cdots = \mathbf{X}_N$ for identical dynamical systems $\dot{\mathbf{X}}_n = \mathbf{F}(\mathbf{X}_n)$. But even for identical systems there can be inhomogeneous synchronized states which, depending on the coupling network, are not easy to obtain analytically.

A linear stability analysis around a stable synchronization manifold (see

Sec. 4.4.2) will only give the exponential time scale at which the attractor is approached. Starting from random initial conditions in the high dimensional state space $T^N$ the time to reach the vicinity of the synchronization manifold may involve intermittent behavior or long transients close to saddle points (Fig. 4.2). We will see in Section 4.2 that for a large system of $N$ oscillators an even larger number $\sim 2^N$ of synchronization manifolds of saddle type stability can exist. The stable and unstable manifolds of these fixed points cannot be crossed. They form the walls of a labyrinth inside the high-dimensional phase space. In order to study the transient approach to synchronization we conducted simulations with random networks of identical Kuramoto phase oscillators. We did experiments (Fig. 4.1) with scale free Barabási-Albert networks [31] as well as connected Rényi Erdös networks (see App. D). As a measure for the distance to the homogeneous synchronization manifold we used

$$d^2 = \sum_{n,m} A_{nm} \sin^2(\vartheta_m - \vartheta_n) \qquad . \tag{4.5}$$

Alternative measures for synchronization of phase oscillators are the variance of the phase velocities or the difference between the fastest and the slowest oscillator

$$\Sigma^2 = \frac{1}{N} \sum_n (\dot{\vartheta}_n - \bar{\vartheta})^2 \qquad \Delta = \dot{\vartheta}_{\max} - \dot{\vartheta}_{\min} \tag{4.6}$$

which must go to zero in complete phase locked synchronization. The distance $d^2$ to the homogeneous state and the support width $\Delta$ of the phase velocity distribution in a regular square lattice of oscillators can be seen in figure (Fig. 4.2 e,f). Between periods of exponential relaxation the distance $d^2$ can become quasi-stationary and non-zero for a long time. In fact, it can settle at a finite value if the homogeneous synchronization manifold does not exist or if it is not the only attracting synchronized state. From random initial conditions the phase profile across the lattice smoothes out quickly. However, a certain type of irregularities remains and only dissolves in pairwise annihilations or across the border of the medium. The nature of these irregularities is that of phase singularities at localized points. In a continuous medium the integral of the phase gradient around a phase singularity is a multiple of $2\pi$. In nonisochronous oscillatory media a phase singularity is usually the center of spiral waves [1]. The dynamics and stability of spiral waves and their interaction can be studied at a kinematic level [62, 63]. This brought up the question whether the reason for meta or multistability in regular lattices and networks is the same. It turns out that in the inhomogeneous state of the random network in figure (Fig. 4.1 b,e) the sum of the phase differences along some closed paths

$$\sum_{e=(n,m)} (\vartheta_m - \vartheta_n) = 2\pi\ l \qquad \text{with } l \in \mathbb{Z} \tag{4.7}$$

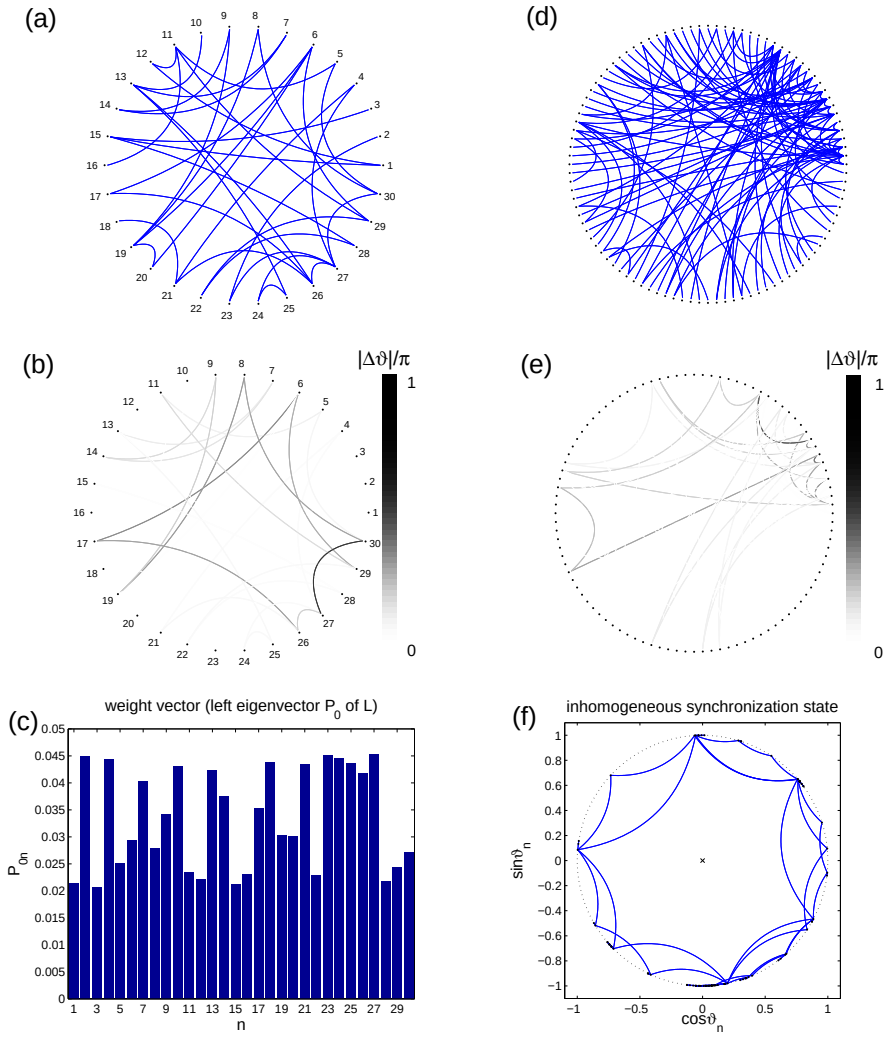


Figure 4.1: Inhomogeneous synchronization states in random networks of identical ($\mathrm{var}(\omega) = \sigma = 0$) phase oscillators (Eq. 4.1). (a-c) N=30, $\gamma = 0.5$. (d-f) N=100, $\gamma = 0.2$. For illustration we used a connected random network with binomial degree distribution $\mathbf{E}[k] = 2.5$ (a-c) and a small Barabasi-Albert [31] random network $k = 1.1$ (d-f). The Coupling structure is shown in (a,d) with links between the nodes for nonzero entries in the adjacency matrix. Subfigures (b) and (e) show the same networks where the phase differences in an inhomogeneous synchronized state across links are drawn in gray scale. Subfigure (c) shows the normalized left eigenvector of the Laplacian (Eqs. 3.6,3.7). It is a measure of the influence of each node on the synchronization frequency (see Sec. 5.1). In subfigure (f) we show the phases of the oscillators in synchronization as points on the unit circle. The connections are made according to the adjacency matrix. Cycles with topological charge can easily be identified.

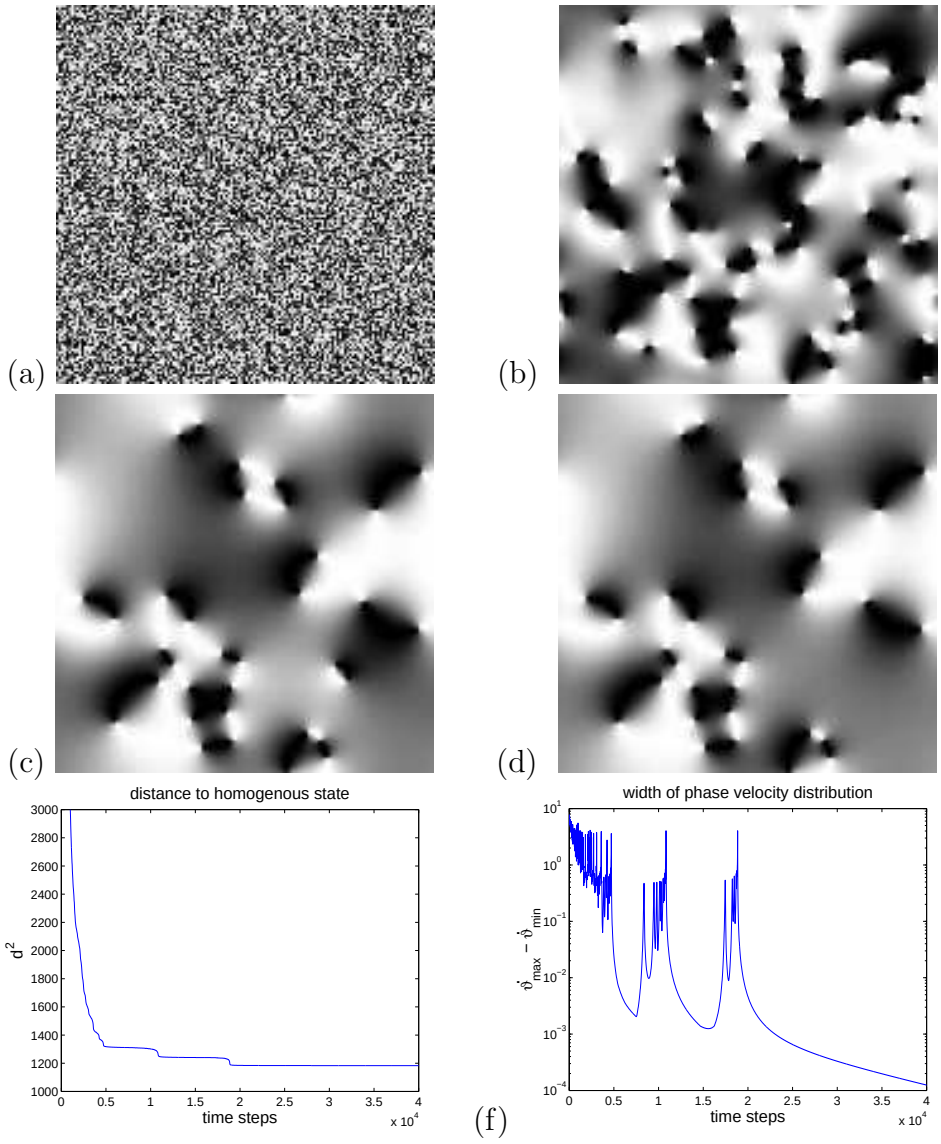


Figure 4.2: A regular square lattice of 150 × 150 identical sine coupled phase oscillators (nearest neighbor coupling, periodic boundary conditions) from random initial conditions does not synchronize to a homogeneous state. Instead an equilibrium or quasi-equilibrium with pairs of opposite topological charges is reached. The topological defects are centers of rotating waves. For nonisochronous oscillators these waves have the form of spirals. Subfigures (a-d) show the sine of the phases in gray levels at time steps t=0 (a), t=1000 (b), t=14000 (c) and t=34000 (d). Subfigures (e) and (f) show the time evolution of the distance measures $d^2$ (Eq. 4.5) and $\Delta$ (Eq. 4.6), respectively. At t≈8000 and t≈17000 topological charges annihilate each other.

is not zero but an integer multiple of $2\pi$. For any given directed circle $L$ in the network, this multiple is called the winding number $l_L$ or topological charge. using the definition of phase difference $(\vartheta_m - \vartheta_n) \in [-\pi, \pi)$ as the shortest arclength on the unit circle the winding number (Eq. 4.7) is defined for a given circle $L$ at all times. Given a simple base $\{L_i\}$ with $(i = 1 \dots E - N + 1)$ of the circle space of the network [55] we can introduce a partition of the state space according to the vector $\boldsymbol{l} = (l_{L_1}, l_{L_2}, \dots, l_{L_{E-N+1}})$ of corresponding winding numbers.

In a systematic approach to study topological charges we proceeded with the simplest system conceivable that can sustain nonzero winding numbers : a ring of $N$ identical phase oscillators with sine coupling

$$\dot{\vartheta}_n = \sin(\vartheta_{n-1} - \vartheta_n) + \sin(\vartheta_{n+1} - \vartheta_n) \tag{4.8}$$

and with periodic boundary conditions $\vartheta_{N+1} = \vartheta_1$ and $\vartheta_0 = \vartheta_N$. The symmetry of the setup yields solutions to the phase differences at synchronization of the form

$$\vartheta_{n+1} - \vartheta_n = \frac{2\pi}{N}\, l \qquad , \; l \in \mathbb{Z} \qquad . \tag{4.9}$$

The off-diagonal elements of the Laplacian in the linear stability analysis (Eq. 3.5) have the value $L_{nn\pm1} = \cos(2\pi l/N)$. If they are not negative the Laplacian is negative semidefinite and positive definite otherwise. Therefore all solutions (Eq. 4.9) with $|l| < N/4$ are stable.

This was, of course not the first time the stability of such a twisted solution or rotating wave has been shown in a discrete system of phase oscillators. Ermentrout [64] went as far as to prove the stability of a single rotating wave in a square lattice with open boundary conditions of phase oscillators with finite nonisochronicity $\gamma$ and then explained spiral waves as the solution of coupled nested rings of increasing lengths. Each ring has the same winding number but a different eigenfrequency

$$\Omega_r = g\left(\frac{2\pi l}{N_r}\right) + g\left(-\frac{2\pi l}{N_r}\right) = 2\gamma\left(1 - \cos\left(\frac{2\pi l}{N_r}\right)\right) \tag{4.10}$$

where $N_r$ is the number of oscillators in the ring. Larger rings farther away from the spiral tip are slower and therefore lag behind in phase. If $\gamma$ is zero one would expect no phase lag, the lines of constant angles should be radial to the center of the rotating wave. This is confirmed by direct simulation (Fig. 4.2 b-d).

An interesting question for us was to determine the size of the basin of attraction for the different synchronization states. Simulating system (Eq. 4.8) we sampled the phase space with random initial conditions and counted the

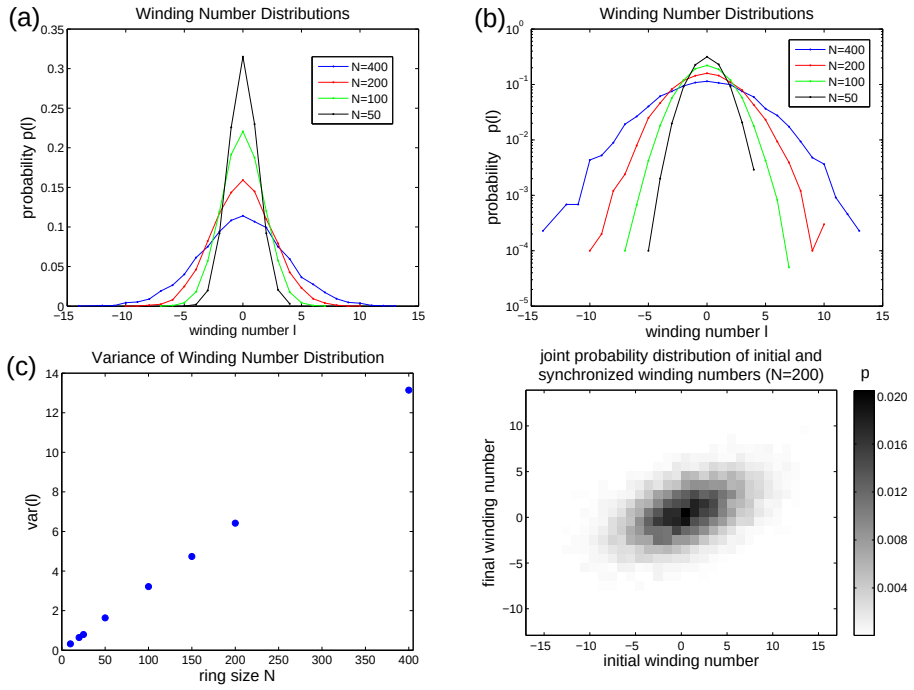


Figure 4.3: We integrated the Kuramoto phase equations for rings of $N$ phase oscillators with nearest neighbor sine coupling (Eq. 4.8) from random initial conditions until the winding number in the synchronized state could be determined. The process was repeated $10^4$ times and the initial and final winding numbers recorded. By this Monte-Carlo integration we could estimate the relative sizes of the basins of attraction for the different synchronized states with charges $l$ from the winding number distribution (a-b). In a logarithmic scale (b) the distribution has the shape of a parabola corresponding to a binomial distribution. The variance of the winding number distribution grows linearly with the size $N$ of the ring (c) This is the same scaling behavior as expected from the displacement distribution of a random walk of length $N$. Subfigure (d) shows the joint histogram of the distribution $p(l(t=0), l(t\to\infty))$ of the winding numbers $l(t=0)$ at random initial conditions and in synchronization $l(t\to\infty)$ for a ring of size $N=200$. They are only weakly correlated with a linear coefficient of correlation $R=0.47$ and mutual information $I=0.21$ *bit*.

number of outcomes for each of the possible winding numbers $|l| < N/4$ in synchronization after integrating the Kuramoto phase equations numerically. For the initial conditions we tried both, a uniform distribution on $T^N$ and importance sampling Monte-Carlo with the Cross Entropy Method [65]. Both gave similar results, while the uniform sampling was much simpler to implement. The results are shown in figure (Fig. 4.3). The distribution of the sizes of the basins of attraction seems to be binomially distributed or gaussian and the variance of the winding number distribution grows linearly with the length $N$ of the ring. We came up with an intuitive explanation, after all, the winding number (Eq. 4.7) is

the sum of random phase differences for random initial conditions, even though they are not independent since they add up to integer multiples of $2\pi$. They are even less independent after the transient time when the winding number does not change anymore before the synchronization manifold is reached. Still, a central limit theorem may be applicable under the more general condition of correlated random variables.

The same results in the case of a ring of phase oscillators with k-neighbor sine coupling was published by Strogatz 2006 [61]. They also used a Monte-Carlo method and gave the same, somewhat handwaving explanation for the winding number distribution. We hope to resolve the geometric shapes of the basins of attraction in future studies to find an analytic expression for the winding number distribution which would answer the questions to the community posed in [61].

In networks of identical oscillators with many or large cycles synchronization states with topological charges, i.e. non-zero winding numbers (Eq. 4.7), are common. Starting from random initial conditions it can be very unlikely to reach the winding number free synchronization state. Topological charges also characterize the states of networks with nonidentical oscillators.

### 4.1.2 Chain of three nonidentical nonisochronous oscillators

While the solution for a system of two nonisochronous, nonidentical Kuramoto phase oscillators, even with asymmetric coupling, is rather straight forward and has been derived elsewhere [66], already a tree network of $N = 3$ oscillators is more complicated to analyze and basically involves finding the roots of fourth degree polynomials. With each node that is added to the network the degree is doubled, so that one can in principle expect a whole spectrum of bifurcations with higher co-dimensions. In fact, for larger values of nonisochronicity $\gamma^2 > 3$ we have found multistability in a cusp-bifurcation for a chain of three nonidentical, nonisochronous phase oscillators.

The first harmonic approximation of the coupling function is often assumed to be a simple sine function. This, however, disregards an important nonlinear effect, as will be shown in the following. The complete first harmonic approximation is given in [1]. Here we restrict ourselves to the case of attractive coupling where $g(0) = 0$ and use

$$g(\Delta\vartheta) = \sin\Delta\vartheta + \gamma\,(1 - \cos\Delta\vartheta) \tag{4.11}$$

as a coupling function. The parameter $\gamma$ breaks the symmetry of the coupling and is directly interpreted as nonisochronicity of a dynamical system around a

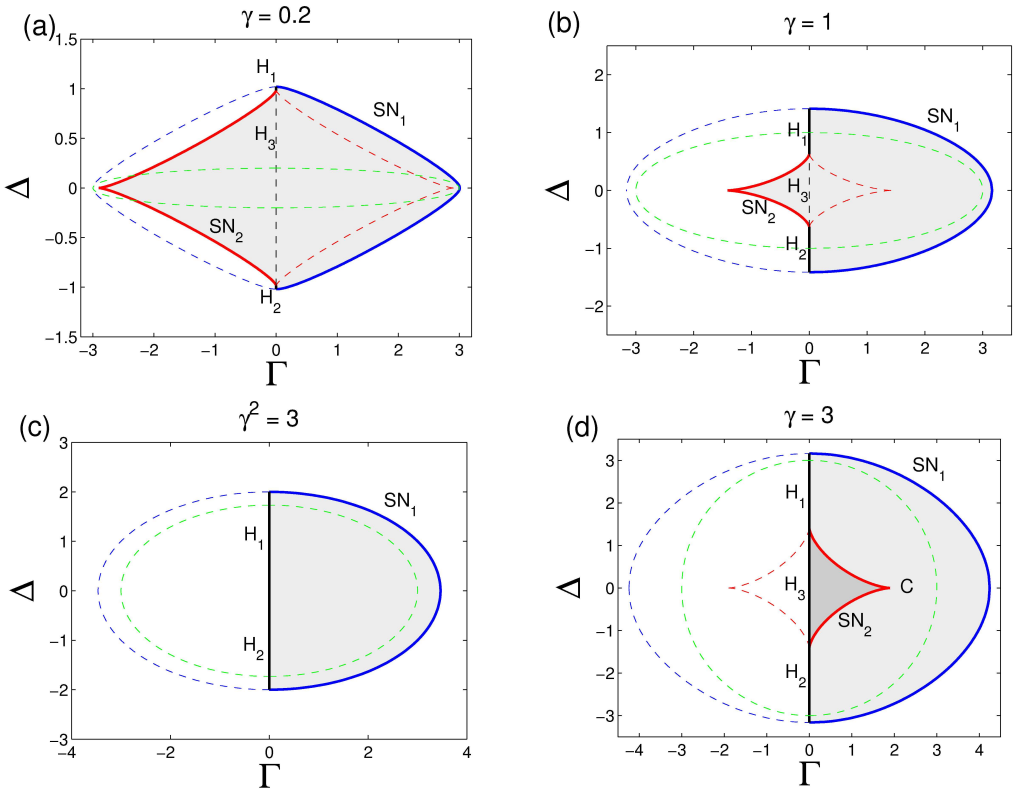


Figure 4.4: Regions in the $\Gamma-\Delta$ parameter space where synchronization manifolds exist for a chain of three nonidentical, nonisochronous Kuramoto phase oscillators (Eq. 4.12) with coupling (Eq. 4.11). Inside the region bounded by the saddle-node bifurcation line $SN_2$ (red line) there are four synchronization manifolds. Two of them vanish in a saddle-node bifurcation at $SN_2$ and the other two at $SN_1$ (blue line). In the gray regions asymptotically stable synchronization exists. Stability is lost across solid lines, either in saddle node bifurcations at $SN_1$ and $SN_2$ or in an Andronov-Hopf bifurcation at $H_1$ and $H_2$ (black lines). The dashed green line marks the inversion of stability when the trace of the Jacobian at a saddle point changes sign. The four diagrams differ in the value of nonisochronicity $\gamma$. For values $\gamma^2 > 3$ we find a regime of bistability (subfig. d, darker gray) bounded by $SN_2$ in a cusp-bifurcation with cusp point C and an Andronov-Hopf bifurcation at $H_3$.

limit cycle before applying a phase reduction (Chap. 2, [1]). A positive $\gamma$ means that a decrease of the oscillation amplitude through coupling will increase the phase velocity. In two attractively coupled oscillators both will experience an acceleration of phase velocity which breaks the antisymmetry of the interaction in the phase variables.

Unlike with odd coupling (Sec. 4.2) the relation between $g(-\Delta\vartheta)$ and $g(\Delta\vartheta)$ is nonlinear in the presence of nonisochronicity and the synchronization states, even

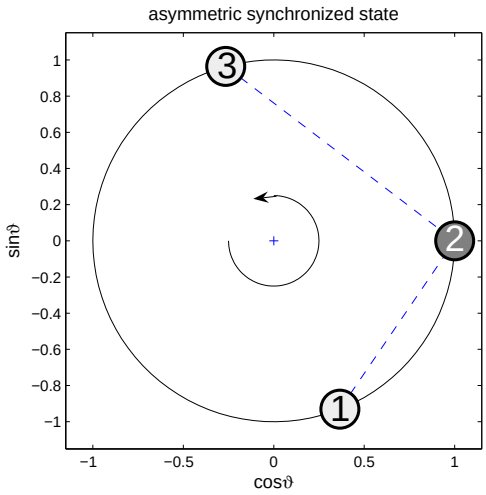


Figure 4.5: Asymmetric synchronized state of a three oscillator chain (Eq. 4.12) on the unit circle, with $\gamma = 3$, $\omega_2 = 0$ and $\omega_1 = \omega_3 = 2.9$. This corresponds to $\Delta = 0$ and $\Gamma = 0.1$ in figure (Fig. 4.4) in the region of bistability. Indeed there is another synchronized state where the first and the third oscillator are exchanged.

in a tree network with $N > 3$, cannot in general be computed analytically. In (Fig. 3.3a-d) one can see, that the region $S$ of potentially stable synchronization on $T^{N-1}$ is folded by the mapping $\Delta\omega(S)$. Especially, for larger values of $\gamma$, the folding makes the map noninjective, i.e. there are regions of multistability in parameter space.

Similar as in a paper by Maistrenko et.al. [13] in the case of a ring of three sine-coupled phase oscillators we will here present the results of a bifurcation analysis of the synchronization states for a chain of three oscillators with the dynamics

$$\begin{aligned} \dot{\vartheta}_1 &= \omega_1 + g(\vartheta_2 - \vartheta_1) \\ \dot{\vartheta}_2 &= \omega_2 + g(\vartheta_1 - \vartheta_2) + g(\vartheta_3 - \vartheta_2) \\ \dot{\vartheta}_3 &= \omega_3 + g(\vartheta_2 - \vartheta_3) \\ g(\Delta\vartheta) &= \sin\Delta\vartheta + \gamma\,(1 - \cos\Delta\vartheta) \qquad . \end{aligned} \tag{4.12}$$

The full analysis can be found in Appendix A. The space $T^2$ of relative phases is a two dimensional torus and the dynamics on it depends on the nonisochronicity and the frequency differences $\omega_2 - \omega_1$ and $\omega_2 - \omega_3$. We use the symmetry of the coupling scheme and parameterize the frequency differences by $\Gamma = \gamma + \frac{1}{2}(2\omega_2 - \omega_1 - \omega_3)$ and $\Delta = \frac{1}{2}(\omega_1 - \omega_3)$. Any bifurcation that occurs at a parameter set $(\Gamma, \Delta, \gamma)$ will also occur at points obtained by varying the signs of the parameters, possibly with inverted stability properties of the synchronization

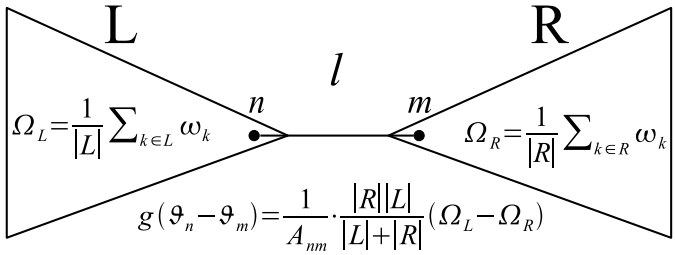


Figure 4.6: If the coupling function is antisymmetric then the value of the coupling function in synchronization across an edge $l = (n, m)$ that separates the coupling network into two otherwise disjoint parts L and R is proportional to the difference of the average frequencies in L and R.

manifolds (see App. A). We will therefore only analyze the bifurcations observed in the $\Gamma - \Delta$ parameter plane for different values of $\gamma \geq 0$. In general there are two saddle-node bifurcation curves (Fig. 4.4). An outer boundary $SN_1$ where no synchronization manifolds exists outside and a region inside $SN_2$ where the torus $T^2$ contains four fixed points. For identical oscillators, i.e. $\Gamma = \gamma$ and $\Delta = 0$ the homogeneous solution $\vartheta_2 - \vartheta_1 = \vartheta_2 - \vartheta_3 = 0$ is always asymptotically stable. If the nonisochronicity is small enough, for values $\gamma^2 < 3$, stability is lost in saddle-node bifurcations at $SN_1$ and $SN_2$ or in Andronov-Hopf bifurcations at the lines $H_1$ and $H_2$ with $\Gamma = 0$ between $SN_1$ and $SN_2$. If the nonisochronicity is large, for values $\gamma^2 > 3$, the region of stability on $T^2$ is folded and we observe a cusp-bifurcation in the $\Gamma - \Delta$ parameter space. Figure (Fig. 4.5) shows that the two synchronized solutions occur in a symmetry break. Even if the two outer oscillators have the same frequency $\omega_1 = \omega_3$ in synchronization they have a different relative phase to the oscillator in the middle. The two stable equilibria vanish either at saddle node bifurcations on $SN_2$, in particular a pitchfork bifurcation at the cusp point C, or become unstable in Andronov-Hopf bifurcations at $H_3$. The existence of Hopf bifurcations in the presence of nonisochronicity is noteworthy since this indicates the presence of another $\gamma$-dependent frequency in the system.

## 4.2 Solutions for odd coupling functions

In the special case of a connected, symmetric coupling network ($A_{nm} = A_{mn}$) without cycles, i.e. a tree network, and an antisymmetric coupling function $g(-\Delta\vartheta) = -g(\Delta\vartheta)$ it is possible to explicitly check whether $\Delta\omega \in \Delta\omega(T^{N-1})$. Moreover one can show the identity $\Delta\omega(S) = \Delta\omega(T^{N-1})$. On the border of $\Delta\omega(T^{N-1})$ all synchronization manifolds disappear through saddle node bifurcations and the linearization of the dynamics orthogonal to the synchronization manifold is degenerate.

Taking the arithmetic mean over all oscillators in equation (Eq. 4.1) the shift of $\Omega$ from the mean frequency is

$$\Omega - \bar{\omega} \;=\; \frac{1}{N} \sum_{n,m} A_{nm}\; g_{mn} \quad . \tag{4.13}$$

Note that only the symmetric terms with respect to the indices $n$ and $m$ contribute to the sum on the right hand side. Because the terms $A_{nm}\; g_{mn}$ are antisymmetric in the indices the right hand side of equation (Eq. 4.13) becomes zero and the synchronization frequency $\Omega$ is exactly equal to the arithmetic mean $\bar{\omega}$ of the natural frequencies. Let $l = (n, m)$ be an edge of the tree network, i.e. $A_{nm} = A_{mn} \neq 0$. Every edge separates the network into two sets of vertices $L$ and $R$ (Fig. 4.6) which are connected via $l$, that is $n \in L$ and $m \in R$. Summing up both sides of equation (Eq. 4.1) over the vertices $k \in L$, using $\Omega = \bar{\omega}$ and rearranging the terms one obtains

$$\sum_{k \in L} (\bar{\omega} - \omega_k) = A_{nm}\; g_{mn} + \sum_{k,n \in L} A_{kn}\; g_{nk} \tag{4.14}$$

The double sum over the all edges $(k, n)$ within $L$ vanishes because of the antisymmetry of the summands so that in synchronization the phase difference must settle at

$$g_{mn} = \frac{1}{A_{nm}} \sum_{k \in L} (\bar{\omega} - \omega_k) \qquad . \tag{4.15}$$

The same argument for the right set of vertices $R$ yields

$$g_{nm} = \frac{1}{A_{mn}} \sum_{k \in R} (\bar{\omega} - \omega_k) \qquad . \tag{4.16}$$

Observing $g_{nm} = -g_{mn}$ and $A_{nm} = A_{mn}$ one can eliminate the mean frequency $\bar{\omega}$ and find

$$g_{nm} = \frac{1}{A_{nm}} \; \frac{|R| \sum_{k \in L} \omega_k - |L| \sum_{k \in R} \omega_k}{|L| + |R|} \qquad . \tag{4.17}$$

Defining the mean frequencies $\Omega_L$ and $\Omega_R$ in the left and right subnetwork, respectively

$$\Omega_L = \frac{1}{|L|} \sum_{k \in L} \omega_k \qquad \Omega_R = \frac{1}{|R|} \sum_{k \in R} \omega_k \tag{4.18}$$

equation (Eq. 4.17) takes the nice form

$$g_{nm} = \frac{1}{A_{nm}} \frac{|L||R|}{|L| + |R|} \, (\Omega_L - \Omega_R) \qquad . \tag{4.19}$$

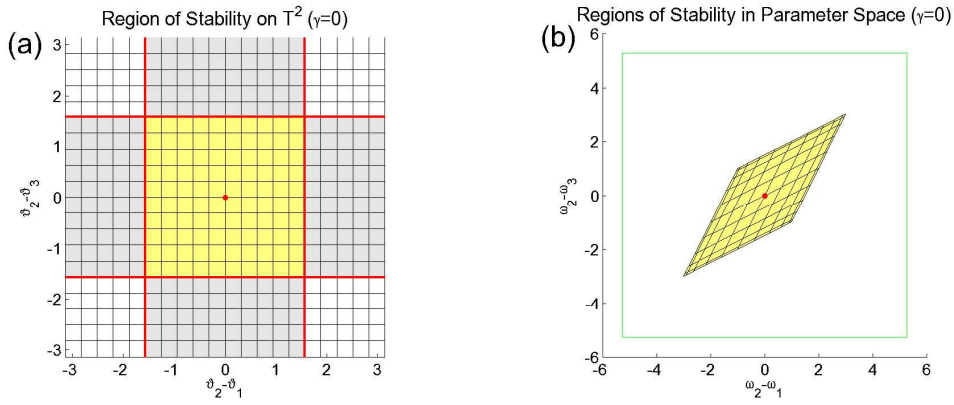


Figure 4.7: Phase space $T^2$ (Fig.(a,c)) and parameter space (Fig.(b,d)) for a chain (Eq. 4.20) of three phase oscillators. The color codes and the coupling structure are that same as in Fig. 3.3. Only here the coupling function is odd. The region of stability and the image of $T^2$ in parameter space are identical (yellow area).

The coupling function across the link $l = (n, m)$ is proportional to the difference of the mean frequencies in the left and right subnetwork. the phase difference is given by all solutions to $g(\vartheta_n - \vartheta_m) = g_{nm}$. If $|g_{nm}| < g_{\max}$ then, since $g(\Delta\vartheta)$ is periodic and continuous, there exist at least two such solutions and there exists at least one solution with $g'_{nm} > 0$. Therefore, since a tree of $N$ vertices has exactly $N - 1$ edges, the number of synchronization manifolds for a parameter set $\omega \in \text{int}\left(\omega(T^{N-1})\right)$ is at least $2^{N-1}$. The matrix $g'_{nm}$ of derivatives is symmetric, so if all $g'_{nm}$ are positive, then the Laplacian (Eq. 3.6) is negative-semidefinite (see Sec. 3.1 or [52]) and the corresponding synchronization manifold is asymptotically stable. Phases $\vartheta_n$ with phase differences such that $g'_{nm} \geq 0$ can be found for any $\Delta\omega \in \Delta\omega(T^{N-1})$ and thus $\Delta\omega(S) = \Delta\omega(T^{N-1})$.

This result is pictured in Fig. 4.7 for the example of a chain of three oscillators with sine coupling

$$\begin{aligned} \dot{\vartheta}_1 &= \omega_1 + \sin(\vartheta_2 - \vartheta_1) \\ \dot{\vartheta}_2 &= \omega_2 + \sin(\vartheta_1 - \vartheta_2) + \sin(\vartheta_3 - \vartheta_2) \\ \dot{\vartheta}_3 &= \omega_3 + \sin(\vartheta_2 - \vartheta_3) \end{aligned} \tag{4.20}$$

for which (Eq. 4.17) gives

$$\sin(\vartheta_2 - \vartheta_1) = \frac{\omega_2 + \omega_3 - 2\omega_1}{3} \qquad \sin(\vartheta_2 - \vartheta_3) = \frac{\omega_2 + \omega_1 - 2\omega_3}{3} \qquad . \tag{4.21}$$

If the frequencies $\omega_k$ are chosen randomly, equation (Eq. 4.19) can be analyzed statistically. For idependent, identically distributed random frequencies $\omega_k$ with

expected value $\mathbf{E}[\omega] = \mu$ and variance $\mathrm{var}(\omega) = \sigma^2$ one finds $\mathbf{E}[g_{nm}] = 0$ and

$$\mathrm{var}(g_{nm}) = \frac{1}{A_{nm}^2}|L||R|\ \sigma^2 \qquad . \tag{4.22}$$

The variance of $g_{nm}$ is largest when $|L| = |R| = N/2$. A central link is therefore more likely to violate the condition $-g_{\max} < g_{nm} < g_{\max}$ that (Eq. 4.19) gives a value inside the interval between the minimum $-g_{\max}$ and the maximum $g_{\max}$ of the antisymmetric coupling function $g(\Delta\vartheta)$. Conversely, however, a network does not necessarily desynchronize most likely across a central link if there are much more links with $|L| = 1$ or $|R| = 1$ as is the case tree networks with scale free degree distribution.

The phase differences $\vartheta_{n+1} - \vartheta_n$ between neighboring vertices and the relative phases $\vartheta_n - \vartheta_1$ in a long chain of phase oscillators with sine coupling and random frequencies $\omega_n$ are shown in Fig. 4.13. According to (Eq. 4.15) the values $g_{n+1n}$ with $n = 1 \ldots N-1$ perform a random walk which must be contained as $|g_{n+1n}| \leq 1$ or synchronization cannot be achieved. The phase differences are approximately proportional to the value of the coupling function and so the phase profile $\vartheta_n - \vartheta_1 = \sum_{k=2}^{n}(\vartheta_k - \vartheta_{k-1})$ is an integrated random walk (Fig. 4.13b). The phase profile is not very regular. It has local maxima (pacemaker region) whenever the random walk crosses the line zero from above and possibly at the boundaries.

Averaging over several realizations of a random tree network and random frequencies the mean phase difference across an edge remains zero, but the variance grows proportionally with the diameter of the tree. Figure (Fig. 4.9) shows the mean phase difference as the function of the distance on the tree. This phase difference is zero. There exists no well defined wave length or direction in the synchronized system.

Note, that (Eq. 4.17) applies for any edge, that separates a network into two otherwise disjoint subnetworks, and not just for tree networks.

## 4.3 Solutions for unidirectional coupling functions

In Section 4.2 we have shown that one can solve the Kuramoto phase equations (Eq. 4.1) for synchronized oscillators for the values of $g_{nm}$ if there are no cycles in the network, i.e. if the coupling network is a tree, and if there is a linear relationship between $g_{nm}$ and $g_{mn}$. At the example of a chain of oscillators with odd coupling function (Fig. 4.13a,b) we have found that the phase differences

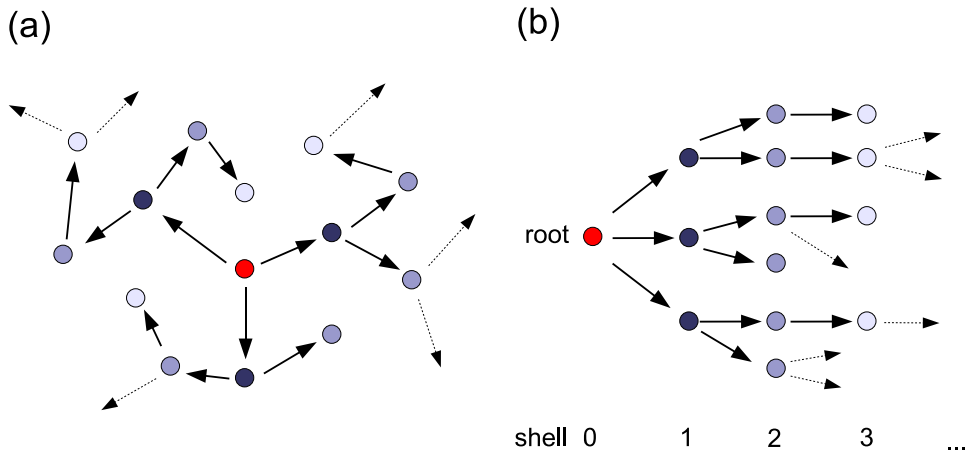


Figure 4.8: Schematics of an excerpt from a tree network. The arrows indicate the direction away from the fastest oscillator (red circle). Subfigure (b) pictures the classification of the vertices into shells (color coded) according to the distance from the fastest oscillator. The influence of the fastest oscillator on the phase profile depends on the asymmetry of the coupling function. For isochronous Kuramoto phase oscillators with $g_{mn} = g_{nm}$ the fastest oscillator has no prominent position on the phase profile in the system and the classification of the network into shells is more or less arbitrary.

perform a random walk and the corresponding phase profile is not very regular in the sense that there is no well defined wave length for different realizations of random frequencies. This situation changes if the coupling function becomes more asymmetric, for instance, if the oscillators are nonisochronous (see Section 4.4). An asymmetry in the coupling function leads to an asymmetric Laplacian $\mathbf{L}$ (Eqs. 3.5, 3.6) if the oscillators are nonidentical and the phase differences at synchronization are not zero. Near the synchronization manifold an asymmetric coupling function is similar to asymmetric coupling $A_{nm} \neq A_{mn}$ which has been studied for example in [39, 40, 36]. The result of these papers was that a network where the couplings $A_{nm}$ are normalized with the out-degree $k_n$ of a node has optimal synchronization properties if the network topology is fixed. Another type of topological asymmetry which increases synchronizability can be found in directionally biased or feed forward networks as defined in [42]. In contrast, the asymmetry of the coupling function is an exclusively dynamical property.

Here we will discuss the extreme case of a unidirectional coupling function of the form

$$g(\Delta\vartheta) = \begin{cases} f(\Delta\vartheta) > 0 & , \text{ for } 0 < \Delta\vartheta < \pi \\ 0 & , \text{ else} \end{cases} \tag{4.23}$$

for instance $g(\Delta\vartheta) = (\sin\Delta\vartheta + |\sin\Delta\vartheta|)/2$. An oscillator $n$ which is ahead of another oscillator $m$ does not feel the influence of $m$ because $g(\vartheta_m - \vartheta_n) = 0$. Thus the coupling $A_{nm}g_{mn}$ describes a directed graph following a phase gradient in the network. Gradient networks, as well, have been discussed to facilitate synchronization [41]. From the equations (Eqs. 4.1, 4.23) follows

$$\Omega - \omega_n = \sum_m A_{nm}\ g_{mn} \geq 0 \qquad . \tag{4.24}$$

The phase gradient in a tree network introduces a strict partial order relation ">" to the set of vertices at synchronization. Two vertices are related as $n > m$ if there exists a a path $(p_1, p_2, \ldots, p_L)$ with $p_1 = n$ and $p_L = m$ and $A_{p_{i+1}p_i}\ g_{p_ip_{i+1}} > 0$. Although phases are periodic, in the absence of circles in the network the asymmetry of the order is ensured (if $n > m$ then not $m > n$). Since the set of vertices is finite, it must contain at least one maximum $n_{\max}$ with respect to the order relation and because there is no $m$ with $m > n_{\max}$ equation (Eq. 4.24) gives $\Omega - \omega_{n_{\max}} = 0$. Equation (Eq. 4.24) tells us that $\Omega - \omega_n \geq 0$ for all $n$ so that the synchronization frequency $\Omega$ is exactly equal to the largest frequency $\Omega = \omega_{n_{\max}} = \omega_{\max}$ in the system. If the frequencies are random, then the probability that two frequencies are equal is zero, although the largest and the second largest frequency may be very close together. We suppose there is only one fastest oscillator in the network then this must be the root of a directed tree (Fig. 4.8). Each node $n$ has exactly one successor $p(n)$ on the path to the root so that

$$\omega_{\max} - \omega_n = A_{np(n)}g_{p(n)n} \qquad . \tag{4.25}$$

If the coupling strengths $A_{nm}$ are uniform and either zero or one then the condition for synchronization is $\omega_{\max} - \omega_{\min} \leq \max_{\varphi} g(\varphi)$. All solutions $\vartheta_{p(n)} - \vartheta_n$ to (Eq. 4.25) with $g'_{p(n)n} > 0$ for all $n$ are phase differences of a stable synchronization manifold.

In contrast to the phase profile for odd coupling, in the case of unidirectional coupling the oscillators in the tree network self-organize in shells around a single pacemaker, the fastest oscillator in the system, and the phase differences between two shells have a nonzero expected value defining a clear wave length along the phase gradient.

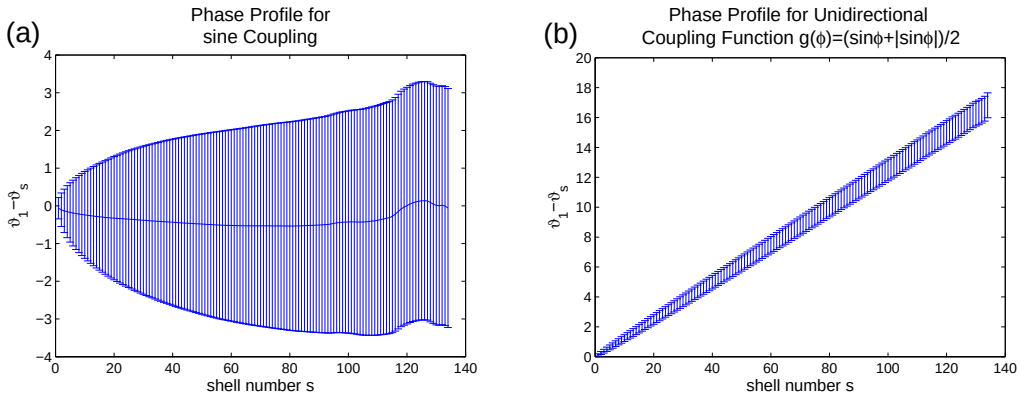


Figure 4.9: Phase profiles in tree networks of synchronized phase oscillators. Shown are the mean relative phase and the variance of of the relative phases (concentric errorbars) as a function of the distance to the fastest oscillator (shell number). The measures where taken from ensembles (1000 trials) of random trees (see App. D) of size $N = 1000$ with uniform coupling $A_{nm} \in \{0, 1\}$ and independent, uniformly distributed random frequencies $\omega_n \in [0, 0.25]$. We have used the analytic expressions (Eq. 4.17, 4.25) to obtain the values of the coupling function across the edges which could be inverted under the condition $g'_{mn} > 0$. We compare sine coupling (Fig.a) and unidirectional coupling (Eq. 4.23, $f(\Delta\vartheta) = \sin\Delta\vartheta$, Fig.b) and find that in the case of unidirectional coupling the system develops a very regular phase profile in synchronization. Originating at the fastest oscillator waves of well defined wavelength travel outwards along the shells of the network around the pacemaker. For $N = 1000$ there are only seldomly more than 80 shells which is why the statistics beyond that shell number is not so good.

## 4.4 Quasi-regular concentric waves

Besides spiral waves and turbulence, target patterns are one of the most prominent features in two dimensional oscillatory media. They are usually associated with the presence of local impurities in the system [1, 67]. These pacemakers change the local oscillation frequency and are able to enslave all other oscillators in the medium, which finally results in regular ring waves ([1, 68] and Fig. 4.11). However, the assumption of a discrete set of localized pacemaker regions in an otherwise homogeneous medium is somewhat artificial. Especially biological systems are often under the constraint of large heterogeneity. In such a disordered system no point can clearly be distinguished as a pacemaker and it is not obvious whether such a system can sustain highly regular target patterns and where they should originate.

The emergence of target patterns in random oscillatory media was first reported and explained in [69] and subsequently also observed in chaotic phase coherent systems [46]. In [10] we showed that the random nature of the medium

itself plays a key role in the formation of the patterns. As the disorder in a rather homogeneous synchronized medium is increased we observed the formation of quasi regular target waves, which result from an intricate interplay between the heterogeneity and a break in the symmetry of the coupling function. We have also studied the scaling properties of the synchronization frequency and wavelength in the limit of small frequency disorder and phase differences between neighboring oscillators. Nonidentical oscillators in the synchronized state are usually separated by fixed nonzero phase differences. These can sum up across spatially extended systems to produce spatio-temporal patterns, which are characterized by stationary relative phases $\vartheta_n - \vartheta_m$. This is demonstrated in figure (Fig. 4.10) where we have simulated system

$$\dot{\vartheta}_n = \omega_n + \sum_{m=1}^{N} A_{nm}\ g(\vartheta_m - \vartheta_n) \tag{4.26}$$

with interaction $g(\Delta\vartheta) = \sin\Delta\vartheta + \gamma(1 - \cos\Delta\vartheta)$ in a two-dimensional square lattice and nearest neighbor coupling.

Let $\eta_n$ be identically distributed random variables with $\mathrm{var}(\eta) = 1$. The frequency heterogeneity of phase oscillators with natural frequencies $\omega_n = \sigma\eta_n$ can be quantified by the variance $\sigma^2 = \mathrm{var}(\omega)$. In Chapter 3 we have shown, that the homogeneous solution $\vartheta_n = \vartheta_m$ for all $n, m$ solves (Eq. 4.1) for identical phase oscillators $\sigma = 0$ and that this synchronization manifold is asymptotically stable if $g'(0) > 0$. The homogeneous synchronization manifold is also structurally stable against small frequency heterogeneities. If the heterogeneity is small the oscillators across the lattice synchronize from homogeneous initial conditions to a rather homogenous phase profile (Fig. 4.10a). However, by increasing the disorder we observe the formation of target waves with decreasing wavelength (Fig. 4.10a-c). The emergence of the concentric waves is due to the symmetry breaking in the interaction function. By reducing the nonisochronicity $\gamma$ in (Eq. 4.11) the pattern becomes more irregular (Fig. 4.10d). The same ordering effect can be seen in sparse connected networks, in particular tree networks (Sec. 4.3, Fig. 4.9) when we compare odd and unidirectional coupling functions. The special case of a chain of coupled phase oscillators is discussed in Section 4.4.1.

It is a somewhat counterintuitive observation that a homogeneous medium with random frequency distributions of no spatial correlation (see Fig. 4.10 insets) can generate and sustain very regular wave patterns. Since the equations (Eq. 4.26) generally approximate the phase dynamics for coupled limit cycle oscillators this effect is not restricted to phase equations. Similar disorder induced target patterns have been observed in lattices of a variety of oscillator

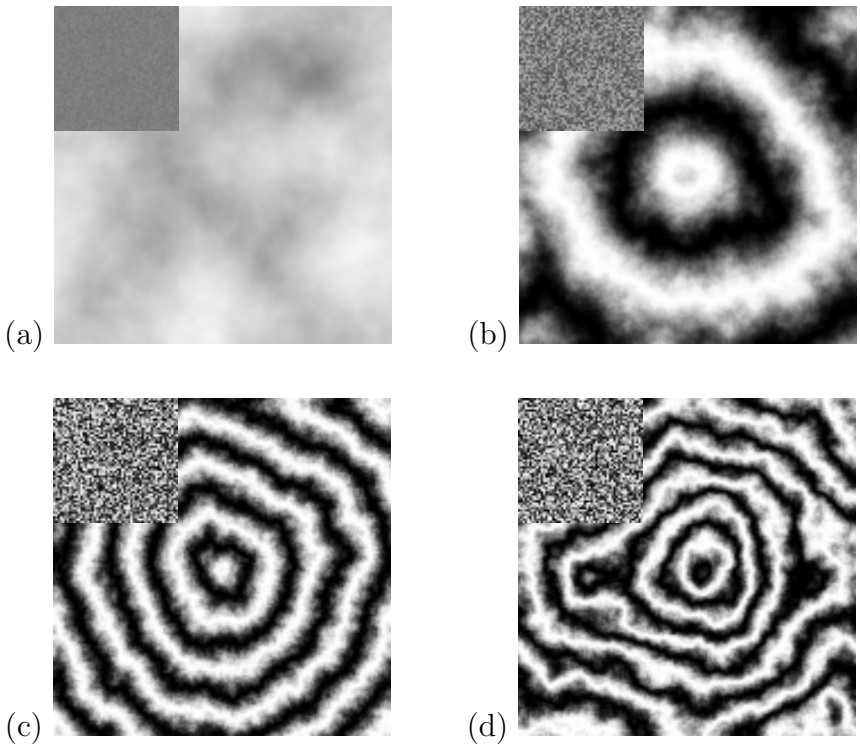


Figure 4.10: Simulation results in a 2-dimensional lattice of 150x150 phase oscillators (Eqs. 4.26, 4.11) with nearest neighbor coupling, $A_{nm} \in \{0, 1\}$, periodic boundary conditions, homogeneous initial conditions and (a) $\gamma = 2$, $\sigma = 0.029$, (b) $\gamma = 2$, $\sigma = 0.173$, (c) $\gamma = 2$, $\sigma = 0.433$ and (d) $\gamma = 0.3$, $\sigma = 0.433$. The random frequencies are taken from a uniform distribution of variance $\sigma^2$. Plotted is the sine of the phases $\vartheta_i$ as grey level. Similar results are obtained for open boundaries. (a)-(c): effect of increased heterogeneity; (c)-(d): influence of nonisochronicity $\gamma$. Insets show the natural frequencies $\omega_i$ as grey levels.

types, including predator-prey systems, chemical reactions and even chaotic oscillators [45, 46, 69, 70].

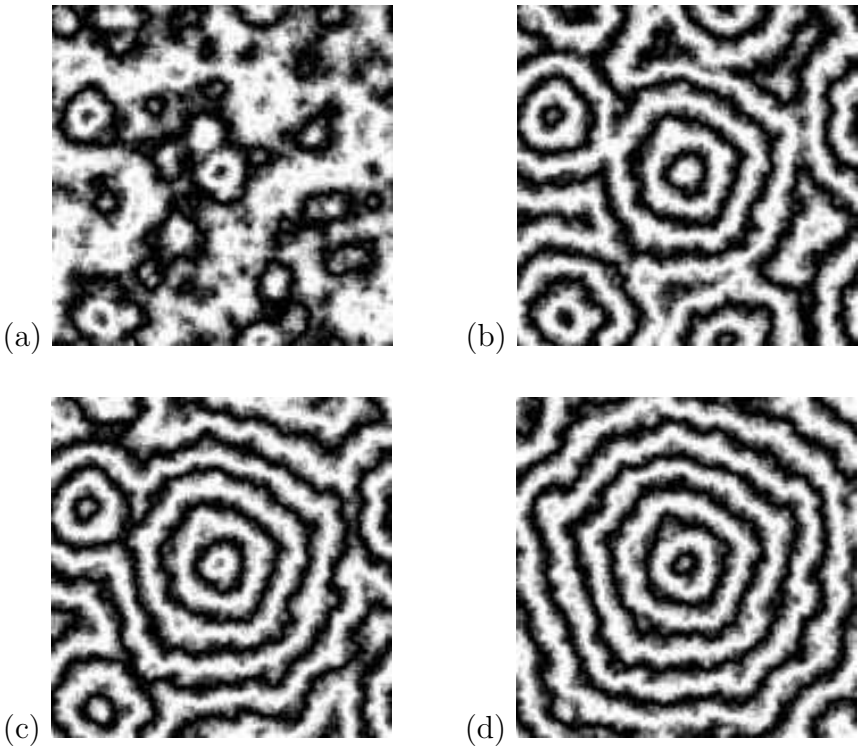


Figure 4.11: Transient to synchronization in a $150 \times 150$ grid of nonisochronous ($\gamma = 1$) Kuramoto phase oscillators with nearest neighbor coupling and periodic boundary conditions. The frequencies used in this simulation where uncorrelated and uniformly distributed with variance var $\omega = \sigma^2$ ($\sigma = 0.6$). Starting from homogeneous initial conditions different regions on the lattice emerge as local pacemakers and compete against each other until a singular quasi-regular concentric target pattern has achieved dominion (d). The subfigures show the sine of the phases in gray levels at different time steps $t = 50$ (a), $t = 300$ (b), $t = 1050$ (c) and $t = 10000$ (d).

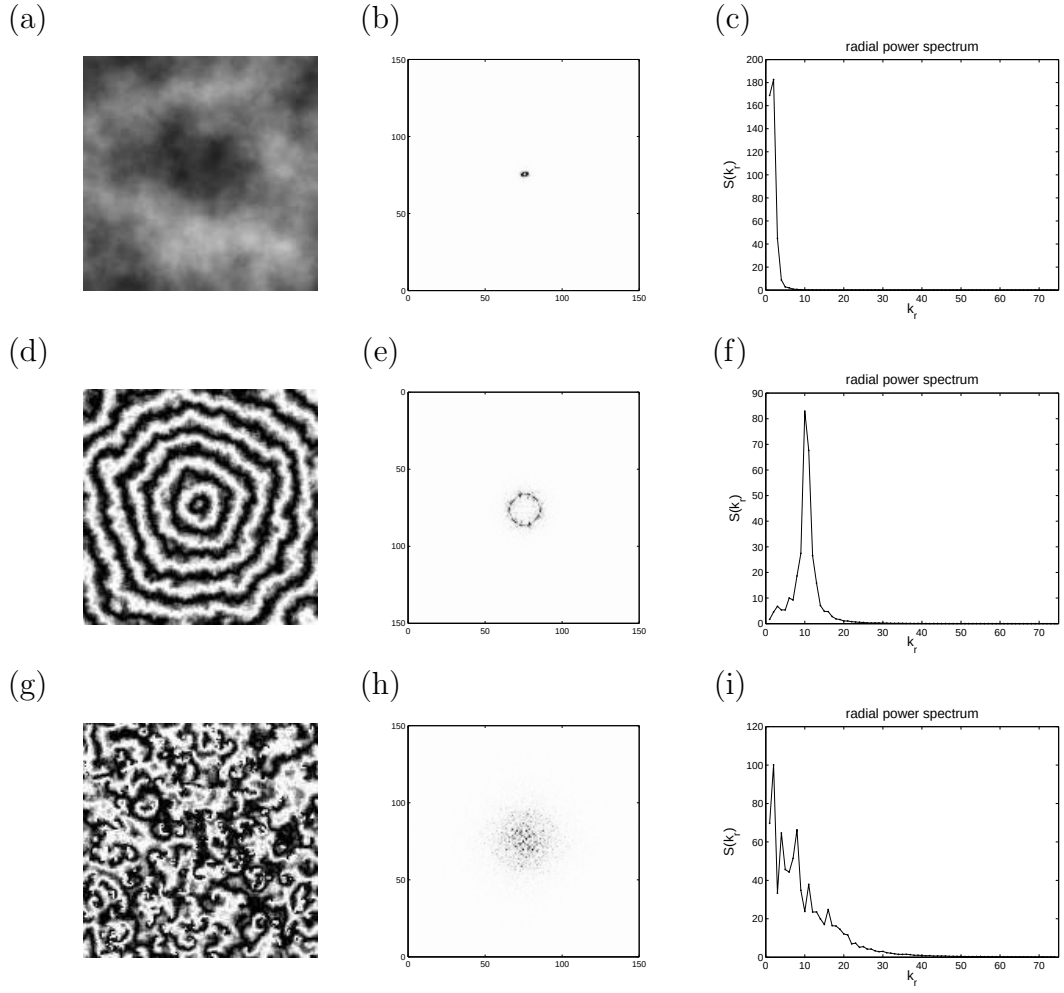


Figure 4.12: Spectral analysis of spatial patterns in 2d grids of $150 \times 150$ non-isochronous ($\gamma = 1$) Kuramoto phase oscillators with nearest neighbor coupling and periodic boundary conditions. The first column (a,d,g) shows the sine of the phases in gray scales after a sufficient transient time. The second column (b,e,h) shows a Fast Fourier Transform (power spectral density) of the images in the first column. In the last column the mean power of all points at a distance $k_r$ from the center is plotted. From this diagram one can in principle find the wavelength and the regularity (coherence) of the waves but only if the wavelength is smaller than the system size. One should also average over many realizations of random frequencies. The heterogeneities in the simulations were $\sigma = 0.05$ (a-c), $\sigma = 0.6$ (d-f) and $\sigma = 0.7$ (g-i) with uncorrelated uniformly distributed random frequencies. The best spectral resolution was achieved in the simulation (d-f), just below the threshold to desynchronization. The last row (g-i) shows the situation of phase turbulence. It is clearly distinguished from synchronization by its broad power spectral density (h,i).

### 4.4.1 Chain of nonidentical nonisochronous oscillators

At the example of tree networks we have shown in Sections 4.2 and 4.3 how the phase profile changes qualitatively depending on the symmetry of the phase coupling function. In this section we are considering the special case of a chain of phase oscillators with nearest neighbor coupling and open boundary conditions.

$$\begin{aligned} \Omega &= \sigma\eta_n + g(\vartheta_{n-1} - \vartheta_n) + g(\vartheta_{n+1} - \vartheta_n) \\ \vartheta_{N+1} &= \vartheta_N \qquad \vartheta_0 = \vartheta_1 \\ g(\Delta\vartheta) &= \sin\Delta\vartheta + \gamma(1 - \cos\Delta\vartheta) \end{aligned} \tag{4.27}$$

In this one dimensional system we find that the break in the symmetry of the coupling function, parameterized by $\gamma \neq 0$, and independent random frequencies $\omega_n = \sigma\eta_n$ with heterogeneity $\mathrm{var}(\omega) = \sigma^2 \neq 0$ lead to the emergence of a characteristic phase difference $\varphi^*$ and hence to a well defined wavelength $\Lambda = 2\pi/\varphi^*$. We can derive a relation between the synchronization frequency $\Omega$ and the wave length $\Lambda$ (Eq. 4.33). We also define measures for the regularity of a phase profile (Eqs. 4.35, 4.38, 4.39) and using the scaling relations reported in [10] and Chapter 5 we find asymptotic expressions for small heterogeneity or nonisochronicity. In addition we can now characterize the regime of high regularity that emerges in a small area before desynchronization for systems with high nonisochronicity (Figs. 4.14c, 4.15a). It turns out, that these very regular phase profiles with short wave lengths occur in the regime of multistability observed in the chain of three oscillators (Sec. 4.1.2).

For isochronous oscillators (Eq. 4.27) with $\gamma = 0$, the coupling function is odd. In that case we can use equations (Eqs. 4.15-4.17) to find the values of the coupling function between neighboring oscillators and by inversion the phase differences. Let us denote

$$\varphi_n = \vartheta_{n+1} - \vartheta_n \qquad . \tag{4.28}$$

Then the value of the coupling function describes a random walk (trend removed) across the lattice

$$g(\varphi_n) = \sin\varphi_n = \sigma \sum_{m=1}^{n} (\bar{\eta} - \eta_m) \qquad . \tag{4.29}$$

For small phase differences we have $\sin\varphi_n \approx \varphi_n$ and the phase profile is given by the sum of the phase differences

$$\vartheta_n - \vartheta_1 = \sum_{k=1}^{n-1} \varphi_k = \sigma \sum_{k=1}^{n-1} \sum_{m=1}^{k} (\bar{\eta} - \eta_k) \quad + \; O(N\sigma^3) \qquad . \tag{4.30}$$

Figure (Fig. 4.13a,b) shows the phase differences and the phase profile in synchronization for a realization of random frequencies. The phase profile is not homogeneous at all but contains several wave trains of irregular length throughout the system originating from different pacemaker regions.

The picture changes when the oscillators are nonisochronous, i.e. $\gamma \neq 0$. The equations (Eqs. 4.27, 4.28) with $\omega_n = \sigma\eta_n$ implicitly define two transfer maps, $T_\Omega : \{\varphi_{n-1}, \omega_n\} \mapsto \varphi_n$ and $T_\Omega^{-1} : \{\varphi_n, \omega_n\} \mapsto \varphi_{n-1}$, which describe the evolution of the phase differences into the right or the left direction of the chain, respectively.

$$\varphi_n \;=\; T_\Omega(\varphi_{n-1}, \omega_n) \;=\; g^{-1}\left(\Omega - \omega_n - g(-\varphi_{n-1})\right) \qquad . \tag{4.31}$$

The random frequencies $\omega_n$ can be seen as noise acting on the map (see Fig. 4.13c,d). We observe that the break in the symmetry of the coupling function leads to a pair of fixed points $\varphi^*$ and $-\varphi^*$ with

$$\varphi^* = T_\Omega(\varphi^*, \bar{\omega}) = g_S^{-1}\left(\frac{\Omega - \bar{\omega}}{2}\right) \tag{4.32}$$

where $g_S(\varphi) = \frac{1}{2}[g(\varphi) + g(-\varphi)]$ is the symmetric part of the coupling function. The mean phase difference is approximately equal to $\varphi^*$ and so we find the relation

$$\frac{2\pi}{\Lambda} \;=\; g_S^{-1}\left(\frac{\Omega - \bar{\omega}}{2}\right) \tag{4.33}$$

between the wavelength $\Lambda$ and the shift $\Omega - \bar{\omega}$ from the mean frequency of the oscillators. By measuring this shift we can determine wavelengths $\Lambda > N$ that are even longer than the system size with high accuracy without having to resort to counting wave trains. By increasing the system size such long waves become visible eventually.

For small fluctuations the transfer map can be linearized at the fixed points so that

$$T(\varphi^* + \psi, \bar{\omega} + \epsilon) \approx \varphi^* + r\psi - \alpha\epsilon \tag{4.34}$$

with

$$r = \frac{g'(-\varphi^*)}{g'(\varphi^*)} \qquad \alpha = \frac{1}{g'(\varphi^*)} \qquad . \tag{4.35}$$

While one fixed point is linearly stable ($|r| \leq 1$) the other fixed point is necessarily unstable. These stability properties are inverted for $T_\Omega^{-1}$. Thus, when iterating to the right of the chain the $\varphi_n$ are concentrated around $\varphi^*$ and around $-\varphi^*$ when iterating to the left. As a consequence, the phase differences that solve

the Kuramoto phase equations (Eq. 4.27) at synchronization organize into two branches

$$\varphi_n = \pm\varphi^* + \psi_n \tag{4.36}$$

around the two fixed points $\pm\varphi^*$, superimposed by autocorrelated fluctuations $\psi_n$ (see Fig. 4.13)

$$\psi_{n+1} \approx r\psi_n - \alpha\epsilon_n \quad . \tag{4.37}$$

Equation (Eq. 4.37) has the form of an autoregressive AR(1) process. If the frequencies $\omega_n$ are independent random variables then the deviations from the arithmetic mean $\epsilon_n = \omega_n - \bar{\omega}$ are almost independent. The constraint $\sum_n \epsilon_n = 0$ correlates the fluctuations. For long chains, where the process (Eq. 4.37) can equilibrate from the open boundary conditions, two consecutive phase differences on the same branch around a stable fixed point are correlated as

$$\begin{aligned} \mathbf{E}\left[\psi_n^2\right] &= \sigma^2\alpha^2\frac{1}{1-r^2} \\ \frac{\mathbf{E}\left[\psi_{n+1}\psi_n\right]}{\mathbf{E}\left[\psi_n^2\right]} &= r \quad . \end{aligned} \tag{4.38}$$

Given the separation of the phase differences into two branches the regularity of the phase profile can be defined by the ratio

$$Q_\psi = \frac{\varphi^{*2}}{\mathrm{var}\psi} \quad . \tag{4.39}$$

Note the difference to [10] where we had defined $Q_\psi = \varphi^*/\mathrm{var}|\varphi|$. The definition in the paper is equivalent to (Eq. 4.39) when the two branches are well separated but both measures go to zero in the limit $\gamma\sigma \to 0$ (see Fig. 4.14c,d).

In [10] we have shown that for small values $\gamma\sigma \ll 1$ we have a scaling relationship of the form

$$\Omega - \bar{\omega} \to \gamma\sigma^2 \cdot C^2 \tag{4.40}$$

with some positive constant $C$ that can be calculated from a perturbation approach (Chap. 5). From equations (Eqs. 4.32, 4.35, 4.38, 4.39) we find for small values of $\gamma\sigma$

$$\begin{aligned} \varphi^{*2} &\approx \sigma^2 \cdot C^2 \\ g'(\varphi^*) \approx 1 + \gamma\sigma \cdot C \qquad & g'(-\varphi^*) \approx 1 - \gamma\sigma \cdot C \\ r &\approx \frac{1-\gamma\sigma\cdot C}{1+\gamma\sigma\cdot C} \\ Q_\psi &\approx 4C^3\,\sigma\gamma \quad . \end{aligned} \tag{4.41}$$

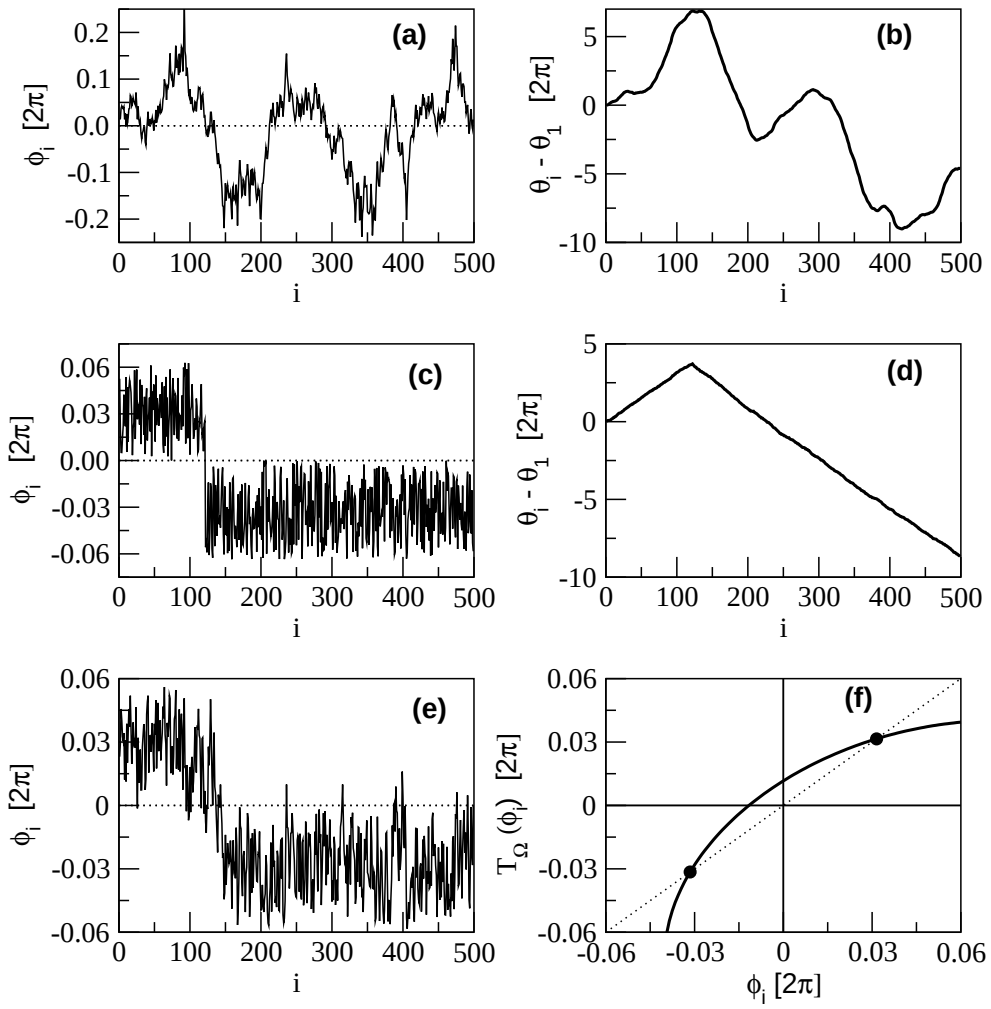


Figure 4.13: Figure (Fig.2) in [10]. Phase differences $\phi_i = \vartheta_{i+1} - \vartheta_i$ (left) and phase profile $\vartheta_i - \vartheta_1$ (b,d) in units of $2\pi$ for a chain of 500 phase oscillators (Eq. 4.27) with uniformly distributed frequencies $\omega_i \in [-0.1, 0.1]$ and open boundaries. (a,b) antisymmetric coupling $g(\delta\vartheta) = \sin\Delta\vartheta$. (c,d) unidirectional coupling $g(\Delta\vartheta) = (\Delta\vartheta + |\Delta\vartheta|)/2$. (e) Synchronized phase profile of the dynamics (Eq. 4.27) with $\gamma = 2$. (f) Transfer map $T_\Omega(\phi_i)$ (Eq. 4.31, solid line) obtained from the phase profile in subfigure (e) and fixed points $\phi^*$ (filled circles).

In the limit $\gamma\sigma \to 0$ the next neighbor correlation $r$ between the phase differences becomes one, corresponding to a random walk at $\gamma = 0$ or the homogeneous phase profile at $\sigma = 0$. At the same time the regularity measure $Q_\psi$ goes to zero.

Only by measuring the shift of synchronization frequency in a one dimensional chain of phase oscillators the characteristic phase difference $\varphi^*$ and thus the wave length $\Lambda$, the next neighbor correlation $r$ of phase differences and the regularity $Q_\psi$ can be determined (Eqs. 4.32, 4.33, 4.35, 4.38, 4.39). Moreover, the quantities $\gamma(\Omega - \bar{\omega})$, $\Lambda/\gamma$, $r$ and $Q_\psi$ are functions of the combined parameter $\gamma\sigma$ (Fig. 4.14) demonstrating the intricate relationship between nonisochronicity and heterogeneity in the formation of quasi-regular concentric waves.

By increasing the heterogeneity $\sigma$ the system will leave the region $\Delta\omega(S)$ of stability at some point leading to phase slips and eventually phase turbulence (Figs. 4.12g-i, 4.16e,f). For nonisochronicities $\gamma \gtrsim 2$ in a small parameter region before desynchronization we observe phase profiles of very high regularity $Q_\psi$. The two fixed points $\pm\varphi^*$ become very well separated while the variance $\mathrm{var}(\psi)$ does not change much. This regime coincides with a negative coefficient of correlation $r$ signifying that the fixed point $\varphi^*$ is located to the right of the local maximum of the transfer map. In simulations (Fig. 4.16) we find multistability in this regime. However, the number of different stable synchronized states with comparatively large basins of attraction does not increase much with the system size.

Unfortunately, the transfermap formalism is restricted to the one dimensional case. In two dimensions the scaled frequency shift $\gamma(\Omega - \bar{\omega})$ and the wave length $\Lambda/\gamma$ are also related via the combined parameter $\sigma\gamma$. This relation however can only be determined experimentally. In fact, the wavelength and measures of regularity in two dimensional media can be derived from a Fourier analysis (Fig. 4.12) but do not yield very accurate results, calling for large ensemble averages. Furthermore, wavelengths that are larger than the system size cannot be resolved.

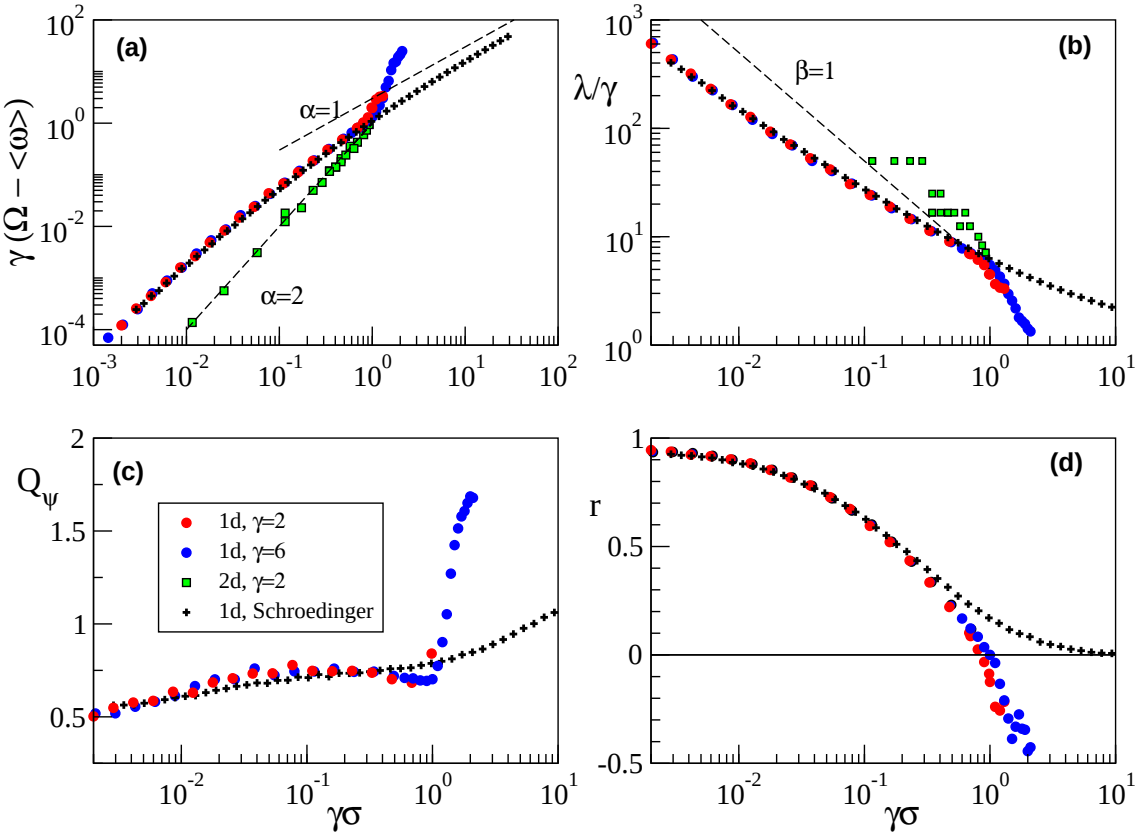


Figure 4.14: Figure (Fig.2) taken from our publication [10]. Shown are the scaled mean frequency shift $\gamma(\Omega - \bar{\omega})$ (a), the scaled wavelength $\lambda/\gamma$ (b), the regularity parameter $Q_\psi = \varphi^*/\mathrm{var}|\varphi|$ (c) and the correlation $r$ of neighboring phase differences (d). We have simulated chains of $N = 500$ oscillators with open boundary conditions and nonisochronicities $\gamma = 2$ (blue dots) and $\gamma = 6$ (red dots). The measurements are averages over 50 runs with different realizations of random frequencies and homogeneous initial conditions until synchronization was reached. The black dots are the corresponding measures taken from the exponential approximation and solving the stationary Schrödinger equation (Sec. 4.4.3). The green squares are measurements on synchronized phase profiles from a single frequency realizations in a $100 \times 100$ square lattice and phase oscillators with nonisochronicity $\gamma = 2$. The wavelength was obtained for one dimension from (Eq. 4.33) and in the two-dimensional system from a Fourier analysis of the phase profile (see Fig. 4.12). The dashed lines are auxiliary power laws with exponents $\alpha$ (a) and $-\beta$ (b) and can be compared with the actual scaling.

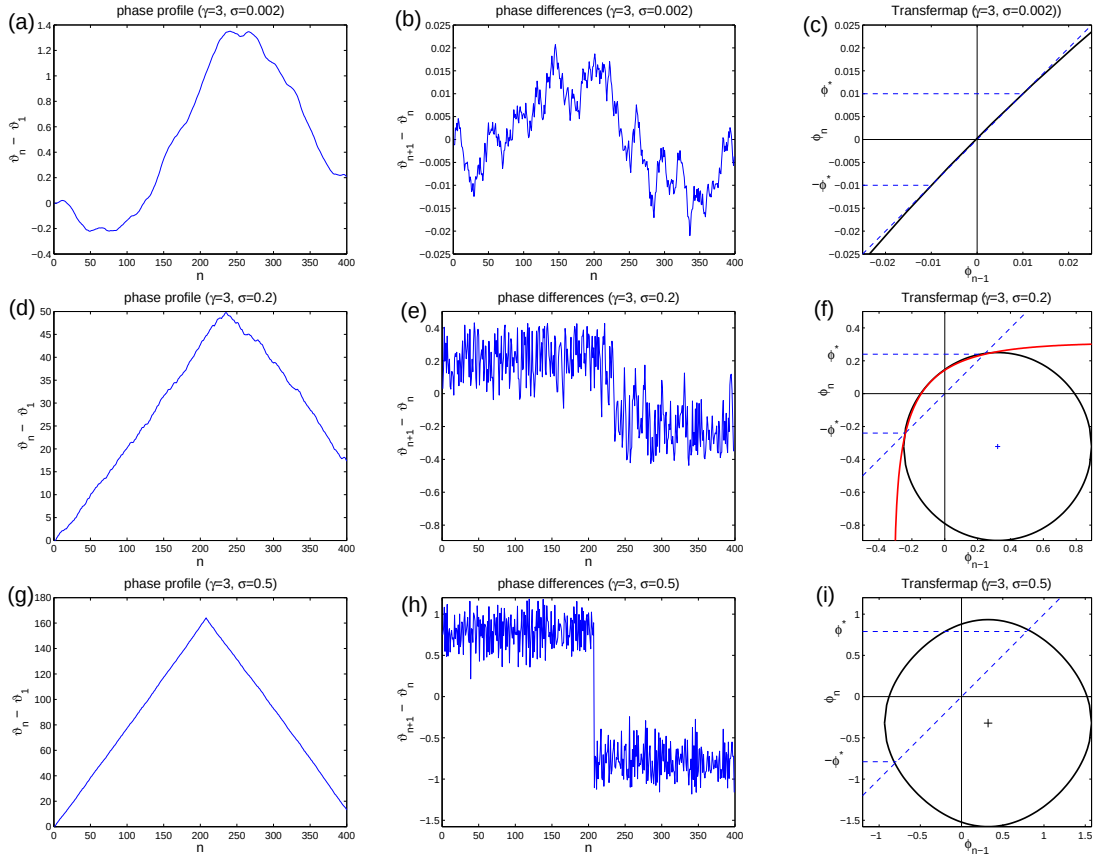


Figure 4.15: phase profiles and next neighbor phase differences for a chain of $N = 400$ nonidentical nonisochronous ($\gamma = 3$) Kuramoto phase oscillators. The frequencies $\omega_n = \sigma\eta_n$ differ only by the heterogeneity factor $\sigma = 0.002$ (a-c) , $\sigma = 0.2$ (d-f) and $\sigma = 0.5$ (f-i). Note the different scales in the corresponding figures. The $\eta_n$ have been drawn from a uniform distribution of variance one. Subfigures (a,d) and (g) show the stationary phase profiles $\vartheta_n - \vartheta_1$ in phase locked synchronization. In the middle column are shown the next neighbor phase differences of the phase profiles. We distinguish three regimes. For very low disorder (b) the phase differences seem to perform a random walk. The transition to a regime with clearly developed mean phase difference (e) for higher disorder is gradually. Only for nonisochronicities $\gamma > 2$ there is a third regime at disorders in the vicinity of the desynchronization transition. The two branches are pulled apart resulting in highly regular concentric waves of very short lengths. The last column (c,f,i) shows the transfer map (Eq. 4.31) deduced from the experimentally established synchronization frequency $\Omega$. The red line in subfigure (f) is the corresponding transfer map obtained from the exponential approximation (Eq. 4.48). This map was omitted in subfigure (c) because it is indistinguishable from the exact transfer map and in subfigure (i) because here the exponential approximation is not valid anymore. The fixed points (Eq. 4.32 have changed side with the maximum of the transfer map.

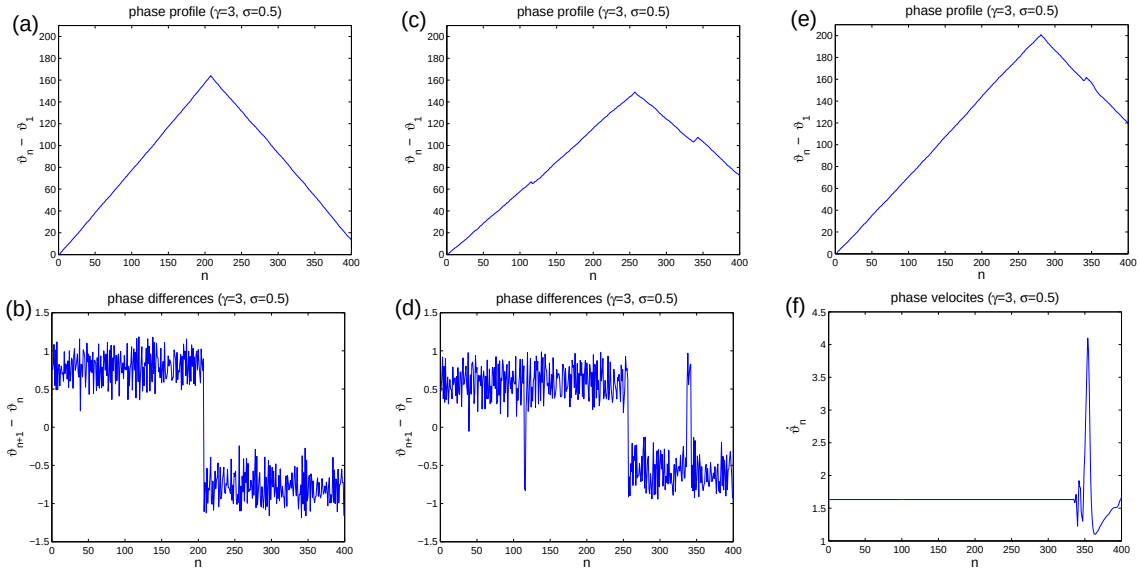


Figure 4.16: For nonisochronicities $\gamma^2 > 3$ we have found multistability in a chain of three nonidentical phase oscillators. Here we show three different phase profiles (chain, open boundary conditions) after a transient time from random initial conditions but with the same realization of random frequencies, $\sigma = 0.5$ and $\gamma = 3$. We used, in fact, the same frequencies $\eta_n$ as in Fig. 4.15. The four panels (a-d) show two stationary phase profiles and their next neighbor phase differences. These are two different synchronized states of the same system. The last two figures (e,f) show the same system in a nonstationary state, where one part of the chain is in synchrony but phase slips occur at the right end of the chain. This can be seen from figure (f) where the phase velocities are shown.

### 4.4.2 Gauge field for topological charges and exponential approximation

In a continuous oscillatory reaction diffusion system Kuramoto (Chap. 2, [1]) derived the nonlinear phase diffusion equations

$$\dot{\vartheta} = \omega(\mathbf{r}) + \alpha\nabla^2\vartheta + \beta(\nabla\vartheta)^2 \qquad . \tag{4.42}$$

For these equations a Cole-Hopf transformation

$$\vartheta = \frac{\alpha}{\beta}\ln\mathbf{q} \tag{4.43}$$

converts the nonlinear PDE (Eq. 4.42) into a linear system

$$\begin{aligned}
\nabla\vartheta &= \frac{\alpha}{\beta}\,\frac{\nabla\mathbf{q}}{\mathbf{q}} \\
\nabla^2\vartheta &= \frac{\alpha}{\beta}\,\frac{\mathbf{q}\nabla^2\mathbf{q} - (\nabla\mathbf{q})^2}{\mathbf{q}^2} \\
\dot{\vartheta} &= \frac{\alpha}{\beta}\,\frac{\dot{\mathbf{q}}}{\mathbf{q}} \;=\; \omega(\mathbf{r}) + \frac{\alpha^2}{\beta}\,\frac{\mathbf{q}\nabla^2\mathbf{q} - (\nabla\mathbf{q})^2}{\mathbf{q}^2} + \frac{\alpha^2}{\beta}\,\frac{(\nabla)\mathbf{q}^2}{\mathbf{q}^2}
\end{aligned} \tag{4.44}$$

and after rearranging

$$\dot{\mathbf{q}} \;=\; -\left[-\frac{\beta}{\alpha}\omega(\mathbf{r}) - \alpha\nabla^2\right]\mathbf{q} \;=\; -\,\mathbf{H}\,\mathbf{q} \qquad . \tag{4.45}$$

The linear second order differential operator $\mathbf{H}$ is the Hamiltonian of a particle moving in a potential $V(\mathbf{r}) = -\omega(\mathbf{r})\beta/\alpha$.

The Cole-Hopf transformation (Eq. 4.43) comes with some pitfalls. On one hand, the dynamics (Eq. 4.45) must guarantee that the function $q(\mathbf{r})$ remains real and positive for all times. And secondly, periodic boundary conditions with $\vartheta + 2\pi l = \vartheta$ cannot be realized with a continuous function $\mathbf{q}$. The synchronized solution obtained by this ansatz is uniquely determined by the equation (Eq. 4.45), and no topological charges are possible. We address this second problem by introducing a stationary gauge field $\vartheta^0$ of which we assume that the first and second derivatives exist (no phase singularities) and which incorporates all topological charges. The deviation $\varphi = \vartheta - \vartheta^0$ can also be transformed as

$$\varphi = \frac{\alpha}{\beta}\ln\mathbf{q} \tag{4.46}$$

to obtain linear equations

$$\begin{aligned} \dot{\mathbf{q}} &= -\left[-\frac{\beta}{\alpha}\omega(\mathbf{r}) - \beta\nabla^2\vartheta^0 - \frac{\beta^2}{\alpha}(\nabla\vartheta^0)^2 - 2\beta\nabla\vartheta^0\nabla - \alpha\nabla^2\right]\mathbf{q} \\ &= -\left[\mathbf{V}_\omega - \tilde{\mathbf{L}}\right]\ \mathbf{q} \ = \ -\tilde{\mathbf{H}}\ \mathbf{q} \end{aligned} \tag{4.47}$$

$$V_\omega(\mathbf{r}) = -\frac{\beta}{\alpha}\omega(\mathbf{r}) \qquad \tilde{\mathbf{L}} = \left[\beta\nabla^2\vartheta^0 + \frac{\beta^2}{\alpha}(\nabla\vartheta^0)^2 + 2\beta\nabla\vartheta^0\nabla + \alpha\nabla^2\right]$$

The linear operator $-\tilde{\mathbf{H}}$ is not necessarily hermitian, but has the same eigenvalues as $-\mathbf{H}$ if $\vartheta^0$ has no topological charges. In that case the two differential operators are just similar with a local scaling $\mathbf{q} \leftrightarrow \mathbf{q}\ e^{\frac{\beta}{\alpha}\vartheta^0}$. If $\vartheta^0$ does have topological charges, then eigenvalues may come in complex conjugated pairs indicating damped oscillations during the transient to synchronization.

This method of transformation for the continuous equations encouraged us to look for a similar ansatz for a general network (Eq. 4.26) of Kuramoto phase oscillators. A Cole-Hopf transformation does not yield immediate success. The idea of the exponential approximation is to replace the harmonic phase coupling function with a different functional form but with identical Taylor expansion around zero up to the second order

$$\tilde{g}(\Delta\vartheta) \ = \ \frac{1}{\gamma}\left(e^{\gamma\Delta\vartheta} - 1\right) \ = \ \sin\Delta\vartheta + \gamma\left(1 - \cos\Delta\vartheta\right) \ + \ O(\Delta\vartheta^3) \tag{4.48}$$

and with $\omega_n = \sigma\eta_n$

$$\dot{\vartheta}_n \approx \sigma\eta_n + \sum_m A_{nm}\ \tilde{g}(\vartheta_m - \vartheta_n) \qquad . \tag{4.49}$$

A similar method is sometimes used to find soliton solutions in discrete media where the interaction potential is approximated by a function with similar properties locally but that allows for an analytical treatment [71]. The approximation (Eq. 4.48) has very similar curvature to the actual phase coupling function for small to intermediate phase differences (Figs. 4.17, 4.15f) but is monotonous globally.

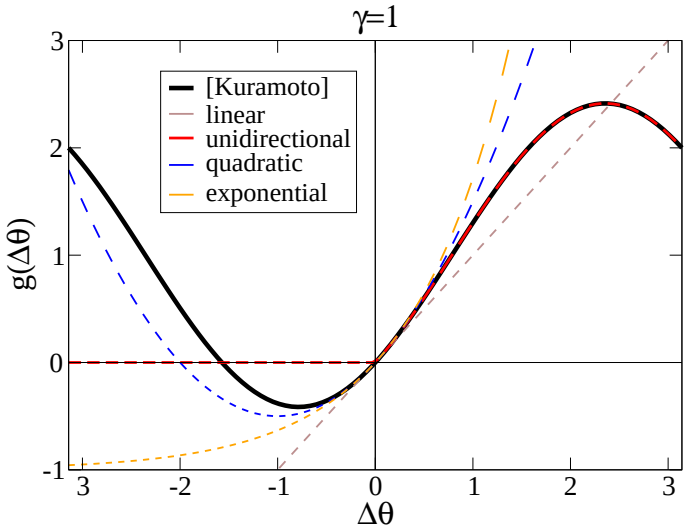


Figure 4.17: For small phase differences at synchronization only the local shape of the phase coupling function plays a role. In the vicinity of a synchronization manifold different approximations of the coupling function are possible. A linear approximation (brown dashed line) makes the Kuramoto model solvable but will not allow for the effect of asymmetry. A unidirectional coupling function (red dashed line) has conceptual advantages but is a poor approximation. A parabolic second order approximation (blue dashed line) gives good simulation results but is analytically not feasible. The exponential approximation (Eq. 4.48, yellow dashed line) is also of order two in the phase differences but allows for an analytical treatment via Cole-Hopf transformation (Eqs. 4.50, 4.51).

As in the continuous case, we want, nevertheless, allow for topological charges. We look therefore at the deviation $\varphi = \vartheta - \vartheta^0$ from a stationary gauge field $\vartheta^0$. The phase dynamics in the vicinity of a gauge field with small phase differences are then

$$\dot{\varphi}_n = \sigma\eta_n + \frac{1}{\gamma}\sum_m A_{nm}\left(e^{\gamma\left(\vartheta^0_{mn}+\varphi_{mn}\right)} - 1\right) \tag{4.50}$$

with phase differences $\vartheta^0_{mn} = (\vartheta^0_m - \vartheta^0_n)$ and $\varphi_{mn} = (\varphi_m - \varphi_n)$ both modulo $[-\pi, \pi)$. It is now possible to apply a Cole-Hopf transformation $\varphi_n = \frac{1}{\gamma}\ln q_n$ resulting in the linear set of equations

$$\dot{q}_n = \sigma\gamma\eta_n q_n + \sum_m A_{nm}\left(e^{\gamma\vartheta^0_{mn}}\ q_m - q_n\right) \tag{4.51}$$

or with $\varepsilon = \sigma\gamma$ and $\mathbf{V}_\eta = -\mathrm{diag}(\eta)$ in vector form

$$\dot{\mathbf{q}} \ = \ -\left[\varepsilon\mathbf{V}_\eta - \tilde{\mathbf{L}}\right]\mathbf{q} \ = \ -\tilde{\mathbf{H}}\ \mathbf{q} \tag{4.52}$$

$$\tilde{L}_{nm} \ = \ A_{nm}\ e^{\gamma\vartheta^0_{mn}} - \delta_{nm}\sum_k A_{nk}$$

This equation is the discrete equivalent of (Eq. 4.47). We will see in the next section that the synchronized solution $\dot{\varphi} = \Omega$ of equation (Eq. 4.50) is directly related to an eigenvector of $\tilde{\mathbf{H}}$ which for a moderately small network $N < 500$ can efficiently be calculated numerically. The linear operator $\tilde{\mathbf{L}}$ is the network Laplacian if $\vartheta^0$ is uniform. Otherwise, for instance in the presence of topological charges, $\tilde{\mathbf{H}}$ is not symmetric and its eigenvalues and eigenvectors may have nonvanishing imaginary components.

### 4.4.3 Solution of the stationary Schrödinger equation and resulting phase profiles

Given a realization of frequencies in a discrete or continuous medium the stationary phase profile in synchronization is related to the asymptotic solution of a linear equation

$$\dot{\mathbf{q}} \;=\; -\,\tilde{\mathbf{H}}\,\mathbf{q} \qquad . \tag{4.53}$$

We will use $q(\mathbf{r})$ to denote the value of a function $\mathbf{q}$ either at a vertex of a network or at a position $\mathbf{r}$ in a continuous medium and $\mathbf{q}(t)$ to denote a function $\mathbf{q}$ at some time $t$. Given a complete set of left and right eigenvectors $\mathbf{Q}_k$ and $\mathbf{q}_k$ of $-\tilde{\mathbf{H}}$ and corresponding eigenvalues $E_k$ the solution $\mathbf{q}(t)$ is formally

$$\mathbf{q}(t) = \sum_k e^{E_k t}\ \left(\mathbf{Q}_k^\dagger \cdot \mathbf{q}(0)\right)\ \mathbf{q}_k \qquad . \tag{4.54}$$

Here we assume that $\tilde{\mathbf{H}}$ has a discrete spectrum. Asymptotically the solution $\mathbf{q}(t)$ will become parallel to the eigenvector $\mathbf{q}_{\max}$ corresponding to the eigenvalue $E_{\max}$ of $-\tilde{\mathbf{H}}$ with the largest real part because the component in this direction, if it is not zero initially, will outgrow all other directions exponentially

$$e^{-E_{\max}t}\ \mathbf{q}(t) = \sum_k e^{(E_k - E_{\max})t}\ \left(\mathbf{Q}_k^\dagger \cdot \mathbf{q}(0)\right)\ \mathbf{q}_k \qquad . \tag{4.55}$$

Taking the limit $t \to \infty$ the right hand side becomes proportional to $\mathbf{q}_{\max}$. In the original variables this means

$$\lim_{t\to\infty}\left(\varphi(t) - \frac{1}{\gamma}E_{\max}\ t\right) = \frac{1}{\gamma}\ln \mathbf{q}_{\max} + C \tag{4.56}$$

$$\lim_{t\to\infty}\left(\varphi(\mathbf{r},t) - \varphi(\mathbf{r}',t)\right) = \frac{1}{\gamma}\ln\left(\frac{q_{\max}(\mathbf{r})}{q_{\max}(\mathbf{r}')}\right) \tag{4.57}$$

or

$$\lim_{t\to\infty}\dot{\varphi}(t) = \frac{1}{\gamma}E_{\max} = \Omega \tag{4.58}$$

These equations beautifully express the relation between the phases $\vartheta = \vartheta^0 + \varphi$ in synchrony and the eigenvector $\mathbf{q}_{\max}$ of the operator $\tilde{\mathbf{H}}$. All other eigenvalues and eigenvectors correspond to damped modes during the transient to synchronization and non vanishing imaginary parts indicate an oscillatory approach to the synchronization manifold.

Since the pioneering work of Anderson [72] it has been recognized that the eigenfunctions of a Hamiltonian with a sufficiently strong diagonal disorder can be localized exponentially, i.e.

$$\mathbf{E}\left[\vartheta(\mathbf{r}_0) - \vartheta(\mathbf{r})\right] = \frac{1}{\gamma}\mathbf{E}\left[\ln\left(\frac{q_{\max}(\mathbf{r}_0)}{q_{\max}(\mathbf{r})}\right)\right] = \frac{2\pi}{\Lambda}\, d(\mathbf{r}_0, \mathbf{r}) \tag{4.59}$$

where $\mathbf{r}_0$ is the position where $\mathbf{q}_{\max}$ is localized, $d(\mathbf{r}_0, \mathbf{r})$ is the distance in the system and $\Lambda$ is a characteristic wavelength. When the localization length of the eigenfunctions in the conduction band of a disordered medium becomes smaller than its length a conductor-insulator transition is observed. Discrete equations of the form (Eq. 4.52) are actually an approximation for strongly localized potentials (tight binding approximation) and often used in the literature about Anderson localization to obtain analytical or simulation results [73, 74] (see App. E).

Both the ground state eigenvalue $E_{\max} = E_{\max}(\varepsilon)$ and the localization length $\lambda = \lambda(\varepsilon)$ of the corresponding eigenvector are random variables but their expected values depend on the strength $\varepsilon$ of the disorder. From (Eqs. 4.57, 4.58) we find the relations

$$\begin{aligned} \gamma\Omega &= E_{\max}(\varepsilon) \\ \frac{\Lambda}{\gamma} &= \lambda(\varepsilon) \qquad . \end{aligned} \tag{4.60}$$

If in some asymptotic regime the eigenvalue and the localization length scale as $(E_{max} - \varepsilon\bar{\eta}) \sim \varepsilon^{\alpha}$ and $\lambda \sim \varepsilon^{-\beta}$ (see Chap. 5 and App. E) we obtain the scaling relations published in [10]

$$\begin{aligned} \Omega - \bar{\omega} &\sim \gamma^{\alpha-1}\sigma^{\alpha} \\ \Lambda &\sim \gamma^{1-\beta}\sigma^{-\beta} \qquad . \end{aligned} \tag{4.61}$$

The relations (Eq. 4.61) are confirmed by direct simulations of one and two dimensional lattices of phase oscillators and no topological charges (Fig. 4.14). For the one dimensional chain we compare the simulations with the results obtained from directly computing the eigenfunction $\mathbf{q}_{\max}$ of $\tilde{\mathbf{H}}$ defined in (Eq. 4.52).

We have to remark that numerical difficulties in computing $\mathbf{q}_{\max}$ can arise

for very short localization lengths compared with the system size. Then the values $q_{\max}(\mathbf{r})$ needed to calculate the phase profile can range over hundreds of orders of magnitude. This can be amended by a good choice of gauge $\vartheta^0$ or by calculating $\mathbf{q}_{\max}$ up to possible precision, changing back to phase variables $\vartheta$ and refining the solution with a Newton method (App. B), direct integration or other heuristic methods.

# Chapter 5

# Perturbation Approach to the Synchronization Frequency

The previous chapters were concerned with general properties of the solutions for the Kuramoto phase equations in synchronization. We have dealt with the difficulties that arise from inverting the function $\Delta\omega(T^{N-1})$, that is, to find the relative phases $\Delta\vartheta \in T^{N-1}$ in synchronization for a realization of relative frequencies $\Delta\omega \in \mathbb{R}^{N-1}$. We could find global solutions, qualitative descriptions and local approximations. Here we will continue in a systematic manner to explore the behavior of a synchronization manifold in response to changes in the natural frequencies in the system. In linear approximation the inverse of a function is locally given by the inversion of a Jacobian. Iterating such an inversion the phase profile of a system of phase oscillators is readily obtained by a Newton method (see App. B). A similar approach is to solve a perturbation series. Such a perturbation series can directly be obtained for the Kuramoto phase equations (Sec. 5.1) or for the linear equations (Eqs. 4.47, 4.52) in Section 5.2.

## 5.1 Perturbation approach for the Kuramoto Phase Equations

For a given field $\omega(\mathbf{r}) = \sigma\eta(\mathbf{r})$ of frequencies we are looking for a solution $\vartheta$ to

$$\Omega = \sigma\eta(\mathbf{r}) + \alpha\nabla^2\vartheta + \beta\left(\nabla\vartheta\right)^2 \qquad . \tag{5.1}$$

Let $\vartheta^0$ be a solution to

$$\Omega^0 = \alpha\nabla^2\vartheta^0 + \beta\left(\nabla\vartheta^0\right)^2 \tag{5.2}$$

for identical oscillators. We consider the deviations $\varphi = \vartheta - \vartheta^0$ with an additional constraint

$$(\mathbf{1}^\dagger \cdot \varphi) = 0 \tag{5.3}$$

were $\mathbf{1}$ is the constant function of unit amplitude. We assume that for small $\sigma$ a solution to (Eqs. 5.1, 5.3) exists and that its Taylor series around zero is absolute convergent. For $\sigma = 0$ the solution obeys (Eq. 5.2). We make the perturbation ansatz

$$\vartheta \;=\; \vartheta^0 + \;\varphi \;=\; \vartheta^0 + \sigma\vartheta^I + \sigma^2\vartheta^{II} + O(\sigma^3) \tag{5.4}$$

and

$$\Omega \;=\; \Omega^0 + \sigma\Omega^I + \sigma^2\Omega^{II} + O(\sigma^3) \tag{5.5}$$

Inserting (Eq. 5.4) into (Eq. 5.1), using (Eq. 5.2) and rearranging the sums we obtain

$$\Omega\ \mathbf{1} \;=\; \Omega^0\ \mathbf{1} + \sum_{j=1}^{\infty} \sigma^j \left(\mathbf{L}\vartheta^{(j)} + \mathbf{b}^{(j)}\right) \tag{5.6}$$

with $j^{\text{th}}$ order perturbation terms $\vartheta^{(j)}$ and

$$\begin{aligned} \mathbf{L} \;&=\; \left[2\beta\nabla\vartheta^0\nabla + \alpha\nabla^2\right] \\ b^{(1)}(\mathbf{r}) \;&=\; \eta(\mathbf{r}) \\ b^{(j>1)}(\mathbf{r}) \;&=\; \beta\sum_{i=1}^{j-1} \nabla\vartheta^{(i)}\nabla\vartheta^{(j-i)} \end{aligned} \tag{5.7}$$

Note, that the functions $\mathbf{b}^{(j)}$ only depend on perturbation terms $\vartheta^{(i)}$ with $i < j$. The differential operator $\mathbf{L}$ is not hermitian if the gauge field solution $\nabla\vartheta^0 \neq 0$ is not homogeneous.

The same perturbation ansatz can be made for the discrete Kuramoto phase equation in synchronization

$$\Omega = \sigma\eta_n + \sum_m A_{nm} g(\vartheta_m - \vartheta_n) \qquad n = 1 \ldots N \tag{5.8}$$

and a gauge field that yields

$$\Omega^0 = \sum_m A_{nm} g(\vartheta^0_m - \vartheta^0_n) \qquad n = 1 \ldots N. \tag{5.9}$$

The perturbation terms are formally derived by using the Taylor expansion of $g(\Delta\vartheta^0 + \Delta\varphi)$ and then collecting the terms proportional to powers of $\sigma$ from the powers of $\Delta\varphi$. For simplicity let us denote $g_{mn} = g(\vartheta^0_m - \vartheta^0_n)$.

$$\Omega = \sigma\eta_n + \sum_m A_{nm} \sum_{j=0}^{\infty} \frac{1}{j!}\, \partial^j g_{mn} \cdot (\varphi_m - \varphi_n)^j \tag{5.10}$$

and after rearranging, using (Eqs. 5.9, 5.4) and writing the equations in vector form one obtains

$$\Omega \mathbf{1} = \Omega^0 \mathbf{1} + \sum_{j=1}^{\infty} \sigma^j \ \left( \mathbf{L} \vartheta^{(j)} + \mathbf{b}^{(j)} \right) \tag{5.11}$$

with

$$\mathbf{L}_{nm} = A_{nm} g'_{mn} - \delta_{nm} \sum_j A_{nj} g'_{jn} \qquad . \tag{5.12}$$

Here $\vartheta^{(j)}$ is the $j^{\text{th}}$ order perturbation term in (Eq. 5.4) and $\mathbf{b}^{(j)}$ is a vector that depends nonlinearly on perturbation terms $\vartheta^{(i)}$ with $i$ strictly smaller than $j$. The first three vectors $\mathbf{b}^I$, $\mathbf{b}^{II}$ and $\mathbf{b}^{III}$ are given by

$$\begin{aligned} b_n^I &= \eta_n \\ b_n^{II} &= \sum_m A_{nm} \frac{1}{2} \ g''_{mn} {\vartheta^I_{mn}}^2 \\ b_n^{III} &= \sum_m A_{nm} \left( g''_{mn} \vartheta^I_{mn} \vartheta^{II}_{mn} + \frac{1}{6} \ g'''_{mn} {\vartheta^I_{mn}}^3 \right) \end{aligned} \tag{5.13}$$

Again, for a shorter notation we have used $\vartheta^{(j)}_{mn} = \vartheta^{(j)}_m - \vartheta^{(j)}_n \mod [-\pi, \pi)$. Equation (Eq. 5.11) is the equivalent of equation (Eq. 5.6) for continuous systems.

Let us suppose the spectrum of $\mathbf{L}$ is discrete and left and right eigenvectors are complete and normalized, i.e.

$$\begin{aligned} \mathbf{L}\mathbf{p}_k &= E_k \ \mathbf{p}_k & \mathbf{L}^\dagger \mathbf{P}_k &= E_k^* \ \mathbf{P}_k \\ \mathbf{P}_k^\dagger \cdot \mathbf{p}_{k'} &= \delta_{kk'} & \sum_k \mathbf{p}_k \mathbf{P}_k^\dagger &= \mathbb{I} \qquad . \end{aligned} \tag{5.14}$$

We see from (Eqs. 5.7, 5.12) that the constant function $\mathbf{p}_0 \sim \mathbf{1}$ is an eigenfunction of $\mathbf{L}$ to the eigenvalue zero. Multiplying equation (Eq. 5.11) from the left with

$$\tilde{\mathbf{P}}_0^\dagger = \frac{\mathbf{P}_0^\dagger}{(\mathbf{P}_0^\dagger \cdot \mathbf{1})} \tag{5.15}$$

we obtain the perturbation expansion of the frequency $\Omega$

$$\Omega = \Omega^0 + \sum_{j=1}^{\infty} \sigma^j \left( \tilde{\mathbf{P}}_0^\dagger \cdot \mathbf{b}^{(j)} \right) \qquad . \tag{5.16}$$

This equation multiplied by $\mathbf{1}$ and subtracted from (Eq. 5.11) leads to a linear equation for each order $j$ of the perturbation series

$$\mathbf{L}\vartheta^{(j)} + \left(\mathbb{I} - \mathbf{1}\ \tilde{\mathbf{P}}_0^\dagger\right)\mathbf{b}^{(j)} = 0 \tag{5.17}$$

which, in a subspace orthogonal to $\mathbf{p}_0$, can be solved successively for each order of perturbation

$$\vartheta^{(j)} = -\sum_{k\neq 0} \frac{\left(\mathbf{P}_k^\dagger \cdot \mathbf{b}^{(j)}\right)}{E_k}\ \left(\mathbf{p}_k - \frac{(\mathbf{1}^\dagger \cdot \mathbf{p}_k)}{(\mathbf{1}^\dagger \cdot \mathbf{p}_0)}\mathbf{p}_0\right) \quad . \tag{5.18}$$

This expression solves (Eq. 5.17) and (Eq. 5.3).

We want to direct the attention to the role of $\tilde{\mathbf{P}}_0^\dagger$ in equation (Eq. 5.16). In first order of $\sigma$ the correction to the synchronization frequency is $\Omega \approx \Omega^0 + \sigma\ \tilde{\mathbf{P}}_0^\dagger \cdot \eta$. The vector $\tilde{\mathbf{P}}_0^\dagger$ assigns to each point of the system a weight that characterizes the influence that a local change of frequency has on the global synchronization frequency. If the gauge $\vartheta^0$ is homogeneous then the Laplacian $\mathbf{L}$ is symmetric and $\tilde{\mathbf{P}}_0 \parallel \mathbf{1}$. Only in the presence of topological charges is it possible for some vertices to have a higher influence on the synchronization frequency than others (Fig. 4.1c). Moreover, equivalent points with respect to a symmetry of $\mathbf{L}$ have identical entries in the corresponding components of $\tilde{\mathbf{P}}_0$. In a completely homogeneous arrangement the left eigenvector $\tilde{\mathbf{P}}_0$ is therefore uniform as well, even if the gauge is not homogeneous. This will be the case in the example studied in Section 5.3, the regular lattice of phase oscillators and periodic boundary conditions, with topological charge. Then the first correction to the synchronization frequency is

$$\Omega^I = \tilde{\mathbf{P}}_0^\dagger \eta = \bar{\eta} \tag{5.19}$$

and in the continuous case the second order correction is

$$\Omega^{II} = \beta \sum_{k,k'\neq 0} \frac{(\mathbf{P}_k^\dagger \cdot \eta)(\eta^\dagger \cdot \mathbf{P}_{k'})}{E_k E_{k'}^*}\ \frac{(\mathbf{p}_{k'}^\dagger \nabla^\dagger \cdot \nabla \mathbf{p}_k)}{|\mathbf{P}_0^\dagger \cdot \mathbf{1}|^2} \quad . \tag{5.20}$$

In the next section we derive expressions for the perturbation terms of the synchronization frequency from the linear equations (Eq. 4.47) and (Eq. 4.52). These expressions have to be compared with the terms we find directly from the Kuramoto phase equations. For continuous systems the Cole-Hopf transformation (Eq. 4.46) is exact. In a discrete system on the other hand we solve two different

problems

$$\begin{aligned} \Omega^0 &= \sum_{m=1}^{N} A_{nm}\; g\left(\vartheta_m^0 - \vartheta_n^0\right) \\ \Omega &= \omega_n + \sum_{m=1}^{N} A_{nm}\; g(\vartheta_m - \vartheta_n) \qquad n = 1 \ldots N \end{aligned} \tag{5.21}$$

and

$$\begin{aligned} \tilde{\Omega}^0 &= \sum_{m=1}^{N} A_{nm}\; \tilde{g}\left(\tilde{\vartheta}_m^0 - \tilde{\vartheta}_n^0\right) \\ \tilde{\Omega} &= \omega_n + \sum_{m=1}^{N} A_{nm}\; \tilde{g}(\vartheta_m - \vartheta_n) \qquad n = 1 \ldots N \quad . \end{aligned} \tag{5.22}$$

Only if the gauge field solutions $\tilde{\vartheta}^0 = \vartheta^0$ are identical the first and the second derivatives of the coupling function $g'_{mn} = \tilde{g}'_{mn}$ and $g''_{mn} = \tilde{g}''_{mn}$ are also identical. In this case the Laplacian $\mathbf{L}$ and the vectors $\mathbf{b}^I$ and $\mathbf{b}^{II}$ (Eq. 5.13) are identical for both problems giving exactly the same first and second order perturbation correction.

## 5.2 Perturbation approach for the exponential approximation

In Sections 4.4.2 and 4.4.3 we showed how the Kuramoto phase equations can be transformed so that finding a synchronized solution becomes the eigenvalue problem of a linear operator. Perturbation theory for a linear system of the form

$$\dot{\mathbf{q}} = -\left[\varepsilon \mathbf{V}_\eta - \tilde{\mathbf{L}}\right] \mathbf{q} = -\tilde{\mathbf{H}}\, \mathbf{q} \tag{5.23}$$

and small perturbations $\varepsilon \mathbf{V}_\eta$ is well established in quantum mechanics (i.e. [75]). The difference here is, that in the presence of topological charges the operator $\tilde{\mathbf{L}}$ does not need to be symmetric or hermitian. Nevertheless Schrödinger perturbation theory can be applied if one distinguishes carefully between left and right eigenvectors. We suppose that the spectrum of $\tilde{\mathbf{L}}$ is discrete and denote the left and right eigenvectors of $\tilde{\mathbf{L}}$ as $\mathbf{Q}_k^0$ and $\mathbf{q}_k^0$ and those of $\tilde{\mathbf{H}}$ as $\mathbf{Q}_k$ and $\mathbf{q}_k$, respectively. Additionally we use the normalization $\mathbf{Q}_k^{0\dagger} \cdot \mathbf{q}_{k'}^0 = \mathbf{Q}_k^\dagger \cdot \mathbf{q}_{k'} = \delta_{kk'}$ and note explicitely that $\mathbf{q}_{\max}^0 = \mathbf{q}_0^0 = \mathbf{1}$. A global phase shift displacement from the gauge field is necessarily the vector with the largest eigenvalue real part if the gauge field belongs to a stable synchronization manifold. The perturbation

series in $\varepsilon$ for the eigenvalues $E_k$ of $-\tilde{\mathbf{H}}$ is then

$$\begin{aligned} E_k &= E_k^0 + \varepsilon E_k^I + \varepsilon^2 E_k^{II} + O(\varepsilon^3) \\ &= E_k^0 - \varepsilon \left( \mathbf{Q}_k^{0\dagger} \cdot \mathbf{V}_\eta \mathbf{q}_k^0 \right) + \varepsilon^2 \sum_{k' \neq k} \frac{\left( \mathbf{Q}_k^{0\dagger} \cdot \mathbf{V}_\eta \mathbf{q}_{k'}^0 \right) \left( \mathbf{Q}_{k'}^{0\dagger} \cdot \mathbf{V}_\eta \mathbf{q}_k^0 \right)}{E_k^0 - E_{k'}^0} + O(\varepsilon^3) \end{aligned} \tag{5.24}$$

The perturbation terms for $\Omega$ and $E_{\max}$ are related as $\Omega^I = E_{\max}^I$ and $\Omega^{II} = \gamma E_{\max}^{II}$. As in the previous section we find that the first order perturbation term

$$\Omega^I = \mathbf{Q}_{\max}^{0\dagger} \cdot \eta \tag{5.25}$$

is equal to a weighted average of natural frequencies. And the second order correction is

$$\Omega^{II} = \gamma \sum_{k \neq 0} \frac{\left( \mathbf{Q}_0^{0\dagger} \cdot \mathbf{V}_\eta \mathbf{q}_k^0 \right) \left( \mathbf{Q}_k^{0\dagger} \cdot \mathbf{V}_\eta \mathbf{q}_0^0 \right)}{E_0^0 - E_k^0} \quad . \tag{5.26}$$

In quantum mechanics it is known that two energy levels can converge and cross each other for certain values $\varepsilon_0$ of a system parameter (Fig. 5.1b). At $\varepsilon_0$ the energy level $E_{\max}$ becomes incidentally degenerate, e.g. $E_{\max} = E_0 = E_1$. Figure (Fig. 5.2) suggests that the ground state eigenfunction changes continuously at this point. This is not trivial, because the eigenspace corresponding to the eigenvalue $E_{\max}$ is two dimensional at $\varepsilon_0$. We interprete such a transition in the original phase variables as a transcritical saddle node bifurcation. We note that, since the exponential approximation is not exact, the bifurcation point for the Kuramoto phase equations is not necessarily identical with $\sigma\gamma = \varepsilon_0$. It is also not clear whether the synchronization manifold at the critical point is indeed two dimensional or if this is only a consequence of the exponential approximation. In either case, the Newton method (App. B) will fail close to the critical point because the eigenvalue zero of $\mathbf{L}$ becomes degenerate.

Since the ground state energy and thus the synchronization frequency is not smooth at the critical point both perturbation approaches fail beyond this point. Indeed, the phase profile in synchronization can change dramatically and one pacemaker region for the whole system can be replaced by a completely different region (Fig. 5.1). On the other hand, if we are only interested in the expected value of equation (Eq. 5.26) then level crossings, if rare for low frequency disorder $\sigma$, will only contribute with a small systematical error.

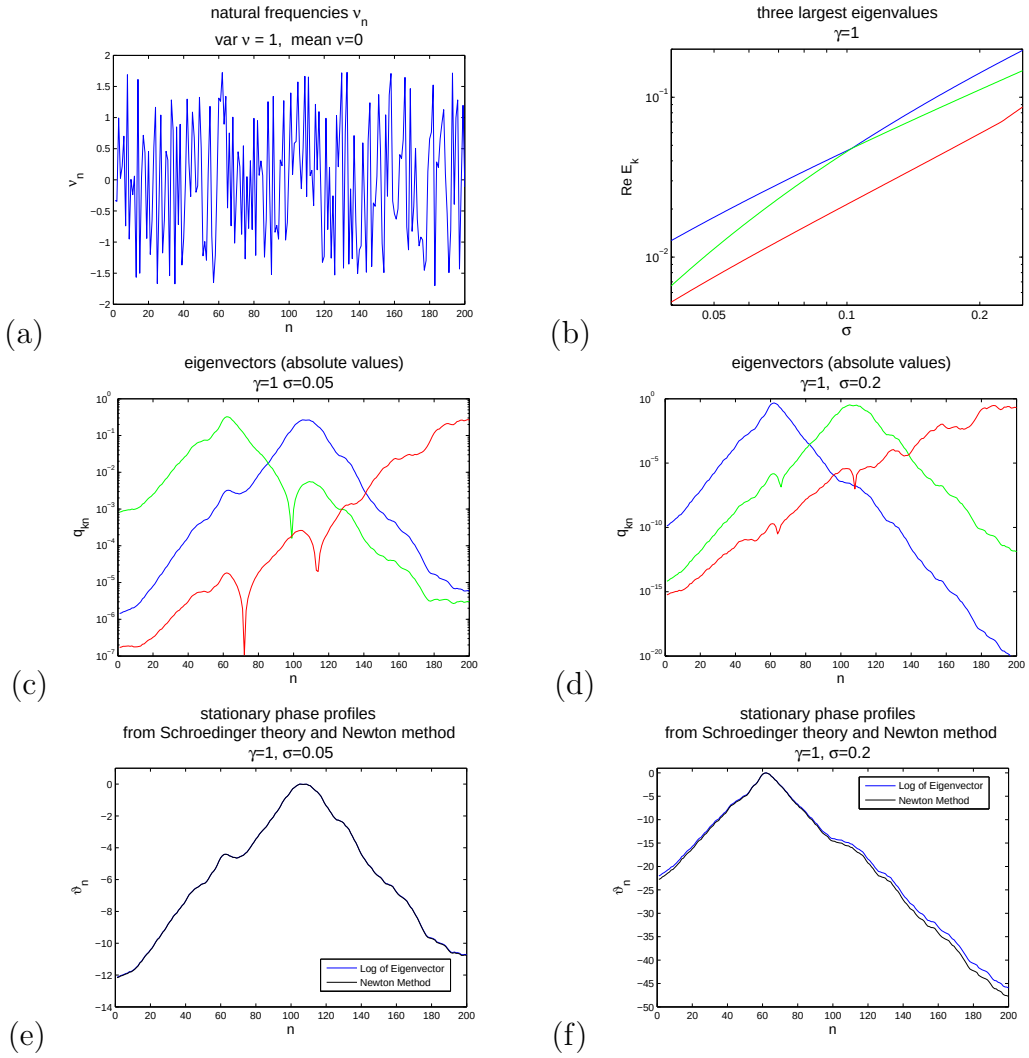


Figure 5.1: Synchronization analysis of a chain (open boundary conditions) of $N = 200$ nonidentical Kuramoto phase oscillators with nearest neighbor coupling. (a) Normalized natural frequencies $\eta_n$ of the oscillators in the chain. The frequencies are shifted so that $\bar{\eta} = 0$. (b) Double logarithmic plot of the three largest eigenvalues of the Schroedinger operator $-\mathbf{H}$. Since there are no topological charges, $\mathbf{H}$ is symmetric and all eigenvalues are real. The largest and the second largest eigenvalue cross each other at $\sigma \approx 0.1$ . (c,d) The absolute values of the corresponding eigenvectors. The eigenvector $\mathbf{q}_{\max}$ corresponding to $E_{\max}$ (blue) does not change sign, while the second eigenvector (green) changes sign once and the third (red) two times. At these positions the logarithm of the absolute value exhibits a sharp peak towards $-\infty$. The first and the second eigenvectors exchange positions resulting in a fast transition of the pacemaker region of the synchronized phase profiles. (e,f) The phase profiles obtained from $\mathbf{q}_{\max}$ and from solving the Kuramoto phase equations are very close so that the Newton method (see App. B) converges.

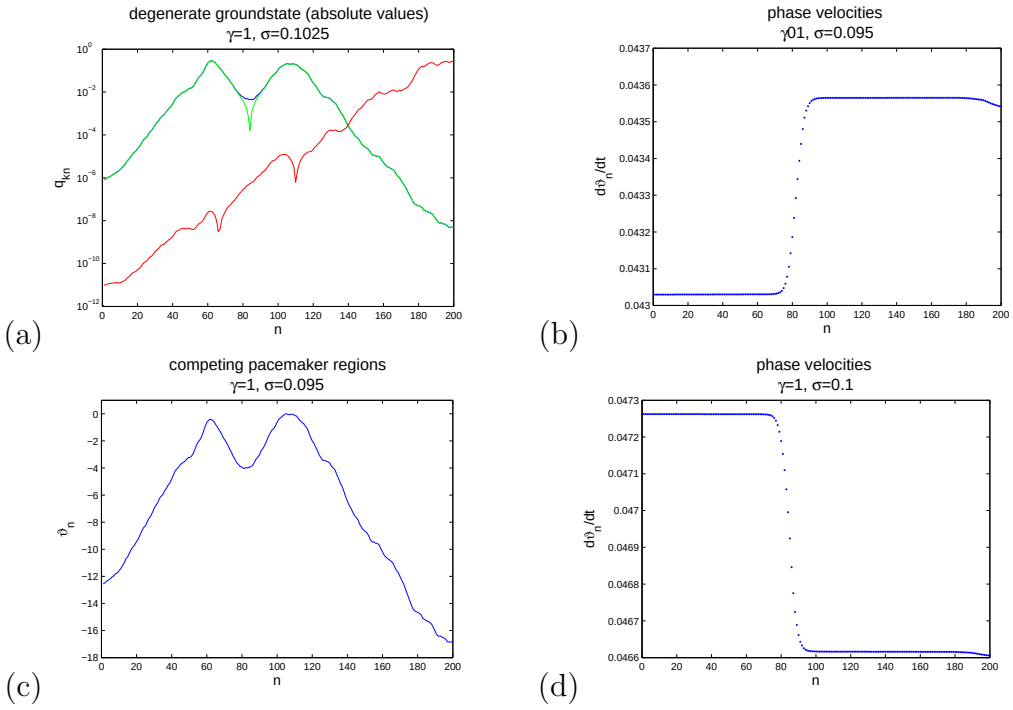


Figure 5.2: Near the point of eigenvalue degeneracy both pacemaker regions coexist and the synchronized state is reached very slowly. In the original phase variables this ground state degeneracy corresponds to a point of bifurcation. This is expressed in a degeneracy of $\mathbf{L}$ and a failure of both, the perturbation theory and the Newton method. In (a) we show the numerically obtained eigenvectors of $\mathbf{H}$ at the point of degeneracy. The first and the second eigenvectors (blue and green) are almost identical in the two competing pacemaker regions except for an opposite sign in one of them. (c) shows the phase profile with two pacemaker regions obtained from the integration of the phase equations (Eq. 2.24). In (b) and (d) the phase velocities across the lattice are plotted for this phase profile and values of $\sigma$ on both sides of the transition. One region is faster than the other region and will pull more and more oscillators over until, after a long transient, both regions have adapted a common phase velocity.

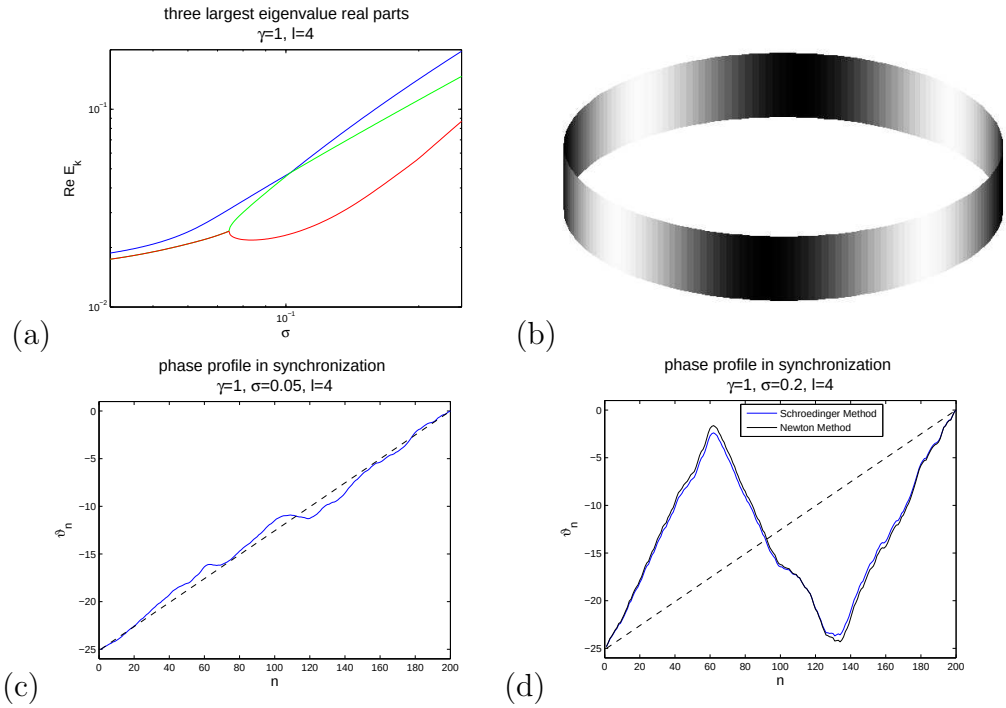


Figure 5.3: Ring of $N = 200$ phase oscillators with the same frequencies as used in (Fig. 5.1) but with periodic boundary conditions and a topological charge of $l = 4$. (a) Double logarithmic plot of the real parts of the eigenvalues of $-\mathbf{H}$. The second and the third eigenvalue are complex conjugated before $\sigma \approx 0.075$. Again, at $\sigma \approx 0.1$ the first and the second eigenvalue cross each other. (b) rotating wave for $\sigma = 0$. Shown is the sine of the phase in gray levels at the faces of a cylinder (for illustration). (c) and (d) show the phase profiles on the ring in synchronization for values of $\sigma$ to either side of the transition. The dotted line indicates the gauge field $\vartheta^0$ which carries the topological charge. In subfigure (b) we also compare the phase profile obtained from the eigenvector method (blue graph) and from the Newton method (black graph, App. B) for the original Kuramoto phase equations. The approximation agrees very well with the actual solution.

## 5.3 Oscillators with random frequencies on a regular cubic lattice

In this section we will explicitely calculate the first and second perturbation terms for nonidentical, nonisochronous phase oscillators on a regular cubic lattice of dimension $d$ with next neighbor coupling and periodic boundary conditions. For that we will use the continuous approximation (Eq. 2.29)

$$\Omega = \sigma\eta + \nabla^2\vartheta \;+\; \gamma\left(\nabla\vartheta\right)^2 \tag{5.27}$$

with $\mu^2/2 = 1$, $L^d = N$ (Eq. 2.27, cubic lattice of unit spacing), $g'(0) = 1$ and $g''(0) = \gamma$ of the KPEs

$$\Omega = \sigma\eta_n + \sum_m A_{nm}\; g(\vartheta_m - \vartheta_n) \qquad . \tag{5.28}$$

We recall that equation (Eq. 5.27) is an approximation of (Eq. 5.28) after a scaling of time $\tau = \frac{1}{2}\mu^2 t$ (Eq. 2.29) so that the heterogeneities $\sigma$ have to be scaled, as well. Let us distinguish them by different subscripts $\sigma_\tau = \frac{2}{\mu^2}\sigma_t$ and in synchronization $\frac{d}{d\tau}\vartheta = \Omega_\tau$ and $\frac{d}{dt}\vartheta = \Omega_t = \frac{1}{2}\mu^2\Omega_\tau$. The perturbation ansatz for the synchronization frequency is

$$\begin{aligned}
\Omega_t &= \Omega_t^0 \;+\; \sigma_t\Omega_t^I \;+\; \sigma_t^2\Omega_t^{II} \;+\; O(\sigma_t^3) \\
\\
\Omega_\tau &= \Omega_\tau^0 \;+\; \sigma_\tau\Omega_\tau^I \;+\; \sigma_\tau^2\Omega_\tau^{II} \;+\; O(\sigma_\tau^3) \qquad .
\end{aligned} \tag{5.29}$$

We can directly compare the perturbation terms and obtain

$$\Omega_t^0 = \frac{1}{2}\mu^2\Omega_\tau^0 \qquad \Omega_t^I = \Omega_\tau^I \qquad \Omega_t^{II} = \frac{2}{\mu^2}\Omega_\tau^{II} \qquad . \tag{5.30}$$

Since $\frac{1}{2}\mu^2 = 1$ for a regular cubic lattice the perturbation terms obtained from the continuous equation (Eq. 5.27) and the discrete equations (Eq. 5.28) coincide up to discretization errors. The eigenvalues and eigenfunctions of the Laplacian for a regular cubic lattice, even in the presence of topological charge are known in principle. However, the expression for the second order frequency shift simplifies greatly in the continuum limit (Eq. 5.37).

We consider a system with side length $L$ in in $d$ dimensions. Due to the periodic boundary conditions we can have non-zero winding numbers $\boldsymbol{l} = (l_1, l_2, \ldots, l_d)$ defining the topological charges of the gauge field $\vartheta^0$. The gauge field $\vartheta^0$ with the constant gradient

$$\nabla\vartheta^0 = \frac{2\pi}{L}\boldsymbol{l} \tag{5.31}$$

solves the Kuramoto phase diffusion equations for the homogeneous system

$$\Omega^0 \;=\; \nabla^2\vartheta^0 + \gamma\left(\nabla\vartheta^0\right)^2 \;=\; \gamma\left(\frac{2\pi}{L}\right)^2 |\boldsymbol{l}|^2 \qquad . \tag{5.32}$$

The gauge modified Laplacian reads

$$\mathbf{L} = 2\gamma\nabla\vartheta^0\nabla + \nabla^2 \tag{5.33}$$

and the left and right eigenfunctions that fulfill the periodic boundary conditions coincide and are simple harmonics

$$\begin{aligned} \mathbf{p_k} &= L^{-\frac{d}{2}} e^{i\frac{2\pi}{L}\mathbf{k}^\dagger\cdot\mathbf{r}} \qquad \text{with } \mathbf{k}^\dagger = (k_1, k_2, \ldots, k_d) \\ \mathbf{L}\mathbf{p_k} &= \left(\frac{2\pi}{L}\right)^2 \left(i\;\; 2\gamma\boldsymbol{l}^\dagger\cdot\mathbf{k} - |\mathbf{k}|^2\right) \qquad \mathbf{p_k} \;=\; E_\mathbf{k}\;\mathbf{p_k} \qquad . \end{aligned} \tag{5.34}$$

The eigenvalue with the largest real part is $E_0$ and the corresponding eigenvector is $\mathbf{p}_0 = L^{-d/2}\mathbf{1}$. The inner product with the vector $\tilde{\mathbf{P}}_0^\dagger = L^{-d}\mathbf{1}^\dagger$ (Eq. 5.15) gives the average of a function across the system. Thus the first order correction of $\Omega$ is (Eq. 5.19)

$$\Omega^I = \bar{\eta} \qquad . \tag{5.35}$$

This agrees with the perturbation term obtained from the linear equations (Sec. 5.2) because $\mathbf{Q}^0_{\max} = \tilde{\mathbf{P}}_0$.

The expected values of the second order perturbation terms (Eqs. 5.24, 5.20) both depend on the two point correlator matrix $\mathbf{C} = \mathbf{E}\left[\eta\eta^\dagger\right]$ of the random frequencies in the system. In the regular lattice with periodic boundary conditions and homogeneous correlator kernel $C(\mathbf{r}, \mathbf{r}') = C(\mathbf{r} - \mathbf{r}')$ the translation symmetries commute with the Laplacian and the correlator kernel (App. C). One can form a complete system of commuting operators from the symmetry operations so that the Laplacian and the correlator kernel must have the same eigenvectors $\mathbf{p}_k$ and $\mathbf{p}_k \cdot \mathbf{C}\mathbf{p}_{k'} = C_{kk}\delta_{kk'}$. Then with

$$\begin{aligned} \beta &= \gamma \\ \mathbf{p_0}\cdot\mathbf{1} &= L^{\frac{d}{2}} \\ \nabla\mathbf{p_k} &= \frac{2\pi}{L}\mathbf{k} \end{aligned} \tag{5.36}$$

from (Eq. 5.20) we find

$$\mathbf{E}\left[\Omega^{II}\right] = \gamma L^{2-d}\frac{1}{4\pi^2}\sum_{\mathbf{k}\neq 0}\frac{C_{kk}|\mathbf{k}|^2}{4\gamma^2(\boldsymbol{l}^\dagger\cdot\mathbf{k})^2 + |\mathbf{k}|^4} \qquad . \tag{5.37}$$

The same expression must follow from the perturbation theory of the linear system (Sec. 5.2). With

$$\begin{aligned} \mathbf{Q}_k^0 &= \mathbf{q}_k^0 = \mathbf{p}_k \\ E_{\mathbf{k}} &= \Omega^0 + \left(\frac{2\pi}{L}\right)^2 \left(i \;\; 2\gamma \boldsymbol{l}^\dagger \cdot \mathbf{k} - |\mathbf{k}|^2\right) \\ \mathbf{Q}_0^{0\dagger}(\mathbf{r})\mathbf{q}_0^0(\mathbf{r}) &= L^{-d} \\ \frac{1}{E_0^0 - E_{\mathbf{k}}^0} &= \left(\frac{L}{2\pi}\right)^2 \frac{-i \;\; 2\gamma \boldsymbol{l}^\dagger \cdot \mathbf{k} + |\mathbf{k}|^2}{4\gamma^2(\boldsymbol{l}^\dagger \cdot \mathbf{k})^2 + |\mathbf{k}|^4} \end{aligned} \tag{5.38}$$

and expression (Eq. 5.26) we find, indeed

$$\mathbf{E}\left[\Omega^{II}\right] = \gamma \mathbf{E}\left[E_0^{II}\right] = \gamma L^{2-d} \frac{1}{4\pi^2} \sum_{\mathbf{k}\neq 0} \frac{C_{kk}|\mathbf{k}|^2}{4\gamma^2(\boldsymbol{l}^\dagger \cdot \mathbf{k})^2 + |\mathbf{k}|^4} \quad . \tag{5.39}$$

The coefficients $C_{kk}$ are crucial for the convergence of the sum. In a continuous system of higher dimension the coefficients $C_{kk}$ must decay as fast as $C_{kk} \sim o(|k|^{2-d})$ so that the infinite sum converges.

In a finite, discrete lattice with $L = N^{\frac{1}{d}}$ and with uncorrelated random frequencies the sums (Eqs. 5.20, 5.26) are finite and we have to assume a cutoff, $C_{kk} = 1$ for $1 \leq |\mathbf{k}| \leq \frac{1}{2}L$ and $C_{kk} = 0$ for $|\mathbf{k}| > \frac{1}{2}L$ in the continuous approximation. Asymptotically for large $N = L^d$ the sum scales like

$$\sum_{|\mathbf{k}|>0}^{|\mathbf{k}|<\frac{1}{2}L} \frac{1}{|\mathbf{k}|^2} \sim O\left(\int_1^{\frac{1}{2}L} k^{d-3} dk\right) \tag{5.40}$$

giving

$$\begin{aligned} \mathbf{E}\left[\Omega^{II}\right] &\sim O(N) \qquad \text{for } d = 1 \\ \mathbf{E}\left[\Omega^{II}\right] &\sim O(\log N) \qquad \text{for } d = 2 \\ \mathbf{E}\left[\Omega^{II}\right] &\sim O(1) \qquad \text{for } d \geq 3 \quad . \end{aligned} \tag{5.41}$$

For a one dimensional ring of $N$ oscillators, winding number $l$, and uncorrelated random frequencies with $C_{kk} = 1$ for $k \neq 0$ we have explicitely

$$\mathbf{E}\left[\Omega^{II}\right] = \gamma N \frac{1}{2\pi^2} \sum_{k>0} \frac{1}{4\gamma^2 l^2 + k^2} \tag{5.42}$$

$$\text{and} \qquad \mathbf{E}\left[\Omega^{II}\right] = \gamma \frac{N}{2\pi^2}\zeta(2) = \gamma \frac{N}{12} \qquad \text{for } l = 0 \quad .$$

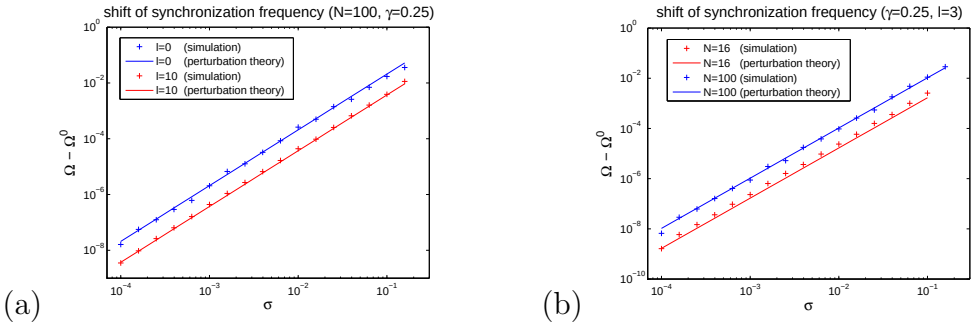


Figure 5.4: Shift of the synchronization frequency from $\Omega_0$, the frequency of the synchronized state with identical oscillators, as a function of the oscillator heterogeneity $\sigma$. We compare simulations (crosses) with the second order perturbation theory (lines, Eq. 5.42). Each cross from the simulations is an average value from 50 runs with different realizations of random frequencies. In order to observe the second order terms the linear contribution to the frequency shift must be exactly zero (not only in expected value). This is achieved by shifting the average frequencies to zero $\bar{\eta} = 0$ for each realization. The second order perturbation term is not affected by this change into a co-rotating frame of reference (see App. C). In subfigure (a) we compare the results for a ring of $N = 100$ nonisochronous ($\gamma = 0.25$) phase oscillators, without topological charge (blue graph) and with a topological charge of $l = 10$ (red graph). Subfigure (b) compares rings of different sizes $N = 16$ (red graph) and $N = 100$ (blue graph) oscillators but with the same nonisochronicity $\gamma = 0.25$ and topological charge $l = 3$.

In figure (Fig. 5.4) we compare the second order perturbation theory (Eq. 5.42) for a ring of phase oscillators with almost independent frequencies. In all ensembles we ensured $\bar{\eta} = 0$ so that the linear perturbation terms are exactly zero and the second order frequency correction can be measured directly. The correlator modes $C_{kk} = 1$ for $k > 0$ are not affected by this shift (App. C).

## 5.4 Oscillators on a sphere without topological Charges

The eingenfunctions of the Laplacian differential operator on the surface of a three dimensional sphere are known to be spherical harmonics. We can therefore readily apply perturbation theory for a continuous oscillating medium on the surface of a sphere. Every nonintersecting closed path separates the surface of the sphere into two regions. Such a path can be contracted to a point in either of the two regions. Topological charges are therefore only possible as pairs of phase defects with opposite charge (clockwise winding numbers) accompanied by spiral waves. Since our theory for continuous media was derived under the assumption of no phase singularities we will not consider topological charges.

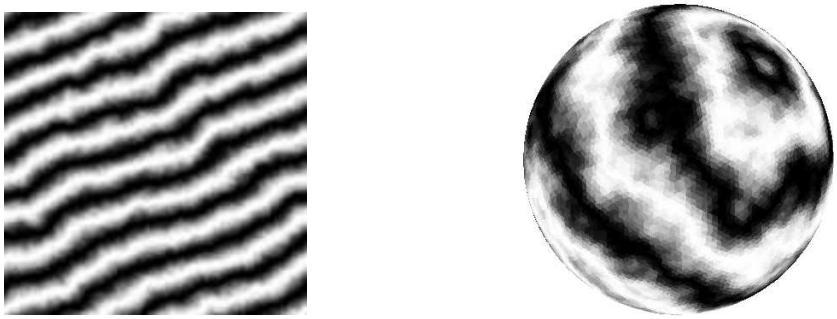

(a) (b)

Figure 5.5: Regular wave patterns in a $150 \times 150$ grid of nonisochronous ($\gamma = 1$) Kuramoto phase oscillators with nearest neighbor coupling and periodic boundary conditions (a) and on a discretization of the sphere surface [76] with $N = 20480$ oscillators (b). The natural frequencies of the individual oscillators where independently uniformly distributed with standard deviation $\sigma = 0.2$. The topology of the square lattice in subfigure (a) is that of a 2-torus and it is possible to have topological charges without phase singularities (large phase differences). We used an initial condition with topological charges $l_x = 3$ and $l_y = 7$. Shown is the sine of the phases in gray levels after a transient time to synchronization.

For a surface discretization we use the face centers of an icosahedron or an iterative refinement thereof [76]. This tessellation is almost homogeneous. Each point has exactly three next neighbors in almost exactly the same distance. The constant $\frac{1}{2}\mu^2$ for the continuum limit is found as $\frac{1}{2}\mu^2 = \frac{3}{4}$ (Eq. 2.27, Fig. 5.6). We will therefore distinguish between $\sigma_\tau$, $\Omega_\tau$ and $\sigma_t$, $\Omega_t$ in the continuous and discrete system, respectively (Eq. 5.30). With a homogeneous gauge field $\vartheta^0 = 0$ and the Laplacian $\tilde{\mathbf{L}} = \nabla^2$ the eigenfunctions and eigenvalues are

$$\begin{aligned} \mathbf{Q}^0_{lm} &= \mathbf{q}^0_{lm} = \frac{1}{R}\mathbf{Y}_{lm} \\ \tilde{\mathbf{L}}\mathbf{Y}_{lm} &= -\frac{1}{R^2} l(l+1)\mathbf{Y}_{lm} \end{aligned} \tag{5.43}$$

with spherical harmonics $Y_{lm}(\theta, \phi)$ [75] and the radius $R$ of the sphere. The two point correlator matrix $\mathbf{C} = \mathbf{E}\left[\eta\eta^\dagger\right]$ is not diagonal in the system of eigenvectors of the Laplacian. However, in the Schrödinger perturbation approach (Sec. 5.2) only the diagonal elements $C_{lm} = \mathbf{Q}^{0\dagger}_{lm} \cdot \mathbf{C}\mathbf{q}^0_{lm}$ are needed for the second order

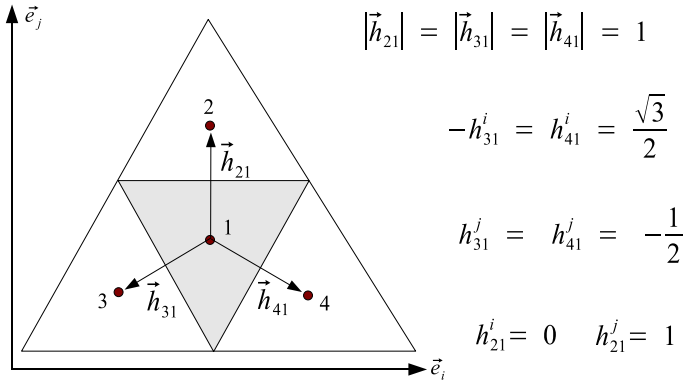


Figure 5.6: Neighbor relations in the triangular grid.

perturbation term $\Omega^{II}$. The first three terms of the perturbation series are thus

$$\begin{aligned} \Omega^0_t &= \Omega^0_\tau = 0 \\ \Omega^I_t &= \Omega^I_\tau = \mathbf{Q}^{0\dagger}_{00} \cdot \mathbf{V}_\eta \mathbf{q}^0_{00} = \bar{\eta} \qquad (5.44) \\ \mathbf{E}\left[\Omega^{II}_t\right] &= \frac{2}{\mu^2}\gamma \frac{1}{4\pi} \sum_{l>0} \sum_{m=-l}^{l} \frac{C_{lm}}{l(l+1)} \quad . \end{aligned}$$

For a discrete system with delta correlated random frequencies the diagonal elements of $\mathbf{C}$ are equal to one. In order to compare the discrete surface grid with the continuous limit, we have again to assume a cutoff at a mode $l_{\max} \sim \sqrt{N}$ because the infinite sum for $\Omega^{II}$ in (Eq. 5.44) does not converge if all $C_{lm}$ are equal. In that case we find

$$\mathbf{E}\left[\Omega^{II}\right] = \frac{1}{3\pi}\gamma \sum_{l=1}^{l_{\max}} \frac{2l+1}{l(l+1)} \qquad (5.45)$$

and with $N \sim l^2_{\max}$ again $\Omega^{II} \sim O(\log N)$.

## 5.5 Random network of oscillators without topological charges

The perturbation terms for the frequency shift in a heterogeneous oscillatory system can be evaluated for a given realization of random frequencies or as expected values obtained by averaging over all possible realizations of frequencies. Beside such dynamical heterogeneity the system itself may be heterogeneous

and only characterized by statistical properties like node degree distribution or loop structure. If topological charges cannot be ruled out then the averaging must be done for all possible network realizations and gauge field solutions $\vartheta^0$. Different mechanisms or algorithms for the generation of random networks sample the set of all networks differently leading to classes of networks for which the statistical properties are known. The most widely used prototypical modell classes in the physical community today are Rényi-Erdös (RE) random graphs [77], Barabási-Albert (BA) scale free networks [31] and Small-World (SM) networks [30]. The spectrum of the Laplacian for these networks follows certain distributions over which expression (Eq. 5.26) can be averaged. As we have seen in Section 4.1.1 the homogeneous solution $\vartheta^0 = \text{const}$ for identical phase oscillators is not the only stable synchronization state. The distribution of topological charges in synchronization after random initial conditions for a random network has not been studied yet. Moreover, we have seen that the gauge modified Laplacian is not symmetric anymore. An averaging over different stable synchronization states for a general network is therefore not feasible.

Instead we will look at the shift of synchronization frequency for a random, connected, undirected network with uncorrelated binomially distributed node degrees and without topological charges (from homogeneous initial conditions). The distribution $\rho_{\mathbf{A}}(E)$ of the eigenvalues of the adjacency matrix for this class of networks follows the Wigner Semicircle-Law ([78, 79]). The Laplacian matrix $\mathbf{L} = \mathbf{A} - \mathbf{D}$ on the other hand, where $\mathbf{D} = \text{diag}(\mathbf{d})$ is the diagonal matrix of node degrees $d_n$, does not follow a semicircle (Fig. D.3). It has one eigenvalue equal to zero and $N-1$ eigenvalues distributed according to a continuous probability density between zero and $N$. From simulations we find that in a connected random Rényi-Erdös like network (see App. D) for a fixed mean degree $\nu = \mathbf{E}[d]$ the density $\rho_{\mathbf{L}}(E, \nu)$ of eigenvalues appears to converge in the limit $N \to \infty$. Keeping the mean degree constant results in ever sparser networks which eventually will have a connection probability $p$ below the perculation threshold [32]. However, by construction (App. D) a large one-component network with very small values of $p$ can be achieved which for $\nu = 2$ in the limit $N \to \infty$ becomes an infinite tree network.

Averaging over many realizations of random networks with uncorrelated random frequencies the sum (Eq. 5.26) can then be replaced by an integral

$$\mathbf{E}\left[\Omega^{II}\right] \;=\; -\gamma \frac{1}{N} \sum_{k=1}^{N-1} \frac{1}{E_k} \approx -\gamma \int \frac{1}{E}\, \rho_{\mathbf{L}}(E)\, dE \qquad . \tag{5.46}$$

If $\rho_{\mathbf{L}}(E)$ is narrow, unimodal and for $E \to 0$ goes to zero fast enough we can expect the integral to be of order $1/\langle E \rangle$. This means, that the exact shape of the

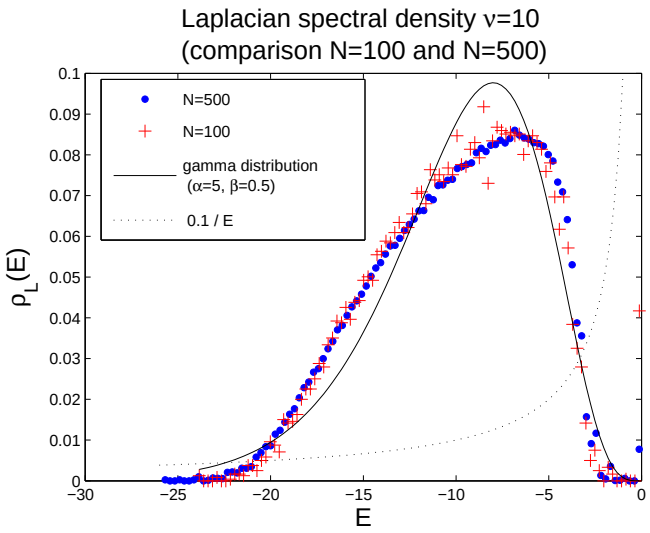


Figure 5.7: The shape of the continuous part of the spectral density of the network Laplacian is independent of the size of the connected random network. The delta component at $E = 0$ is of order $1/N$. Shown is a normalized histogram of all eigenvalues obtained from 100 realizations of random connected networks with mean node degree $\nu = 10$, size $N = 100$ (red crosses) and $N = 500$ (blue circles). We compare the spectral densities with a gamma distribution on the negative real axis (Eq. 5.47) with shape parameters $\alpha = 5$ and $\beta = 0.5$ (solid line). The dotted line is the quantity $\sim 1/E$ which we need the average for.

spectral density is not very important for an approximation of (Eq. 5.46). As a hypothesis for the distribution of nonzero eigenvalues of the Laplacian we use the gamma distribution on the negative axis

$$\rho_{\mathbf{L}}\left(E|\alpha(\nu),\beta(\nu)\right) = \frac{\beta^{\alpha}}{\Gamma(\alpha)}(-E)^{\alpha-1}e^{\beta E} \qquad . \tag{5.47}$$

From Monte-Carlo simulations and maximum likelihood parameter estimation (Fig. 5.8) we conclude that $\beta = \frac{1}{2}$ is independent of $\nu$ and $\alpha/\beta = \nu$. Then the integral (Eq. 5.46) becomes

$$\mathbf{E}\left[\Omega^{II}\right] \;=\; \gamma\frac{\beta}{\alpha-1} = \gamma\frac{1}{\nu-2} \qquad . \tag{5.48}$$

In figures 5.7 and D.3 one can see that the hypothesis (Eq. 5.47) should be rejected but it leads to a good approximation (Eq. 5.48) of the sum and integral (Eq. 5.46) and also gives $\nu = 2$, the infinite tree network, as a critical parameter value. Expression (Eq. 5.48) is an empirical result. Analytical expressions for the Laplacian spectral density based on a virial expansion exist [80] but are rather complicated.

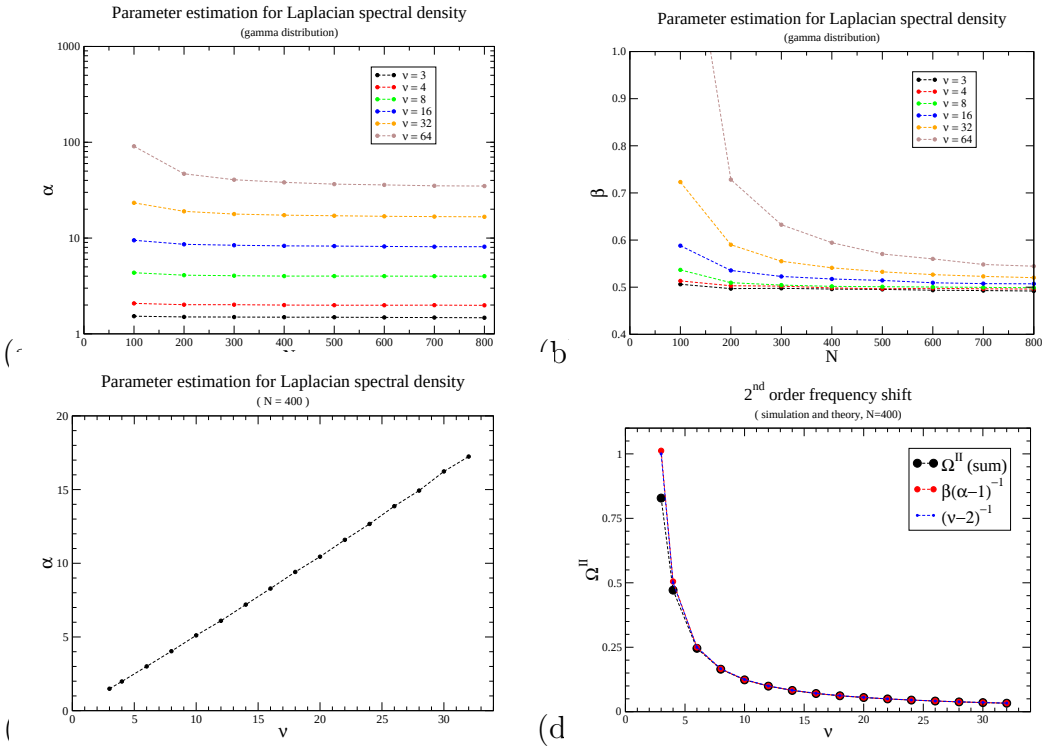


Figure 5.8: We estimated the shape parameters $\alpha$ and $\beta$ of a gamma distribution from all eigenvalues of 100 realizations of connected random networks. Subfigures (a,b) show the dependence of $\alpha$ and $\beta$ on the system size $N$. They converge for large networks $N \gg 1$. We plotted the shape parameters for system sizes between $N = 100$ and $N = 800$ for different mean node degrees $\nu = 3, \ldots, 64$. In semilogarithmic scales in (a) one can see that $\alpha$ is equally spaced for a geometric progression of $\nu$. Subfigure (c) shows that $\alpha$ depends, indeed, linearly on the mean node degree $\nu$. In subfigure (d) we show the expected second order frequency shift $\mathbf{E}\left[\Omega^{II}\right]$ with nonisochronicity $\gamma = 1$ directly obtained from the perturbation series (Eq. 5.46, black circles) and averaged over 100 random networks and compare it with the approximations (Eq. 5.48, red and blue circles). We find them in very good agreement.

Note that $\mathbf{E}\left[\Omega^{II}\right]$ is independent of the system size. The diameter of an RE random network scales as $R \sim \log N / \log \nu$ [32]. It has therefore an infinite dimension $\dim = \lim_{N\to\infty} \log N / \log R$ and can be compared with the situation for regular cubic lattices where the second order perturbation terms do not scale with the system size for dimensions larger than two (Eq. 5.41).

# Chapter 6

# Summary and Discussion

In this chapter we will summarize this thesis and discuss the implications of our results. We will also address open questions which should be considered in future work.

Our goal was to study the characteristics of complete synchronization states in discrete systems of nonidentical Kuramoto phase oscillators. In that state the phase differences or relative phases of all oscillators form a stationary phase profile and evolve unisonous with the same constant synchronization frequency $\Omega$. This phase locked state is actually a special case scenario. Much attention in the literature today is given to clusters of synchronization which can arise spontaneously from a completely disordered state and merge in a transition to the limiting state of complete synchronization. Our approach was essentially from the opposite direction, i.e. to study the change of a synchronization state of identical oscillators in response to increasing heterogeneity. Given a realization $\omega_n$ of natural frequencies of the isolated oscillators it is a very complicated problem to find the stationary phase profile and the synchronization frequency $\Omega$ in the system of coupled oscillators. Such a synchronized solution may not be stable, not unique or might not even exist. We have observed, however, that the inverse problem is trivial. Given a phase profile one can directly and uniquely up to a constant compute the natural frequencies $\omega_n$ which make this phase profile stationary. We have explored this dichotomy in Chapter 3 where we have formalized the problem by introducing a mapping between the space of relative frequencies and the torus $T^{N-1}$ of relative phases between $N$ phase oscillators in synchronization. This formalism helped us to formulate the problem and to visualize the complexity of finding a synchronized state. Because the space of relative phases is compact, so is its image under the mapping and we could find boundaries for the heterogeneity beyond which no complete synchronization is possible (Eq. 3.15).

We then moved on in Chapter 4 to look for situations in which we actually can find or approximate the stationary phase profile. This is the case in connected networks without circular paths, i.e. in tree networks, and for special phase coupling functions. From the analytic solutions (Eqs. 4.17 and 4.25, Figs. 4.6 and 4.9) we have learned that an asymmetry in the phase coupling function has an ordering effect which favors faster oscillators as centers of waves and suppresses wave front diffusion thus leading to more regular and concentric waves. The effect is very similar for asymmetries introduced through the coupling topology of a system, which has recently been studied by others [36, 42], but it differs from such situations because an asymmetric phase coupling is a purely dynamical property. A parameter which can break the coupling symmetry in the phase variables is the non-isochronicity $\gamma$ of the oscillators. It measures the dependence of the angular velocity of an oscillator on deviations from the limit cycle. The importance of $\gamma$ for synchronization has been remarked on by Kuramoto and Sakaguchi already two decades ago [69] (there $\alpha$, same effect) but it is most often neglected for analytical reasons [11, 22, 61]. An odd coupling function and identical oscillators make the Kuramoto model a gradient system for which one can show that it always synchronizes. A slightly asymmetric phase coupling function or even nonidentical oscillators destroy this property of the equations and usually lead to considerable analytical difficulties.

Before looking for approximations in Section 4.4 we have presented exact results in Section 4.1, in particular, multistability - the existence of more than one stable synchronized state for a given set of frequencies. It is often overlooked that even for identical oscillators there may be other synchronized states than the trivial homogeneous solution of complete identical synchronization. The torus topology of the phase space is responsible for the existence of inhomogeneous synchronized solutions with nonzero winding numbers. For real valued scalar variables one expects that the integral of the gradient over closed loops or the sum of the nearest neighbor differences along circular paths is zero. This is not the case for elements of a circle. Periodic boundary conditions make it possible to have a locally well defined phase gradient but the sum or integral around a closed path can be an integer multiple of $2\pi$, the so called topological charge of the circle. We had encountered multiple heterogeneous stable synchronized solutions in random networks of identical phase oscillators in simulations and had started to study this phenomenon systematically before we became aware of a recent publication on the same topic by Stephen Strogatz [61]. The results in Section 4.1.1 are therefore not new but present our own original work. Aside from this, topological charges play an important role later on in Chapter 5 in the analysis of the synchronization frequency. If the symmetry of the coupling function is broken by nonisochronicity then the symmetry of the Jacobian around such an inhomogeneous synchronized state is also broken even if the coupling network

is undirected. An important question is the size of the basin of attraction whenever different attractors in a dynamical system coexist. We have found that the winding numbers in a ring of identical sine-coupled phase oscillators are distributed in a binomial fashion after synchronizing from random initial conditions. The variance of the winding number distribution grows linearly with the size of the ring making the homogeneous solution just one among many other, almost equally probable solutions. While in a random network the number of circles grows as it becomes more connected at the same time the length of the cycles decreases. We expect therefore that the steady state entropy, i.e. the amount of information contained in different stable synchronization states, strongly depends on the topology of the network. We did not explore this question further in this thesis but would like to continue working on it.

Beside this topologically induced multistability we have also found multistability of dynamical origin. In Section 4.1.2 and Appendix A we have solved the problem of complete synchronization for a chain of three nonidentical, nonisochronous Kuramoto phase oscillators. We have found that multistability arises for large nonisochronicites and nonidentical natural frequencies in a cusp-bifurcation. The regime of large nonisochronicity also leads to multiple stable states of synchronization in larger systems of nonidentical phase oscillators (Fig. 4.16). The findings in Section 4.1 suggest that multistability is a common feature of the Kuramoto model.

In Section 4.4.1 and [10] we have introduced a transfer map formalism for the phase differences in a one dimensional chain of phase oscillators and have found that nonisochronicity $\gamma \neq 0$ has an ordering effect on the phase differences just like the extreme asymmetric case of a unidirectional phase coupling function and a tree network (Sec. 4.3). We have obtained an important relation (Eq. 4.33) between the synchronization frequency and the emergent mean wavelength in the system and define measures of regularity of the resulting quasi-regular concentric waves. We have found a first hint on the connection between the nonisochronicity and the heterogeneity of the oscillators, measured by the frequency variance $\sigma$, for the effect of quasi-regular concentric waves. The autocorrelations between neighboring phase differences in synchrony as well as the regularity measure $Q_\psi$ defined as the ratio between the fluctuations of the phase differences and the mean phase difference are functions of the combined parameter $\gamma\sigma$. The regularity $Q_\psi$ goes to zero if either $\gamma$ or $\sigma$ go to zero. Heterogeneity is therefore a key ingredient for quasi-regular concentric waves. For isochronous oscillators $\gamma = 0$ there can still be concentric waves in the system but the phase differences and wave fronts diffuse freely. Averaged over many realizations of random frequencies the mean wavelength with respect to any point on the chain is zero.

It has turned out that the phenomenon of quasi-regular concentric waves is directly related to the effect of Anderson localization. To see this one can change the Kuramoto phase diffusion equation with a Cole-Hopf transformation (Sec. 4.4.2) into a linear equation of the Schrödinger type for a wave function of a particle moving in a random potential. We have followed in principle the argument of Kuramoto and Sakaguchi [1, 69] but we have introduced two new ingredients. The first is the idea of a gauge field which carries the topological charges in the system. A gauge field corresponds to a local choice of phase coordinates. This approach generalizes the analysis to include the possibility of nonzero winding numbers and has enabled us to apply linear theory (Eq. 4.47) and derive higher order expansions in the vicinity of inhomogeneous synchronized solutions. The second idea is the exponential approximation of the coupling function for discrete systems of phase oscillators (Eqs. 4.48, 4.50). This approximation leads to a system of phase equations which can be transformed with a Cole-Hopf transformation into a discrete Schrödinger equation, retaining the overall coupling structure. We have therfore found a way to transcribe the Kuramoto phase equations into linear equations (Eq. 4.52) not only for regular coupling topologies but for networks in general. The major advantage over a mere tangent space linearization of the dynamics is that the asymmetry $\gamma$ of the coupling function is taken into account. In fact, a nonzero $\gamma$ is a prerequisite for the Cole-Hopf transformation to be defined. Equations (Eqs. 4.56-4.58) relate the phase profile in synchronization and the synchronization frequency $\Omega$ to the ground state and the ground state energy of a Hamiltonian. Quasi-regular concentric waves correspond to exponentially localized ground states. Scaling theory of Anderson localization prompted us to look for scaling properties of both the localization length and the synchronization frequency (Fig. 4.14). The role of the scaling parameter $\varepsilon = \gamma\sigma$ becomes clear in the transformed system. It measures the diagonal disorder of the Hamiltonian.

The last chapter (Chap. 5) is concerned only with the temporal aspect of pattern formation through synchronization. The diagonal disorder of strength $\varepsilon = \gamma\sigma$ in the potential of the linear Schrödinger equations is an open invitation to apply quantum mechanical perturbation theory. The most important consequence is that, in homogeneous coupling topologies or with a homogeneous gauge field, the linear term in the perturbation series is equal to the mean frequency of the phase oscillators and for small diagonal disorder the synchronization frequency will scale as $(\Omega - \bar{\omega}) \sim \gamma\sigma^2$. If, on the other hand, we expand around an inhomogeneous synchronized state and the coupling topology is not homogeneous this relation is not valid anymore. Some oscillators will have a stronger influence on the linear perturbation term of the synchronization frequency than others. In contrast to the situation found in quantum mechanics the linear operator can be non-hermitian so that we had to carefully distinguish

between left and right eigenvectors in our perturbation approach. Since the linear equations for a discrete system of phase oscillators have been derived using an approximation for the coupling function we were faced with the question of how to relate the results of a perturbation analysis for the new equations to the original Kuramoto model. This could only be addressed by developing a perturbation theory for the Kuramoto model first (Sec. 5.1). At the end of this section we were able to answer the question. The linear and the second order perturbation terms for the Kuramoto model and the Schrödinger theory are identical if the gauge field solution is the same, e.g. a constant gauge in the absence of topological charges. This is due to the fact that the phase coupling function and its exponential approximation have the same Taylor expansion up to the second order. We have derived first and second order perturbation terms for the Schrödinger theory in Section 5.2.

The equations (Eqs. 5.20 and 5.26) have been the main tools in our analysis of examples in the concluding Sections 5.3-5.5. Without further assumptions we can calculate (Sec. 5.3) the expected synchronization frequency in a continuous or discrete ring of nonidentical, nonisochronous Kuramoto phase oscillators with or without topological charges and with independent identically distributed random frequencies. For continuous systems of higher dimension the frequencies cannot be delta correlated or the second order perturbation term becomes infinite. We have addressed this problem by introducing a cutoff in the Fourier expansion of the frequency correlation matrix at a length scale smaller than the distance of neighboring oscillators in a discretization of the oscillatory medium. With this technique we have found the scaling behavior of the second order perturbation term with respect to the number of oscillators and the dimension of the medium (Eq. 5.41). The shift of the synchronization frequency from the mean frequency in a one dimensional system is proportional to the number $N$ of oscillators, it grows as $\log N$ in a two dimensional system, e.g. a rectangular lattice (Sec. 5.3) or the surface of a sphere (Sec. 5.4), and it is asymptotically independent of $N$ for higher system dimensions. These scaling results have yet to be confirmed in simulations for the publication [54] of this work. In the last section (Sec. 5.5) we have found an empirical expression for the expected shift of synchronization frequency in connected random networks with binomial degree distribution (Rényi-Erdös type). The dimension of such a network is larger than two and we have found accordingly that the shift of the synchronization frequency depends on the mean degree in the network but not its size $N$. Expression (Eq. 5.48) is a fair approximation for larger mean degrees $\mathbf{E}[d] \gg 1$. Corresponding examinations need yet to be done for random networks of other statistical ensembles, like scale-free or small-world networks. Coupled oscillators with correlated frequencies can be analyzed with our theory readily, since the two point correlator enters the equations. It would be interesting to study

the effect of power-law correlated frequencies, which one can expect in fractal frequency landscapes [81, 82], on the scaling of the synchronization frequency.

We have put a large portion of the calculations and method details in the appendices. Appendices A and D contain novel results, the steady state analysis for the chain of three nonidentical, nonisochronous phase oscillators and an algorithm that samples uniformly from all undirected, connected random graphs of given size $N$. After the conclusion of this work we will be looking into appropriate forms of publication. The Newton method described in Appendix B is interesting as a numerical tool in combination with the linear equations from our exponential approximation. We will include it in the manuscript [54].

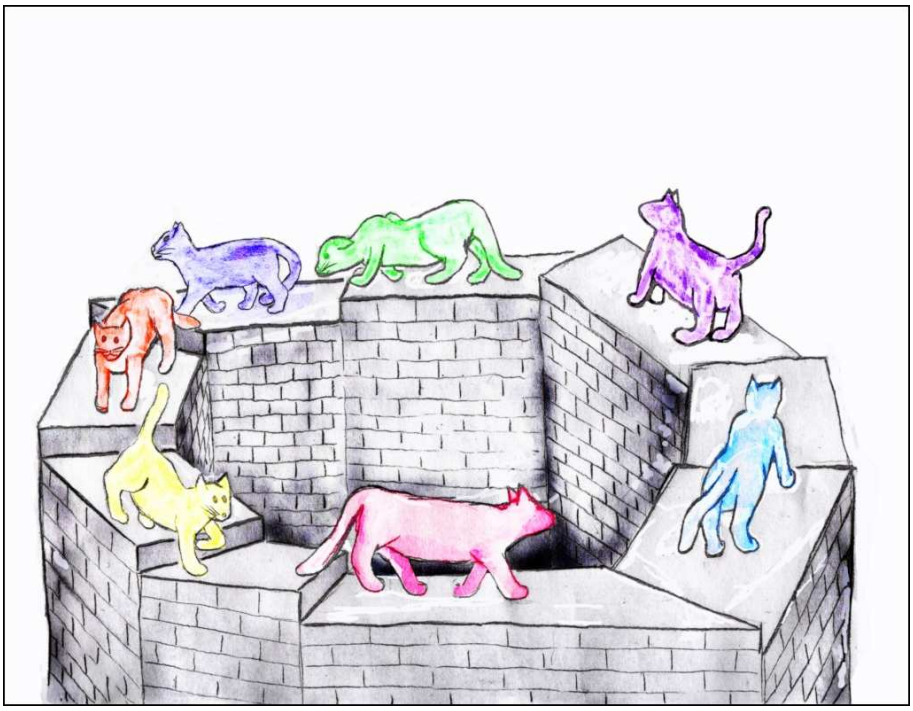

# Appendix A

# Bifurcation Analysis for a Chain of Three Oscillators

We are looking for fixed points of the relative phases, corresponding to synchronized solutions of the phase equations

$$\begin{aligned} \dot{\vartheta}_1 &= \omega_1 + g(\vartheta_2 - \vartheta_1) \\ \dot{\vartheta}_2 &= \omega_2 + g(\vartheta_1 - \vartheta_2) + g(\vartheta_3 - \vartheta_2) \qquad \text{(A.1)} \\ \dot{\vartheta}_3 &= \omega_3 + g(\vartheta_2 - \vartheta_3) \\ g(\Delta\vartheta) &= \sin\Delta\vartheta + \gamma\,(1 - \cos\Delta\vartheta) \qquad \text{(A.2)} \end{aligned}$$

The torus $T^2$ of relative phases can be parameterized by the new phases $\phi_1 = \frac{1}{2}(2\vartheta_2 - \vartheta_1 - \vartheta_3)$ and $\phi_2 = \frac{1}{2}(\vartheta_1 - \vartheta_3)$ so that $\vartheta_2 - \vartheta_1 = \phi_1 - \phi_2$ and $\vartheta_2 - \vartheta_3 = \phi_1 + \phi_2$. This transformation rotates the torus locally by 45° which makes the fixed point analysis easier. Additionally we use the parameters $\Delta = \frac{1}{2}(\omega_1 - \omega_3)$ and $\Gamma = \gamma + \frac{1}{2}(2\omega_2 - \omega_1 - \omega_3)$. The time dynamics of the phases $\phi_1$ and $\phi_2$ simplify to

$$\begin{aligned} \dot{\phi}_1 &= \Gamma - F_1(\phi_1, \gamma)\ \cos\phi_2 \qquad \text{(A.3)} \\ \dot{\phi}_2 &= \Delta - F_2(\phi_1, \gamma)\ \sin\phi_2 \end{aligned}$$

with

$$F_1(\phi_1, \gamma) = \gamma\cos\phi_1 + 3\sin\phi_1 \quad , \quad F_2(\phi_1, \gamma) = \cos\phi_1 + \gamma\sin\phi_1 \qquad . \qquad \text{(A.4)}$$

The functions $F_1$ and $F_2$ are simple harmonics and as such have the reflection and translation symmetries

$$\begin{aligned} F_1(\phi + \pi, \gamma) &= -F_1(\phi, \gamma) \quad , \quad F_2(\phi + \pi, \gamma) = -F_2(\phi, \gamma) \qquad \text{(A.5)} \\ F_1(-\phi, -\gamma) &= -F_1(\phi, \gamma) \quad , \quad F_2(-\phi, -\gamma) = F_2(\phi, \gamma) \qquad . \qquad \text{(A.6)} \end{aligned}$$

The equations (Eq. A.3) are therefore invariant under the following transformations

$$\phi_2 \to -\phi_2 \quad , \quad \Delta \to -\Delta \tag{A.7}$$
$$\phi_1 \to -\phi_1 \quad , \quad \Gamma \to -\Gamma \ , \ \gamma \to -\gamma \tag{A.8}$$
$$\phi_1 \to \phi_1 + \pi \quad , \quad \Delta \to -\Delta \ , \ \Gamma \to -\Gamma \ , \ t \to -t \quad . \tag{A.9}$$

By combining the symmetry transformations (Eqs. A.7, A.8 and A.9) the signs of the parameters $\Gamma$, $\Delta$ and $\gamma$ can be switched individually while the number of fixed points remains invariant. The bifurcation analysis can therefore be restricted to the case where all three parameters are positive if one notes that the time inversion involved in the symmetry (Eq. A.9) also switches stable and unstable manifolds of the fixed points.

There is another symmetry which is artificially introduced by the definition of the phases $\phi_1$ and $\phi_2$. Note that $(\phi_1, \phi_2)$ and $(\phi_1 + \pi, \phi_2 + \pi)$ designate the same point on the torus $T^2$ of phase differences $\vartheta_2 - \vartheta_1$ and $\vartheta_2 - \vartheta_3$. The dynamics (Eq. A.3) has always twice as many fixed points on the 2-Torus parameterized by $\phi_1$ and $\phi_2$ as the dynamics of the phase differences on $T^2$.

The Jacobian of the dynamics (Eq. A.3) is

$$\mathbf{J} = \begin{pmatrix} -F_1{}' \cos\phi_2 & F_1 \sin\phi_2 \\ -F_2{}' \sin\phi_2 & -F_2 \cos\phi_2 \end{pmatrix} \tag{A.10}$$

with trace $\tau$ and determinant $D$

$$\begin{aligned} \tau &= -\cos\phi_2 (F_1{}' + F_2) = -4\cos\phi_1 \cos\phi_2 \\ D &= \cos^2\phi_2 \ F_1{}' F_2 + \sin^2\phi_2 \ F_1 F_2{}' \quad . \end{aligned} \tag{A.11}$$

The functions $F_1$, $F_2$ and their derivatives $F_1{}'$ and $F_2{}'$ with respect to $\phi_1$ are

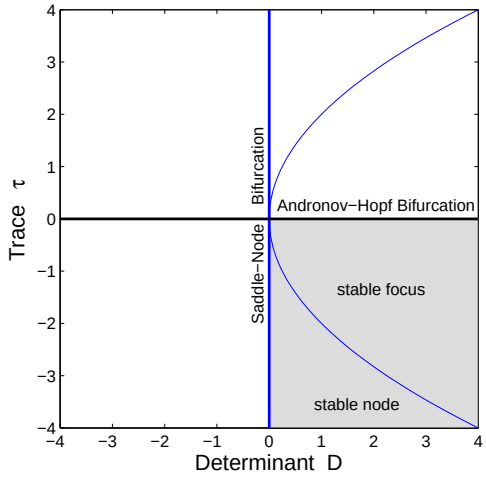


Figure A.1: In a two dimensional system the stability of a fixed point can be determined by the trace $\tau$ and the determinant D of the Jacobian of the dynamics at the fixed point [83]. Only if $\tau < 0$ and $D > 0$ both eigenvalues can be negative and the fixed point is asymptotically stable. The parabola marks the line $\tau^2 - 4D = 0$. To the right of this line the eigenvalues are complex conjugated and the dynamics near the fixed point is oscillatory (damped or amplified).

related in a number of ways

$$F_1 = \gamma \cos\phi_1 + 3\sin\phi_1 \quad , \quad F_2 = \cos\phi_1 + \gamma \sin\phi_1 \tag{A.12}$$

$$F_1{}' = 3\cos\phi_1 - \gamma \sin\phi_1 \quad , \quad F_2{}' = \gamma\cos\phi_1 - \sin\phi_1 \tag{A.13}$$

$$\cos\phi_1 = \frac{F_2 + \gamma F_2{}'}{1+\gamma^2} = \frac{3F_1{}' + \gamma F_1}{9+\gamma^2} = \frac{3F_2 - \gamma F_1}{3-\gamma^2} \tag{A.14}$$

$$\sin\phi_1 = \frac{\gamma F_2 - F_2{}'}{1+\gamma^2} = \frac{3F_1 - \gamma F_1{}'}{9+\gamma^2} = \frac{F_1 - \gamma F_2}{3-\gamma^2} \tag{A.15}$$

$$F_2 = \frac{(3-\gamma^2)F_1{}' + 4\gamma F_1}{9+\gamma^2} \qquad F_2{}' = \frac{4\gamma F_1{}' - (3-\gamma^2)F_1}{9+\gamma^2} \tag{A.16}$$

$$F_1^2 + F_1{}'^2 = 9+\gamma^2 \quad , \quad F_2^2 + F_2{}'^2 = 1+\gamma^2 \tag{A.17}$$

$$F_1{}'F_2 - F_1F_2{}' = 3-\gamma^2 \quad , \quad F_1F_2 + F_1{}'F_2{}' = 4\gamma \tag{A.18}$$

Additionally at the fixed points of (Eq. A.3) we have

$$\Gamma = F_1 \cos\phi_2 \qquad \Delta = F_2 \sin\phi_2 \tag{A.19}$$

In a two dimensional dynamical system there are two bifurcations that change the stability of a fixed point (Fig. A.1). The determinant $D$ of the Jacobian has

to be positive and the trace $\tau$ must be negative for a fixed point to be stable. Two fixed points coincide in a saddle-node bifurcation for $D = 0$ and a stable focus can become unstable across the line where $\tau = 0$ (Fig. A.2). The parabola $\tau^2 - 4D = 0$ marks the transition from a node to a focus. Two real eigenvalues collide and become a pair of complex conjugated eigenvalues. The stability of the fixed point, however does not change, which is why we will not look for this transition in the parameter space.

The trace $\tau$ (Eq. A.11) vanishes for points on the torus where $F_1{}' + F_2 = 0$.

$$
\begin{aligned}
&F_1{}' + F_2 = 0 \overset{(A.16)}{\longleftrightarrow} 12F_1{}' + 4\gamma F_1 = 0 \longleftrightarrow F_1{}' = -\gamma F_1/3 \\
&\overset{(A.17)}{\longrightarrow} F_1{}'^2 + F_1^2 = F_1^2(\gamma^2/9 + 1) = (9 + \gamma^2) \\
&\overset{(A.17,A.18)}{\longleftrightarrow} F_1^2 = 9,\ F_1{}'^2 = \gamma^2, F_2^2 = \gamma^2,\ F_2{}'^2 = 1,\ F_1{}'F_2 = -\gamma^2,\ F_1F_2{}' = -3 \\
&\overset{(A.19)}{\longleftrightarrow} \cos^2\phi_2 = \Gamma^2/9,\ \sin^2\phi_1 = \Delta^2/\gamma^2 \longleftrightarrow D = -\gamma^2\Gamma^2/9 - 3\Delta^2/\gamma^2 \leq 0.
\end{aligned}
$$

With $\cos^2\phi_1 + \sin^2\phi_1 = 1$ we find that the trace at one fixed point is zero for $\gamma^2\Gamma^2 + 9\Delta^2 = 9\gamma^2$ which describes an ellipse in the $\Gamma$-$\Delta$ parameter space (Fig. A.2 dashed green line). Since the determinant of the Jacobian at this fixed point is smaller than zero the fixed point is a saddle which changes stable and unstable directions when this ellipse is crossed.

The trace is also zero if $\cos\phi_2 = 0$ from which with (Eq. A.19) follows $\Gamma = 0$. There are four fixed points of the dynamics (Eq. A.3) with $\cos\phi_2 = 0$ corresponding to two synchronization states on $T^2$. The determinant $D$ of $J$ at these fixed points follows as

$$
\cos\phi_2 = 0 \longleftrightarrow \sin^2\phi_2 = 1 \overset{(A.11,A.19)}{\longrightarrow} D = F_1F_2{}',\ \Delta^2 = F_2^2 \overset{(A.17)}{\longrightarrow} F_2{}'^2 = 1 + \gamma^2 - \Delta^2.
$$

For the parameters $\Gamma = 0$ and $\Delta = 0$, since $\sin\phi_2 \neq 0$, $F_2$ in (Eq. A.19) must be zero. With (Eq. A.18) we obtain $D = -(3 - \gamma^2)$ for the fixed points where $\cos\phi_2 = 0$. This means that across the line $H_3$ (Fig. A.2) two synchronization states loose stability in an Andronov-Hopf bifurcation if $\gamma^2 > 3$. If $\gamma^2 < 3$ the fixed points with $\cos\phi_2 = 0$ are saddles for parameters $\Gamma$ and $\Delta$ in the inner area circumscribed by the curve $\mathrm{SN}_2$ (Fig. A.2) where the determinant changes. On the line $\Gamma = 0$ the determinant is zero if $F_1 = 0$ or $F_2{}' = 0$.

$$
\begin{aligned}
&F_2{}' = 0 \longrightarrow F_2^2 = \Delta^2 = 1 + \gamma^2 \\
&F_1 = 0 \longrightarrow F_1{}'^2 = 9 + \gamma^2 \overset{(A.18)}{\longrightarrow} F_1{}'^2F_2^2 = (3 - \gamma^2)^2 = (9 + \gamma^2)\Delta^2 \\
&\longleftrightarrow \Delta^2 = (3 - \gamma^2)^2/(9 + \gamma^2)
\end{aligned}
$$

Conversely, if $\Delta^2 = (3-\gamma^2)^2/(9+\gamma^2)$ and $\cos\phi_2 = 0$ it does not follow that $F_1 = 0$.

$$F_2^2 = \Delta^2 = \frac{(3-\gamma^2)^2}{9+\gamma^2} \overset{\text{(A.16)}}{=} \left(\frac{(3-\gamma^2){F_1}' + 4\gamma F_1}{9+\gamma^2}\right)^2$$

$$\longleftrightarrow (3-\gamma^2)^2(9+\gamma^2) - (3-\gamma^2)^2 {F_1}'^2 - 16\gamma^2 F_1^2 = 8\gamma(3-\gamma^2)F_1{F_1}'$$
$$\overset{\text{(A.17)}}{\longleftrightarrow} \left((3-\gamma^2)^2 - 16\gamma^2\right) F_1^2 = 8\gamma(3-\gamma^2)F_1{F_1}'$$
$$\overset{F_1\neq 0}{\longleftrightarrow} \left((3-\gamma^2)^2 - 16\gamma^2\right) F_1 = 8\gamma(3-\gamma^2){F_1}'$$
$$\overset{\text{(A.17)}}{\longrightarrow} \left((3-\gamma^2)^2 - 16\gamma^2\right)^2 F_1^2 = 8^2\gamma(3-\gamma^2)^2(1+\gamma^2-F_1^2)$$
$$\longleftrightarrow F_1^2(((3-\gamma^2)^2 - 16\gamma^2)^2 + 8^2\gamma^2(3-\gamma^2)^2) = 8^2\gamma^2(3-\gamma^2)^2(1+\gamma^2)$$

$$\longleftrightarrow F_1^2 = \frac{64\gamma^2(3-\gamma^2)^2}{(1+\gamma^2)(9+\gamma^2)^2} \tag{A.20}$$

This means, that only at one fixed point with $\cos\phi_2 = 0$ the determinant changes sign when $SN_2$ is crossed. For $\gamma^2 < 3$ this fixed point becomes a center outside of $SN_2$ and for $\gamma^2 > 3$ one of the centers becomes a saddle. Therefore $H_1$ and $H_2$ are Hopf bifurcation lines for all values of $\gamma$ and $H_3$ is a Hopf bifurcation line only for $\gamma^2 > 3$.

The saddle-node bifurcation lines $SN_1$ and $SN_2$ are determined implicitely.

$$D = \cos^2\phi_2 {F_1}' F_2 + \sin^2\phi_2 F_1 {F_2}'$$
$$\overset{\text{(A.18,A.19)}}{=} \cos^2\phi_2(3-\gamma^2) + F_1{F_2}' = {F_1}'F_2 - \sin^2\phi_2(3-\gamma^2)$$
$$\overset{\text{(A.11)}}{\longrightarrow} DF_1^2 = \Gamma^2(3-\gamma^2) + F_1^3{F_2}'$$
and $DF_2^2 = {F_1}'F_2^3 - \Delta^2(3-\gamma^2)$.

Note from (Eq. A.12) that $F_1$ and $F_2$ cannot be zero at the same time unless $\gamma^2 = 3$. This case will be discussed separately. Otherwise we have

$D = 0 \longleftrightarrow DF_1^2 = DF_2^2 = 0$ yielding equations for the parametric curves $SN_1$ and $SN_2$.

$$\Gamma^2 = -\frac{F_1^3{F_2}'}{3-\gamma^2} \quad , \quad \Delta^2 = \frac{{F_1}'F_2^3}{3-\gamma^2}$$

Both $F_1^3{F_2}'$ and $F_2^3{F_1}'$ have a period of $\pi$. There are two intervals within $[-\pi/2, \pi/2]$ where $F_1^3{F_2}' \leq 0$ and $F_2^3{F_1}' \geq 0$ and thus $\Gamma^2, \Delta^2 \geq 0$. The line $\Gamma = 0$ has already been discussed. The critical points on the line $\Delta = 0$ are found to yield

$\Delta^2 = 0 \longleftrightarrow F_2 = 0$ or $F_1{}' = 0$

(i) $F_2 = 0 \overset{(A.17)}{\longleftrightarrow} F_2{}'^2 = 1 + \gamma^2$
$- F_1 F_2{}' \overset{(A.18)}{=} 3 - \gamma^2 \longrightarrow \Gamma^2 = F_1^2 = (3-\gamma^2)^2/(1+\gamma^2)$

(ii) $F_1{}' = 0 \overset{(A.17)}{\longleftrightarrow} F_1^2 = 9 + \gamma^2$
$- F_1{}' F_2 \overset{(A.18)}{=} 3 - \gamma^2 \longrightarrow \Gamma^2 = F_1^2 = 9 + \gamma^2$

Finally we consider the degenerate case $\gamma^2 = 3$ and $F_1 = F_2 = 0$.

$F_1 = 0, F_2 = 0 \longrightarrow \Gamma = 0,\ \Delta = 0$
$F_2 = 0 \overset{(A.12)}{\longrightarrow} \cos\phi_1 = -\gamma \sin\phi_1$
$\overset{(A.13)}{\longrightarrow} F_1{}' = 3\cos\phi_1 - \gamma\sin\phi_1 = 4\cos\phi_1$
$\overset{(A.17)}{\longrightarrow} F_1^2 + F_1{}'^2 = 9 + \gamma^2 = 12 \longrightarrow F_1{}'^2 = 12 = 16\cos^2\phi_1$
$\longleftrightarrow \cos^2\phi_1 = \frac{3}{4},\ \sin^2\phi_1 = \frac{1}{4}$
and $\cos^2\phi_2 + \sin^2\phi_2 = 1$

At the critical value $\gamma^2 = 3$ of nonisochronicity with $\Gamma = \Delta = 0$ there exists a whole line of fixed points with $\phi_2 \in [-\pi, \pi]$ at which the determinant $D$ is zero. This is the onset of the cusp-bifurcation found for larger values $\gamma^2 > 3$.

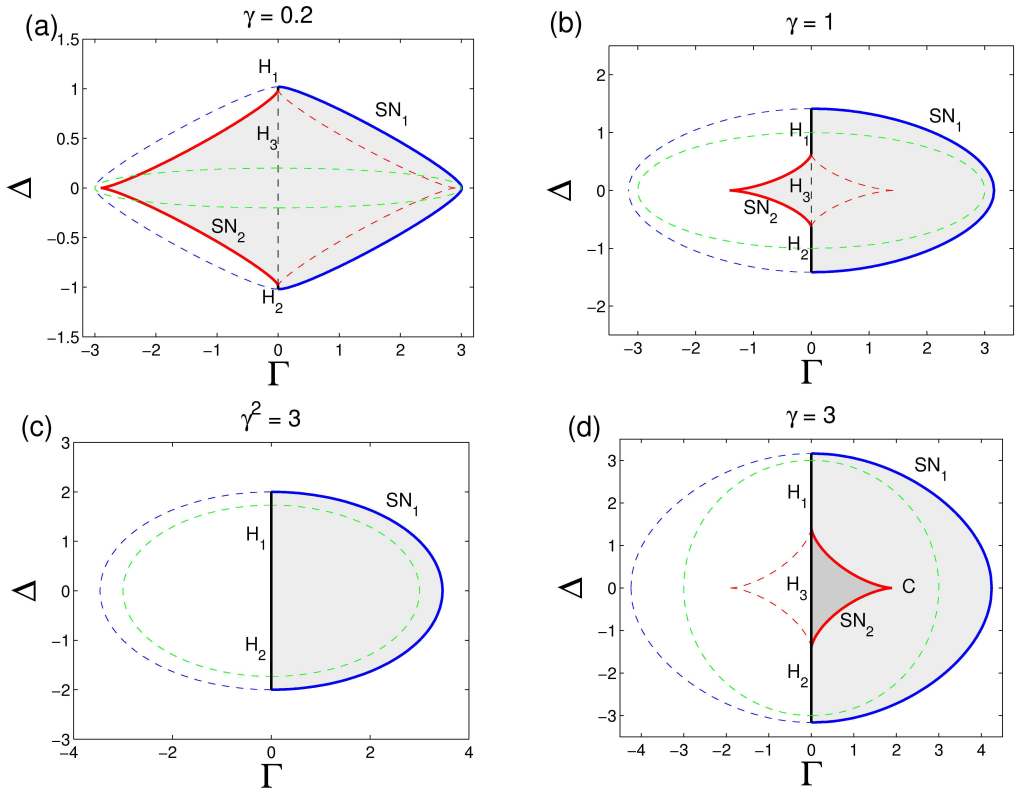


Figure A.2: Regions in the $\Gamma - \Delta$ parameter space where synchronization manifolds exist for a chain of three nonidentical, nonisochronous Kuramoto phase oscillators (Eq. A.1). Inside the region bounded by the saddle-node bifurcation line $SN_2$ (red line) there are four synchronization manifolds. Two of them vanish in a saddle-node bifurcation at $SN_2$ and the other two at $SN_1$ (blue line). In the gray regions asymptotically stable synchronization exists. Stability is lost across solid lines, either in saddle node bifurcations at $SN_1$ and $SN_2$ or in an Andronov-Hopf bifurcation at $H_1$ and $H_2$ (black lines). The dashed green line marks the inversion of stability when the trace of the Jacobian at a saddle point changes sign. The four diagrams differ in the value of nonisochronicity $\gamma$. For values $\gamma^2 > 3$ we find a regime of bistability (subfig. d, darker gray) bounded by $SN_2$ in a cusp-bifurcation with cusp point C and an Andronov-Hopf bifurcation at $H_3$.

# Appendix B

# Newton Method for the Synchronization Manifold

Searching for a stable synchronization manifold inside the huge state space of a large network of phase oscillators is like following a will-o-wisp through a dark forrest. We can integrate the Kuramoto phase equations in the hope to achieve synchronization but the ghost light will not go the direct route and once it is in the larger vicinity of the target it slows down exponentially. In a regular medium we may be in the regime of two competing pacemaker regions, which means that parts of the phase profile are still very different from the synchronized solution. Especially since we are interested in the exact shape of the phase profile we had to look for heuristic methods to bridge the long transient times to synchronization. We start by choosing a gauge field $\vartheta^0$. This is usually homogeneous but we have also used constant phase differences $\vartheta^0_{n+1} - \vartheta^0_n = l2\pi/N$ for a ring of oscillators with topological charge $l$.

If the oscillators are nonisochronous we could use the exponential approximation described in Section 4.4.2 and calculate the ground state vector of the corresponding Hamiltonian. One could called this a nonlinear Newton step. The phase profile obtained from the approximation of the phase coupling function should be very close to the actual synchronized solution in the sense that the phase relations between coupled oscillators are already correct and competing pacemaker regions are already suppressed. From this approximation we started to integrate the phase equations but also tried to speed up the process with the help of a Newton method.

Suppose we are looking for a synchronized solution $\vartheta$ of

$$\Omega = \omega_n + \sum_m A_{nm}\ g(\vartheta_m - \vartheta_n) \tag{B.1}$$

and we know that the phases $\vartheta^0$ are close to the solution. They may yield

$$\Omega_n = \omega_n + \sum_m A_{nm}\ g(\vartheta^0_m - \vartheta^0_n) \tag{B.2}$$

with yet non-identical phase velocities $\Omega_n$. The idea of the (linear) Newton method is to linearize the equation (Eq. B.1) with respect to the displacement $\varphi = \vartheta - \vartheta^0$ and solve

$$\sum_m A_{nm}\ g'_{mn}\ (\varphi_m - \varphi_n) \approx \Omega - \Omega_n \tag{B.3}$$

with $g'_{mn} = g(\vartheta^0_m - \vartheta^0_n)$ in the subspace orthogonal to a global phase shift. Because only the phase differences enter the equation we can impose the additional condition $\varphi_N = 0$. With the possibly asymmetric Laplacian

$$L_{nm} = A_{nm}g'_{mn} - \delta_{nm}\sum_p A_{np}g'_{pn} \tag{B.4}$$

we obtain from (Eq. B.3)

$$\sum_m (L_{nm} - L_{Nm})\,\varphi_m = \Omega_N - \Omega_n \qquad . \tag{B.5}$$

The matrix $\mathbf{M}$ with

$$M_{nm} = L_{nm} - L_{Nm} \qquad \text{for } n, m < N \tag{B.6}$$

is in general not singular, except at bifurcation points, and can be inverted to obtain the phases $\varphi_n$ for $n < N$ from equation (Eq. B.5). The phase profile $\vartheta^0 + \varphi$ will be closer to the actual synchronization manifold. This Newton step can be iterated and the deviation from the synchronization manifold decreases algebraically instead of exponentially. A Newton step should only be performed if the amplitude of the frequency differences $\Omega_N - \Omega_n$ is small but still larger than machine precision. It should be rejected if the synchronized state is likely to be a saddle, i.e. if $\mathbf{M}$ has positive eigenvalues.

# Appendix C

# Symmetry and the Correlator Matrix

A symmetry of a system is an automorphism $\mathbf{S} : M \to M$ which maps a point $\mathbf{r}$ uniquely to another point $S(\mathbf{r})$. One would say a function $\mathbf{f}$ is symmetric with respect to $\mathbf{S}$ if $f(\mathbf{r}) = f(S(\mathbf{r}))$ for all $\mathbf{r}$. Associated with $S$ is an operator $\mathbf{\Sigma}$ with

$$(\mathbf{\Sigma f}) = \mathbf{f} \circ \mathbf{S} \qquad . \tag{C.1}$$

A constant function $\mathbf{f}_0 \parallel \mathbf{1}$ is an eigenfunction of $\mathbf{\Sigma}$ with eigenvalue $\sigma_0 = 1$. In fact, with node permutations, rotations and translations we will only consider unitary transformations

$$\mathbf{\Sigma}^\dagger = \mathbf{\Sigma}^{-1} \qquad . \tag{C.2}$$

An operator $\mathbf{L}$ is symmetric with respect to a symmetry if it commutes with $\mathbf{\Sigma}$

$$\mathbf{\Sigma L} = \mathbf{L\Sigma} \qquad . \tag{C.3}$$

The set of symmetric transformations is called the symmetry group of $\mathbf{L}$. Let $\mathbf{P}_k$ and $\mathbf{p}_k$ be a complete system of orthonormal left and right eigenvectors of $\mathbf{L}$ with eigenvalues $E_k$. For any symmetry $\mathbf{\Sigma}$ of $\mathbf{L}$ one observes

$$\mathbf{L\Sigma p}_k = E_k \mathbf{\Sigma p}_k \tag{C.4}$$

which means that $\mathbf{\Sigma p}_k$ is an eigenvector of $\mathbf{L}$ to the eigenvalue $E_k$. If the eigenvalue $E_k$ is not degenerate then $\mathbf{p}_k$ is also an eigenvector of $\mathbf{\Sigma}$ with

$$\mathbf{\Sigma p}_k = \sigma_k \mathbf{p}_k \qquad \text{(if } E_k \text{ is not degenerate).} \tag{C.5}$$

In that case the left eigenvector $\mathbf{P}_k$ is also an eigenvector of $\mathbf{\Sigma}$

$$\begin{aligned} \mathbf{\Sigma}^\dagger \mathbf{P}_k &= \sigma_k^* \mathbf{P}_k \\ \mathbf{P}_k &= \mathbf{\Sigma}\mathbf{\Sigma}^\dagger \mathbf{P}_k = \sigma^* \mathbf{\Sigma} \mathbf{P_k} \\ \mathbf{\Sigma} \mathbf{P}_k &= \frac{1}{\sigma_k^*} \mathbf{P}_k = \sigma_k \mathbf{P}_k \quad . \end{aligned} \tag{C.6}$$

Here we have used the fact that $\mathbf{\Sigma}$ is unitary and has eigenvalues on the complex unit circle.

Of particular interest for our perturbation approach is the left eigenvector $\mathbf{P}_0$ of the Laplacian operator $\mathbf{L}$ to the eigenvalue $E_0 = 0$. If this eigenvalue is not degenerate, which means that the only neutrally stable phase shift in synchronization is global, then with $\sigma_0 = 1$ we have

$$\mathbf{\Sigma} \mathbf{P}_0 = \mathbf{P_0} \qquad \text{and} \qquad P_0(r) = P_0(S(r)) \tag{C.7}$$

for all symmetry transformations of $\mathbf{L}$. The left eigenvector $\mathbf{P}_0$ assigns identical weights to equivalent nodes or positions $\mathbf{r}$ with respect to the symmetry. It is therefore uniform if the system is homogeneous but also if the Laplacian is hermitian, which is the case for identical oscillators on the uniform synchronization manifold.

We are now interested in the consequence of symmetry for the correlator matrix $\mathbf{C} = \mathbf{E}[\eta\eta^\dagger]$ with random functions $\eta(\mathbf{r})$. If the joint probability distribution $p(\eta(\mathbf{r}), \eta(\mathbf{r}'))$ is symmetric with respect to a symmetry of the system, i.e. equivalent node pairs have the same distribution, then the symmetry groups of $\mathbf{C}$ and $\mathbf{L}$ are identical. This does not necessarily mean, however, that $\mathbf{C}$ and $\mathbf{L}$ commute and that $\mathbf{C}$ is diagonal for a complete set of eigenvectors $\mathbf{P}_k$ and $\mathbf{p}_k$ of $\mathbf{L}$. Suppose $\mathbf{L}$ and $\mathbf{\Sigma}$ commute and $\mathbf{P}_k$ and $\mathbf{p}_k$ are a complete set of common eigenvectors (discrete). The operator $C$ can be written as

$$\mathbf{C} = \sum_{k,k'} C_{kk'} \mathbf{p}_k \mathbf{P}_{k'}^\dagger \quad . \tag{C.8}$$

If $\mathbf{C}$ and $\mathbf{\Sigma}$ commute then from $\mathbf{\Sigma}\mathbf{p}_{k'} = \sigma_{k'}\mathbf{p}_k$ and $\mathbf{P}_k^\dagger \mathbf{\Sigma} = \mathbf{P}_k^\dagger \sigma_k$ follows

$$\mathbf{P}_k^\dagger \cdot \mathbf{\Sigma}\mathbf{C}\mathbf{p}_{k'} = \sigma_k C_{kk'} = \mathbf{P}_k^\dagger \cdot \mathbf{C}\mathbf{\Sigma}\mathbf{p}_{k'} = C_{kk'}\sigma_{k'} \tag{C.9}$$

and

$$C_{kk'}\left(\sigma_k - \sigma_{k'}\right) = 0 \quad . \tag{C.10}$$

Off-diagonal elements $C_{kk'}$ with $k \neq k'$ are zero if the eigenvalues $\sigma_k$ and $\sigma_{k'}$ are different. If there is a complete set of commuting symmetry operations of $\mathbf{C}$ then for each $k \neq k'$ such a symmetry can be found that $\sigma_k \neq \sigma_{k'}$ and $\mathbf{C}$ is diagonal. This is the case for a continuous cubic medium with periodic boundary conditions and constant gradient $\nabla\vartheta^0 = \boldsymbol{l}\, 2\pi/L$. The symmetry group of this system is $SU(2) \times SU(2) \times \cdots \times SU(2)$. The infinitesimal translations $\mathbf{\Sigma}^{(i)} = \partial_i$ of the corresponding Lie-algebra form a complete set of commuting operators.

On the surface of a 2-sphere the situation is different. The infinitesimal rotations $\mathbf{\Sigma}^x$, $\mathbf{\Sigma}^y$ and $\mathbf{\Sigma}^z$ around the $x$, $y$ and $z$ axes do not commute with each other. The Laplacian differential operator and $\mathbf{\Sigma}^z$ form a complete system of commuting operators with eigenfunctions $\mathbf{p}_{lm}$ [75] so that

$$\mathbf{L}\mathbf{p}_{lm} = l(l+1)\mathbf{p}_{lm} \qquad \mathbf{\Sigma}^z\mathbf{p}_{lm} = m\mathbf{p}_{lm} \tag{C.11}$$

Since $\mathbf{\Sigma}^z$ is also a symmetry of $\mathbf{C}$ from equation (Eq. C.10) follows $C_{lml'm'} = 0$ if $m \neq m'$.

Assuming furthermore that left and right eigenvectors are identical, either because the Laplacian is symmetric or because all positions in the system are equivalent with respect to a symmetry group. Let $\nu$ be a function of random frequencies with correlator entries

$$\tilde{C}_{kk'} = \mathbf{p}_k^\dagger \cdot \mathbf{E}\left[\nu\nu^\dagger\right] \mathbf{p}_{k'} \tag{C.12}$$

and

$$\eta = \left(\mathbb{I} - c\ \mathbf{p}_0\mathbf{p}_0^\dagger\right)\nu \qquad . \tag{C.13}$$

Then the correlator $\mathbf{C}$ of $\eta$ is given by

$$C_{kk'} \;=\; \tilde{C}_{kk'} \;-\; c\ \delta_{k0}\ \tilde{C}_{0k'} \;-\; c\ \delta_{0k'}\ \tilde{C}_{k0} \;+\; c^2\ \delta_{kk'}\ \tilde{C}_{00} \qquad . \tag{C.14}$$

In particular for $c = 1$ the shift makes the arithmetic mean $\bar{\eta}$ zero. Since only correlator terms with $k, k' \neq 0$ enter the equations for the expected second order perturbation terms (Eqs. 5.20 or 5.26), they are independent of a change into a co-rotating frame of reference.

# Appendix D

# Connected Random Networks

This section describes a way to sample uniformly from connected, undirected networks of a given size $N$ with labeled vertices and gives expressions for the degree distribution. We will use the following notations for different distributions - a binomial distribution for $n$ successes of $N$ Bernoulli trials with success probability $p$ is denoted by $P_p(n|N)$. A Poissonian distribution of $n$ events and with the mean $\nu$ will be denoted by $P_\nu(n)$. These distributions are distinguished in notation by the number of their arguments. The degree distributions of random networks on $N$ vertices are denoted by $P_{RE}(k|N)$, $P_T(d|N)$, $P_{CN}(k|N)$ for a Rényi-Erdös random network, a random tree and a random connected network respectively. For large networks $N \gg 1$ these distributions become Poissonian asymptotically and independent of $N$. Then the conditional argument is omitted.

The usual Rényi-Erdös method [77] to generate the adjacency matrix $A_{ij}$ for $i, j = 1 \ldots N$ vertices is to set $A_{ij} = 1$, thus allowing the link from vertex $j$ to vertex $i$, with a probability $p$ or $A_{ij} = 0$ otherwise. The total number $k_{in} = \sum_j A_{ij}$ of links to a node $i$ is the in-degree of this node and the total number of links from this node $k_{out} = \sum_j A_{ji}$ is called the out-degree. In-degree and out-degree are random variables for each node. If $A_{ij}$ is constrained to be symmetric then $k_{in} = k_{out} = k$, otherwise and if there are no self-loops $k_{in}$ and $k_{out}$ are independent. We will only consider the symmetric case without self loops in the following.

The method of Rényi and Erdös samples uniformly from all possible (symmetric) graphs on $N$ vertices. Only a certain fraction of these graphs are connected. Even the probability $P_{RE}(k = 0)$ for a node to have no links at all is nonzero. The degree distribution $P_{RE}(k|N)$ of a Rényi-Erdös (RE) network of $N$ vertices is in fact a binomial distribution for $k$ successes in $N - 1$ Bernoulli trials of

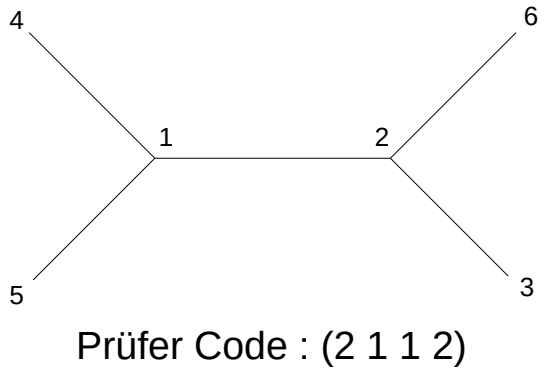


Figure D.1: A labeled tree and its corresponding Prüfer Code. The leaf with the smallest label is 3. It has 2 as parent, the first number in the PC. After removing vertex 3 the leaf with the smallest label is 4. This one has 1 as parent, the second number in the PC, and so on.

success probability $p$

$$P_{RE}(k|N) = P_p(k|N-1) = \frac{(N-1)!}{k!(N-1-k)!} p^k (1-p)^{(N-1-k)} \tag{D.1}$$

The idea for guaranteeing the connectedness of the network is to first generate a random tree with $N$ vertices and then allow additional edges with a probability $q$. It turns out that the degree distribution $P_{CN}(k|N)$ of such a connected network is a shifted binomial distribution (Eq. D.3).

The Prüfer Code [84] is a bijection between the set of labeled trees with $N$ vertices and the set of length $N-2$ integer sequences $\{n_i \mid i = 1 \ldots N-2\}$ of the numbers $n_i \in \{1 \ldots N\}$. A Prüfer Code (PC) provides a recipe for the construction of the corresponding tree. The numbers $n_i$ are the labels of parent nodes and the number $n_1$ is the parent of the tree leaf with the smallest index. This leaf is uniquely determined, since the set of leaves are all vertices which are not parents, i.e. whose indices do not appear in the PC (Fig. D.1). The generation of a tree from a given PC and the inverse task are of complexity $O(N \log N)$.

The number $k_n$ of links to a vertex $n$ is one more (!) than the number of times the index $n$ appears in the PC. If we sample uniformly from the set of PCs by drawing the $n_i$ randomly and independently the degree distribution $P_T(k|N)$ of the corresponding random trees is binomial but shifted by one :

$$P_T(k|N) = P_{\frac{1}{N}}(k-1|N-2) \tag{D.2}$$

As one expects from a tree, all vertices have at least one link to another vertex. From $N-1$ possible links only $N-2$ are randomly either on or off with probability

$p_0 = \frac{1}{N}$ and $(1 - p_0)$, respectively. If additionally to the edges of the tree links are added with a probability $q$ the probability $1 - p_1$ for a link not to be added is $(1 - p_1) = (1 - p_0)(1 - q)$. The degree distribution $P_{CN}(k|N)$ of the connected network is binomial with the single trial success probability $p_1$ but shifted by one.

$$P_{CN}(k|N) = P_{p_1}(k - 1|N - 2) \tag{D.3}$$

The expected degree is $\mathbf{E}[k] = 1 + p_1(N - 2)$. Note that $p_1 = p_0 + q(1 - p_0) \geq p_0$ and therefore $\mathbf{E}[k] \geq 1 + \frac{N-2}{N}$. Demanding that $\mathbf{E}[k] = \nu$ the probability $q$ to allow additional links has to be chosen as

$$q = \frac{N(\nu - 1) - (N - 2)}{(N - 1)(N - 2)}. \tag{D.4}$$

Letting $N \gg 1$ become large, the degree distribution approaches a Poissonian distribution which is shifted by one.

$$P_{CN}(k) \to P_{\nu-1}(k - 1) = \frac{(\nu - 1)^{(k-1)}}{(k - 1)!}\, e^{(1-\nu)} \tag{D.5}$$

and

$$\nu \geq 2 \qquad , \qquad q \to \frac{\nu - 1}{N} \qquad . \tag{D.6}$$

In Section 5.5 we ask for the eigenvalue spectrum of the network Laplacian. Both, the spectrum of the adjacency matrix $\mathbf{A}$ and of the normalized Laplacian $\mathbb{I} - \mathbf{D}^{-\frac{1}{2}}\mathbf{A}\mathbf{D}^{-\frac{1}{2}}$ with the degree matrix $\mathbf{D} = \mathrm{diag}(\mathbf{k})$ have compact support and a semi-circle like shape (Fig. D.3, [85, 79]) for an RE network. But we need the spectral density $\varrho_{\mathbf{L}}(E)$ of the Laplacian $\mathbf{L} = \mathbf{A} - \mathbf{D}$ in our perturbative analysis. We find in Monte-Carlo simulations that $\varrho_{\mathbf{L}}(E)$ is unimodal on the negative real axis and has a delta peak of magnitude $1/N$ at $E = 0$. If $\nu \to 2$ approaches the value for a tree network the maximum of the spectral density goes to zero. For large $N$ the spectral density only depends on the mean degree $\nu$ (Fig. 5.8). The functional form of $\varrho_{\mathbf{L}}(E)$ is not a gamma distribution on the negative real axis (Fig. 5.7). Nevertheless, the integration (Eq. 5.46) is not very sensitive to the shape, as long as $\varrho_{\mathbf{L}}(E)$ goes fast enough to zero for $E \to 0$. With the hypothesis of a gamma distribution the quantity $x = -E$ is distributed according to the density

$$p(x|\alpha, \beta) = \frac{\beta^\alpha}{\Gamma(\alpha)} x^{\alpha-1} e^{-\beta x} \qquad . \tag{D.7}$$

Mean $\mu$ and variance $\sigma^2$ are given as

$$\mu = \frac{\alpha}{\beta} \qquad \sigma^2 = \frac{\alpha}{\beta^2} \tag{D.8}$$

so that as a rough estimate of the parameters from a set of eigenvalues one can use the method of moments with

$$\beta = -\frac{\bar{E}}{\text{var } E} \qquad \alpha = \frac{\bar{E}^2}{\text{var } E} \qquad . \tag{D.9}$$

These expressions should be used as initial values for a maximum likelihood estimation. For the results shown in figure (Fig. 5.8) we used the maximum likelihood estimator provided in the *statistical toolbox* of the popular Matlab software. We see that the two parameters of the gamma-distribution are independent of the system size for $N \gg 1$. In fact, $\beta \approx 1/2$ and $\alpha \approx \nu/2$.

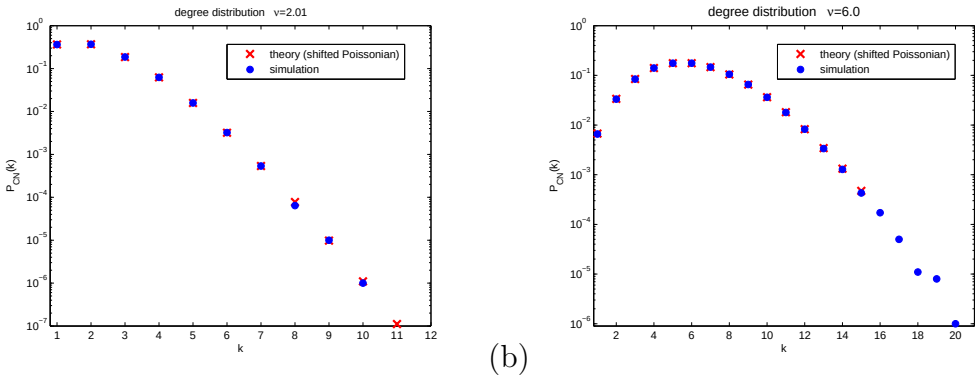


(a) (b)

Figure D.2: Degree distribution (blue dots) from 1000 realizations of random connected networks (CN) with $N = 1000$ nodes, and probability $q$ for additional edges from (Eq. D.4). The parameter $\nu$ for the construction of the networks in subfigure (a) was set to be $\nu = 2.01$. The mean degree obtained from the simulations was $\mathbf{E}[k] = 2.0102$. The parameter $\nu$ for the construction of the networks in subfigure (b) was set to be $\nu = 6.0$. The mean degree obtained from the simulations was $\mathbf{E}[k] = 6.002$. The red crosses are the theoretical shifted Poissonian degree distributions (Eq. D.5).

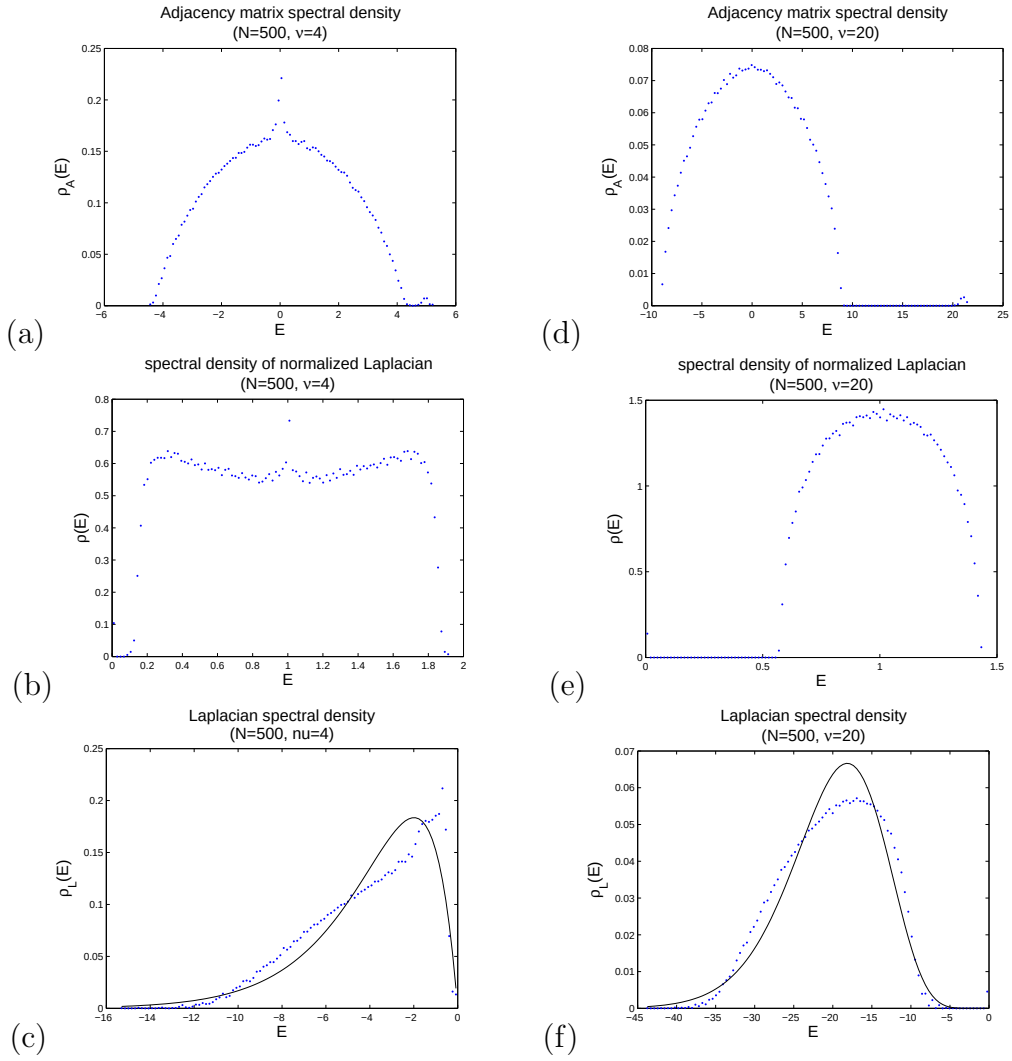


Figure D.3: Spectral densities of the Adjacency matrix (a,d) the normalized network Laplacian (b,e) and the Laplacian of a connected random network of size $N = 500$ (c,f) from an ensemble 100 realizations. The densities were computed from all eigenvalues of an ensemble of 100 realizations. The mean node degree on the left (a-c) is $\nu = 4$ and on the right (d-f) it is $\nu = 20$. Subfigures (c) and (f) also show the gamma distributions which fit the spectral densities best (solid line, parameters from maximum likelihood estimations).

# Appendix E

# Anderson Localization

In Section 4.4.3 we have seen that for nonisochronous oscillators ($\gamma \neq 0$) the phase profile in synchronization corresponds to the ground state solution of a stationary Schrödinger equation of a particle in a potential. The solution is reached at a time scale proportional to the difference of the largest and second largest real parts of the eigenvalues of the Hamiltonian, which may be non hermitian if the gauge field is not uniform. As Sakaguchi, Shinomoto and Kuramoto before [69] we have argued [10] that quasiregular concentric waves are the result of exponential localization of the ground state in a random potential. This effect was first analytically studied 1958 by P. W. Anderson [72] and has since become known as Anderson localization. It is experimentally observed in many different mechanical and quantum mechanical systems [72, 73, 86] as a loss of transport or diffusion due to heterogeneity in the system. The original work of Anderson was concerned with the transport of spin waves in a three dimensional discrete medium with random site potentials. The equations were quickly used in the tight binding model in condensed matter physics. A high number of defects in a two or three dimensional conductor leads to a metal-insulator phase transition corresponding to a localization of the electron wave functions. In the tight binding model electrons do not interact and are subject to a potential of random delta functions. The Schrödinger equation for this problem becomes a discrete equations for the wave function of an electron at the different sites and the Laplacian becomes the discrete Laplacian matrix of the system. If in a one dimensional system only next neighbor interaction is considered the tight binding model gives exactly the equations obtained from the exponential approximation for the Kuramoto model on a chain without topological charges

$$Eq_n = \varepsilon\eta_n + q_{n+1} - 2q_n + q_{n-1} \qquad . \tag{E.1}$$

This one dimensional problem can be solved, for instance with a transfer matrix formalism [87]. For $\varepsilon = 0$ all solutions compatible with open, periodic or no-flux boundary conditions are plain waves $q_n = e^{ikn}$. For arbitrarily small disorder $\varepsilon \neq$

0 the eigenvectors become localized. This can be seen by rearranging (Eq. E.1)

$$q_{n+1} = (E + 2 - \varepsilon\eta_n)q_n + q_{n-1} \tag{E.2}$$

and looking at the expected values $\mathbf{E}[q_n]$. We observe that equation (Eq. E.2) is causal, that is, $q_n$ depends only on $q_{n'}$ with $n' < n$ and $q_n$ is independent of $\eta_n$. With $x_n = \mathbf{E}[q_n]$, $y_n = \mathbf{E}[q_{n-1}]$ and $\mathbf{E}[\eta_n] = 0$, given an energy $E$ the evolution of the expected values of the eigenfunction along the system is

$$\begin{pmatrix} x_{n+1} \\ y_{n+1} \end{pmatrix} = \begin{pmatrix} E+2 & -1 \\ 1 & 0 \end{pmatrix} \begin{pmatrix} x_n \\ y_n \end{pmatrix} \quad . \tag{E.3}$$

The eigenvalues of the transfer matrix are

$$\lambda_\pm = \frac{E+2}{2} \pm \sqrt{\frac{(E+2)^2}{4} - 1} \quad . \tag{E.4}$$

Unless $E = -2$ (band center) the eigenfunctions will grow or decay exponentially from the boundary of the system. The localization length depends only on the eigenvalue $E$, just as the wave length of the stationary phase profile for the Kuramoto oscillators in one dimension depends on the synchronization frequency (Eq. 4.32). Indeed, Anderson Localization occurs at arbitrary disorder. For finite system sizes a transition between conductor and insulator occurs if the localization length is smaller than the system size.

The situation is more complicated in systems of higher dimension. Here, even in the limit of an infinite system size, electrical transport can be possible below a critical disorder $\varepsilon_c$. The Metal-insulator transition is a real phase transition. Until recently it was accepted that it was a second order phase transition. Discrepancies in experiments to the scaling theory of Anderson localization were attributed to the faults of the tight binding approximation. It is accepted doctrine that the wave functions are not localized for arbitrary small disorders and that localization in higher dimensions is not exponential. This poses the question whether quasi-regular concentric waves are still solutions of the nonisochronous Kuramoto model in synchronization in higher or even in two dimensions if the system size is increased and the disorder decreased. Recent analytical work [74] has challenged the scaling theory of Anderson localization. They predict the coexistence of localized and and non-localized wave functions of the same energy from the tight binding model in higher dimensions. The metal-insulator transition would therefore be a first order phase transition. The analysis reveals that the ground state of the system, which lies outside the energy band, will always be localized for a nonvanishing disorder but not necessarily exponentially.

# References


[1] Y. Kuramoto. *Chemical Oscillations, Waves and Turbulence*. Springer, Berlin, 1985, 1985.

[2] Arkady Pikovsky, Michael Rosenblum, and Jürgen Kurths. *Synchronization: A Universal Concept in Nonlinear Sciences*. Cambridge University Press, 2003.

[3] Steven H. Strogatz. *Sync: The Emerging Science of Spontaneous Order*. Hyperion, 2006.

[4] P. Bak. *How Nature Works: The Science of Self-Organized Criticality*. New York: Copernicus, 1996.

[5] Stephen P. Hubbell. *The Unified Neutral Theory of Biodiversity and Biogeography*. Princeton University Press, 2001.

[6] Hermann Haken. *Synergetik*. Springer-Verlag Berlin, Heidelberg, New York, 1982.

[7] Hermann Haken. *Synergetics, an Introduction: Nonequilibrium Phase Transitions and Self-Organization in Physics, Chemistry, and Biology*. Springer, 3rd rev enl edition, 1983.

[8] Michael G. Rosenblum and Arkady S. Pikovsky. Controlling synchronization in an ensemble of globally coupled oscillators. *Phys. Rev. Lett.*, 92, 114102, 2004.

[9] Natalia Tukhlina, Michael Rosenblum, Arkady Pikovsky, and Jürgen Kurths. Feedback suppression of neural synchrony by vanishing stimulation. *Phys. Rev. E*, 75, 011918, 2007.

[10] B. Blasius and R. Tönjes. Quasiregular concentric waves in heterogeneous lattices of coupled oscillators. *Phys. Rev. Lett.*, 95, 084101, 2005.

[11] J. G. Restrepo, E. Ott, and B. R. Hunt. Onset of synchronization in large networks of coupled oscillators. *Phys. Rev. E*, 71, 036151, 2005.

[12] M. Rosenblum and A. Pikovsky. Self-organized quasiperiodicity in oscillator ensembles with global nonlinear coupling. *Phys. Rev. Lett.*, 98, 064101, 2007.

[13] Y. L. Maistrenko, O. Popovych, O. Burylko, and P. A. Tass. Mechanism of desynchronization in the finite-dimensional Kuramoto model. *Phys. Rev. Lett.*, 93, 084102, 2004.

[14] Y. L. Maistrenko, Borys Lysyansky, Christian Hauptmann, Oleksandr Burylko, and Peter A. Tass. Multistability in the Kuramoto model with synaptic plasticity. *Phys. Rev. E*, 75, 066207, 2007.

[15] J. A. Freund, L. Schimansky-Geier, and P. Hänggi. Frequency and phase synchronization in stochastic systems. *Chaos*, 13:225–238, 2003.

[16] I. Z. Kiss, C. G. Rusin, H. Kori, and J. L. Hudson. Engineering complex dynamical structures: Sequential patterns and desynchronization. *Science*, 316 no. 5833:1886 – 1889, 2007.

[17] H. G. Schuster and P. Wagner. A model for neuronal oscillations in the visual cortex. *Bio. Cyb.*, 64:77–82, 83–85, 1990.

[18] R. E. Mirollo and S. H. Strogatz. Synchronization of pulse-coupled biological oscillators. *SIAM J. Appl. Math.*, 50, 1645, 1990.

[19] C. Schäfer, M. G. Rosenblum, J. Kurths, and H.-H. Abel. Heartbeat synchronized with ventilation. *Nature (London)*, 392:239, 1998.

[20] P. A. Tass. Desynchronization of brain rhythms with soft phase-resetting techniques. *Bio. Cyb.*, 87(2):102, 2002.

[21] Francisco Varela, Jean-Philippe Lachaux, Eugenio Rodriguez, and Jacques Martinerie. The brainweb: Phase synchronization and large-scale integration. *Nature Rev. Neurosci.*, 2(4):229, 2001.

[22] H. Kori and A. S. Mikhailov. Entrainment of randomly coupled oscillator networks by a pacemaker. *Phys. Rev. Lett.*, 93, 254101, 2004.

[23] K. Wiesenfeld, P. Colet, and S. H. Strogatz. Synchronization transitions in a disordered Josephson series array. *Phys. Rev. Lett.*, 76, 404, 1996.

[24] K. Wiesenfeld, P. Colet, and S. H. Strogatz. Frequency locking in Josephson arrays: Connection with the Kuramoto model. *Phys. Rev. E*, 57, 1563, 1998.

[25] R. Li and T. Erneux. Stability conditions for coupled lasers: series coupling versus parallel coupling. *Opt. Commun.*, 99:196, 1993.

[26] M. Silber, L. Fabiny, and K. Wiesenfeld. Stability results for in-phase and splay-phase states of solid-state laser arrays. *J. Opt. Soc. Am. B*, 10:1121, 1993.

[27] Kurt Wiesenfeld and James W. Swift. Averaged equations for Josephson junction series arrays. *Phys. Rev. E*, 51, 1020, 1995.

[28] Steven H. Strogatz, Daniel M. Abrams, Allan McRobie, Bruno Eckhardt, and Edward Ott. Theoretical mechanics : Crowd synchrony on the millennium bridge. *Nature*, 438:43–44, 2005.

[29] J. A. Acebrón, L. L. Bonilla, C. J. Pérez Vicente, F. Ritort, and R. Spigler. The kuramoto model: A simple paradigm for synchronization phenomena. *Rev. Mod. Phys.*, 77, 2005.

[30] Duncan J. Watts and Steven H. Strogatz. Collective dynamics of 'small-world' networks. *Nature*, 393:440–442, 1998.

[31] Albert-László Barabási and Réka Albert. Emergence of scaling in random networks. *Science*, 286:509–512, 1999.

[32] Albert-László Barabási and Réka Albert. Statistical mechanics of complex networks. *Rev. Mod. Phys.*, 74, 2002.

[33] L. M. Pecora and T. L. Carroll. Master stability functions for synchronized coupled systems. *Phys. Rev. Lett.*, 80, 2109, 1998.

[34] Junji Ito and Kunihiko Kaneko. Spontaneous structure formation in a network of chaotic units with variable connection strengths. *Phys. Rev. Lett.*, 88, 028701, 2002.

[35] Junji Ito and Kunihiko Kaneko. Spontaneous structure formation in a network of dynamic elements. *Phys. Rev. E*, 67, 046226, 2003.

[36] Changsong Zhou and J. Kurths. Dynamical weights and enhanced synchronization in adaptive complex networks. *Phys. Rev. Lett.*, 96, 164102, 2006.

[37] T. Gross, C. Dommar D'Lima, and B. Blasius. Epidemic dynamics on an adaptive network. *Phys. Rev. Lett.*, 72, 208701-4, 2006.

[38] Thilo Gross and Bernd Blasius. Adaptive coevolutionary networks - a review. *to appear in Journal of the Royal Society - Interface*, 2007.

[39] A. E. Motter, Changsong Zhou, and J. Kurths. Network synchronization, diffusion, and the paradox of heterogeneity. *Phys. Rev. E*, 71, 016116, 2005.

[40] Changsong Zhou, A. E. Motter, and J. Kurths. Universality in the synchronization of weighted random networks. *Phys. Rev. Lett.*, 96, 034101, 2006.

[41] Xingang Wang, Ying-Cheng Lai, and Choy Heng Lai. Enhancing synchronization based on complex gradient networks. *Phys. Rev. E*, 75, 056205, 2007.

[42] H. Kori and A. S. Mikhailov. Strong effects of network architecture in the entrainment of coupled oscillator systems. *Phys. Rev. E*, 74, 066115, 2006.

[43] J. Wolff, M. Stich, C. Beta, and H. H. Rotermund. Laser-induced target patterns in the oscillatory co oxidation on pt(110). *J. Phys. Chem. B*, 305:14282–14291, 2004.

[44] O.-U. Kheowan, E. Mihaliuk, B. Blasius, I. Sendi na Nadal, and K. Showalter. Wave mediated synchronization of nonuniform oscillatory media. *Phys. Rev. Lett.*, 98, 074101, 2007.

[45] Derek M. Johnson, Ottar N. Bjørnstad, and Andrew M. Liebhold. Landscape geometry and traveling waves in the larch budmoth. *Ecology Letters*, 7:967–974, 2004.

[46] B. Blasius, A. Huppert, and L. Stone. Complex dynamics and phase synchronization in spatially extended ecological systems. *Nature (London)*, 399:354–359, 1999.

[47] B. Blasius and L. Stone. Chaos and phase synchronization in ecological systems. *J. Bif. Chaos*, 10 (10):2361–2380, 2000.

[48] J. Schlesner, V. Zykov, H. Engel, and E. Schöll. Stabilization of unstable rigid rotation of spiral waves in excitable media. *Phys. Rev. E*, 74, 046215, 2006.

[49] R. Bracewell. *The Fourier Transform and Its Applications*. McGraw-Hill, 1999.

[50] A. T. Winfree. *The geometry of biological time*. Springer-Verlag (2nd edition), 2001.

[51] M. Nakahara. *Geometry, Topology and Physics (Graduate Student Series in Physics)*. Taylor & Francis, 2nd edition, 2003.

[52] F. R. K. Chung. *Spectral graph theory (CBMS Regional Conference Series in Mathematics, No. 92)*. American Mathematical Society, 1997.

[53] S. Gershgorin. Über die Abgrenzung der Eigenwerte einer Matrix. *Izv. Akad. Nauk. USSR Otd. Fiz.-Mat. Nauk*, 7:749–754, 1931.

[54] R. Tönjes and B. Blasius. Perturbation analysis for networks of phase oscillators subject to quenched frequency disorder. *in preparation*, 2007.

[55] Franziska Berger, Peter Gritzmann, and Sven de Vries. Minimum cycle bases for network graphs. *Algorithmica*, 40:51–62, 2004.

[56] A. Pikovsky and Ph. Rosenau. Phase compactons. *Physica D*, 218, 1:56–69, 2006.

[57] J. J. Hopfield. Neural networks and physical systems with emergent collective computational abilities. *PNAS*, 79 (8):2554–2558, 1982.

[58] Roberto Benzit, Alfonso Sutera, and Angelo Vulpiani. The mechanism of stochastic resonance. *J. Phys. A: Math. Gen.*, 14:L453–L457, 1981.

[59] Bruce McNamara, Kurt Wiesenfeld, and Rajarshi Roy. Stochastic resonance in a ring laser. *Phys. Rev. Lett.*, 60, 25:2626, 1988.

[60] Takashi Nishikawa, Ying-Cheng Lai, and Frank C. Hoppensteadt. Capacity of oscillatory associative-memory networks with error-free retrieval. *Phys. Rev. Lett.*, 92, 108101, 2004.

[61] S. H. Strogatz. The size of the synch basin. *Chaos*, 16, 015103, 2006.

[62] A. S. Mikhailov and V. S. Zykov. Kinematical theory of spiral waves in excitable media: Comparison with numerical simulations. *Physica D*, 52:379–397, 1991.

[63] Markus Bär, Anil K. Bangia, and Ioannis G. Kevrekidis. Bifurcation and stability analysis of rotating chemical spirals in circular domains: Boundary-induced meandering and stabilization. *Phys. Rev. E*, 67, 056126, 1991.

[64] J. E. Paullet and G. B. Ermentrout. Stable rotating waves in two-dimensional discrete active media. *SIAM J. Appl. Math.*, 54(6):1720–1744, 1994.

[65] P. T. de Boer, D. P. Kroese, S. Mannor, and R. Y. Rubinstein. A tutorial on the cross-entropy method. *Annals of operations research*, 134 (1):19–67, 2005.

[66] B. Blasius, E. Montbrió, and J. Kurths. Anomalous phase synchronization in populations of nonidentical oscillators. *Phys. Rev. E*, 67, 035204, 2003.

[67] A. N. Zaikin and A. M. Zhabotinsky. Concentration wave propagation in two-dimensional liquid-phase self-oscillating system. *Nature*, 225:535, 1970.

[68] A. S. Mikhailov and A. Engel. Multiple target pattern creation and synchronization phenomena. *Physics Letters A*, 117:257, 1986.

[69] H. Sakaguchi, S. Shinomoto, and Y. Kuramoto. Mutual entrainment in oscillator lattices with nonvariational type interaction. *Prog. of Theor. Phys.*, 79, 1069, 1988.

[70] L. Schimansky-Geier, J. Kurths, B. Fiedler, and E. Schöll. *Analysis and Control of Complex Nonlinear Processes*. World Scientific, 2007.

[71] Philip Rosenau. Hamiltonian dynamics of dense chains and lattices: or how to correct the continuum. *Phys. Lett. A*, 311:39–52, 2003.

[72] P. W. Anderson. Absence of diffusion in certain random lattices. *Prog. of Theor. Phys.*, 109, 1492, 1958.

[73] S. Russ. Scaling of the localization length in linear electronic and vibrational systems with long-range correlated disorder. *Phys. Rev. B*, 66, 12204, 2002.

[74] V.N. Kuzovkov and W. von Niessen. The phase diagram of the multidimensional anderson localization via analytic determination of lyapunov exponents. *Eur. Phys. J. B*, 42:529–542, 2004.

[75] W. Nolting. *Grundkurs Theoretische Physik 5 Quantenmechanik (Teil 2).* Vieweg, 3rd edition, 1997.

[76] J. R. Baumgardner and P. O. Frederickson. Icosahedral discretization of the two sphere. *SIAM J. Numer. Anal.*, 22:6, 1985.

[77] Paul Erdös and Alfréd Rényi. On random graphs. i. *Publ. Math.*, 6:290–297, 1959.

[78] Eugene Wigner. On the distribution of the roots of certain symmetric matrices. *Ann. of Math.*, 67:325–328, 1958.

[79] I. J. Farkasi, I. Derényi, A.-L. Barabási, and T. Vicsek. Spectra of 'real-world' graphs: Beyond the semicircle law. *Phys. Rev. E.*, 64, 026704, 2001.

[80] G. Biroli and R. Monasson. A single defect approximation for localized states on random lattices. *J. Phys. A: Math. Gen.*, 32:L255–L261, 1999.

[81] M. A. Zaks. Localized desynchronized states in weakly disordered lattices of coupled phase oscillators. *unpublished*, 2007.

[82] M. A. Zaks, A. S. Pikovsky, and J. Kurths. On the correlation dimension of the spectral measure for the thue-morse sequence. *Journal of Statistical Physics*, 88:1387–1392, 1997.

[83] Steven H. Strogatz. *Nonlinear Dynamics and Chaos*. Perseus Books Group, 2001.

[84] H. Prüfer. Neuer Beweis eines Satzes über Permutationen. *Arch. Math. Phys.*, 27:742–744, 1918.

[85] Fan Chung, Linyuan Lu, and Van Vu. Spectra of random graphs with given expected degrees. *PNAS*, 100(10):6313–6318, 2003.

[86] D. S. Wiersma, P. Bartolini, A. Lagendijk, and Roberto Righini. Localization of light in a disordered medium. *Nature*, 390:671–673, 1997.

[87] J. B. Pendry. The evolution of waves in disordered media. *J. Phys. C: Condensed Matter Phys.*, 15 No 16:3493–3511, 1982.